

IMPACT-GENERATED VOLATILE MOVEMENT
AND REDISTRIBUTION IN THE ROSE CITY METEORITE

A Thesis
Presented to
the Faculty of the Graduate School
University of Houston

In Partial Fulfillment
of the Requirements for the Degree
Master of Science

by
Ruth M. Fruland

December, 1975

IMPACT-GENERATED VOLATILE MOVEMENT
AND REDISTRIBUTION IN THE ROSE CITY METEORITE

Abstract
of Thesis
Presented to
the Faculty of the Graduate School
University of Houston

In Partial Fulfillment
of the Requirements for the Degree
Master of Science

by

Ruth M. Fruland

December, 1975

ABSTRACT

Ordinary chondrites contain textures and mineralogies which indicate a range in intensity of shock and thermal metamorphism. It has been proposed that the metamorphic sequence in ordinary chondrites is the result of thermal metamorphism in ejecta blankets deposited by impact events on the parent meteorite bodies. Because of the association of vapor phase crystallization with recrystallized (thermally-metamorphosed) lunar breccias, a search for vapor phase crystallization was undertaken with the Rose City meteorite (H-group). The Rose City meteorite is a high iron chondrite that underwent brecciation, shock-melting, vaporization and recrystallization in an impact event about 400 million years ago as interpreted from rare gas data. It contains a variety of lithologies: (1) clasts of moderately-shocked H6 lithology, (2) matrix, between clasts, of shock-melted and recrystallized silicate veins, depleted in metal and sulfide but containing numerous mineral fragments and vesicles, (3) matrix veins of metal and sulfide with a cotectic texture, (4) clasts in which the metal-sulfide and silicate portions show a range in degree of shock melting. Many of the larger clasts which are still coherent are surrounded by a band of metal-sulfide with the same cotectic texture common in the matrix metal bands.

A striking array of apparently vapor-grown crystals in cavities was found in both the recrystallized matrix and in the clasts of the Rose City meteorite, using the scanning electron microscope and energy dispersive x-ray analyzer. Euhedral to subhedral crystals of troilite, iron, iron-nickel, pyroxene, olivine, and apatite were found attached

to the walls of vugs. Similar morphologies and mineralogies of crystals in vuggy lunar breccias and the Rose City meteorite suggest similar processes caused loss of volatiles plus redistribution of volatiles in both ordinary chondrites and lunar breccias. Cooling of hot ejecta blankets on parent meteorite bodies would include movements of vapors (such as oxides, halides, sulfides, iron) from hotter to cooler areas, and result in eventual loss of noncondensable species and deposition of condensable species in cooler areas. This would explain some of the volatile depletions in ordinary chondrites. Cooling of large thermally-zoned ejecta blankets would partially explain the progressive thermal metamorphism of ordinary chondrites with the more recrystallized meteorites originating in the hotter zones of the ejecta blanket.

CONTENTS

ABSTRACT.....	iv
LIST OF FIGURES.....	viii
LIST OF TABLES.....	xii
CHAPTER 1. INTRODUCTION.....	1
Purpose and Scope.....	1
Nomenclature and Classification of Ordinary Chondrites.....	2
Shock Metamorphism in Chondrites.....	9
Description of the Rose City Meteorite.....	11
Impact-Generated Lunar and Terrestrial Analogs to Shocked Meteorites.....	18
Laboratory Work.....	20
Previous Work.....	22
Vapor Phase in Lunar Rocks.....	22
Criteria for Identification of Vapor-Derived Crystals.....	23
Vapor Phase in Terrestrial Pyroclastic Ash Flows.....	24
Vapor Phase in Meteorites.....	26
CHAPTER 2. PETROGRAPHY OF THE ROSE CITY METEORITE.....	28
Clast Lithology.....	28
Matrix Lithology.....	38
CHAPTER 3. SCANNING ELECTRON MICROSCOPE STUDY OF THE ROSE CITY METEORITE.....	46
Vug Morphology and Vug Mineralogy in Clast Lithology.....	46
Vug Morphology and Vug Mineralogy in Matrix Lithology.....	46
CHAPTER 4. ALTERATION PRODUCTS IN THE ROSE CITY METEORITE.....	88
CHAPTER 5.....	97
Summary.....	97
Discussion.....	100

CONTENTS

ACKNOWLEDGEMENTS.....	105
REFERENCES.....	106
APPENDIX A.....	114

LIST OF FIGURES

	Page
FIGURE 1: Five Chemical Groups of Chondrites.....	5
2. The Rose City Meteorite Sample.....	15
3. Photomicrograph of Clast Lithology.....	29
4. Metal and Sulfide in Clast Lithology.....	32
5. Metal and Sulfide in Clast Vug.....	32
6A. Shock Veins in Clast Lithology.....	34
6B. Shock Veins, Reflected Light.....	34
7. Pyroxene Crystals in Vug.....	35
8. Vesicle in Clast Lithology.....	35
9. Olivine Crystals in Vug.....	37
10. Calcium Phosphate in Vug.....	37
11A. Photomicrograph of Matrix Lithology, Metal-Rich Area...	39
11B. Total Matrix Thin Section.....	39
11C. Photomicrograph of Matrix Lithology, Silicate-Rich Area.....	40
12A. Metal-Sulfide Cotectic Texture.....	42
12B. Vug in Metal-Sulfide-Rich Area.....	42
13. Partially Melted Clast.....	44
14. Glass Vein with Aligned Metal Spheres.....	44
15A. Shock-Melted Glassy Area, Reflected Light.....	45
15B. Shock-Melted Glassy Area, Transmitted Light.....	45
16A. SEM Photograph of Clast Vugs.....	47
16B. Troilite Crystal.....	47
16C. Rose City Meteorite Troilite Growth Steps.....	49

	Page
FIGURE 17A. Lunar Troilite Growth Steps.....	49
17B. Lunar Troilite Crystal.....	51
18. Iron Crystal, Rose City Meteorite.....	51
19. Calcium Phosphate, Rose City Meteorite.....	53
20. Silicate Crystals in Vug.....	53
21A. Iron and Silicates in Vug.....	55
21B. High Magnification of Silicate Crystal.....	55
22A. Iron Crystal in Irregular Vug.....	59
22B. Iron Crystal, High Magnification.....	59
23. Common Crystal Forms.....	60
24. Cubic Iron Crystal.....	61
25A. Troilite Crystal.....	62
25B. Growth Steps, Troilite Crystal.....	62
26A. Calcium Phosphate, Iron in Vugs.....	64
26B. Skeletal Calcium Phosphate Crystals.....	64
26C. Euhedral Calcium Phosphate Crystals.....	65
27. Lunar Apatite Crystal.....	65
28A. Large Iron Crystal in Vug.....	67
28B. Silicates on Vug Wall.....	67
29A. Iron Crystal in Vesicle.....	69
29B. Crystal Faces on Iron Crystal.....	69
29C. Lunar Iron Crystal.....	70
29D. Chromite Crystal, Rose City Meteorite.....	70
30A. High-Calcium Silicates, Growth Steps on Silicates, Rose City Meteorite.....	72
30B. Growth Steps on Lunar Pyroxene.....	72

	Page
FIGURE 31A. Pyroxene Crystals, Rose City Meteorite.....	74
31B. Pyroxene Crystals, Lunar Breccia.....	74
31C. Pyroxene Crystals, Rose City Meteorite, Stereo Pair....	75
32A. Vug in Recrystallized Silicate Vein.....	76
32B. Equant Crystal, Silicate Vein.....	76
32C. Doubly-Terminated Olivine Crystal.....	77
33. Doubly-Terminated Silicate Crystal with Button Features.....	77
34. Elongate Vesicle.....	80
35. Spherical Vesicle.....	80
36A. Irregular Vug, Metal-Rich Area.....	82
36B. Iron Crystals.....	82
36C. Chromite Crystal.....	83
36D. Skeletal Chromite Crystals.....	83
36E. Whitlockite Crystals, Rose City Meteorite.....	85
36F. Whitlockite Crystals, Lunar Breccia.....	85
36G. Whitlockite Crystals, Rose City Meteorite.....	86
36H. Calcium-Phospho-Silicate Crystal, Rose City Meteorite..	86
36I. Twinned Iron Crystal, Rose City Meteorite.....	87
36J. Lunar Iron Crystal.....	87
37A. Large Vug with Alteration Products.....	90
37B. Spheroidal Iron Alteration Forms.....	90
38A. Small Vug with Iron Alteration Forms.....	92
38B. Iron Spheres.....	92
39. Iron Alteration in Vesicle.....	93

	Page
FIGURE 40A. Bladed Iron Alteration Forms in the Rose City Meteorite.....	94
40B. Bladed Iron Alteration Forms in a Lunar Breccia.....	94
41A. Iron Crystal, Stereo Pair.....	95
41B. Surface Texture, Iron Crystal.....	95
42. Schematic Diagram of Ejecta Blanket.....	102

LIST OF TABLES

	Page
TABLE 1. Chemical Analysis of the Rose City Meteorite.....	3
2. Mineral Content of the Rose City Meteorite.....	5
3. Fe, Mg and Si Distributions in the Five Chemical Groups of Chondrites.....	7
4. Petrologic Types of Chondrites.....	8
5. Classification of Chondrites.....	10
6. Comparison of H-Group Chondrite Averages with the Rose City Meteorite.....	13
7A. Microprobe Analyses of Clast Silicates.....	31
7B. Microprobe Analyses of Matrix Silicates.....	31

CHAPTER ONE

INTRODUCTION

Purpose and Scope

The purpose of this study is to characterize and determine the importance of the redistribution of volatile species, initiated by shock metamorphism and evidenced by vapor phase crystallization, in the Rose City meteorite. A detailed study was undertaken of the pore space, vapor-derived vugs (cavities) and vapor-grown mineral assemblages in the vugs of the highly shock-metamorphosed Rose City meteorite. The study included extensive use of the scanning electron microscope (SEM), the petrographic microscope and the electron microprobe.

The vapor-grown mineral assemblages in the Rose City meteorite are similar to vapor-derived features in lunar breccias. These features are directly related to shock metamorphism, and it was hoped that volatile movement and redistribution in the thermally metamorphosed ordinary chondrites also could be related to shock metamorphism. The morphology and physical association of the different vug crystals as observed with the SEM are given considerable attention because this tool has not been used before to any extent on this problem. Before the study of lunar rocks, vapor phase crystallization was not suspected to have occurred in meteorites.

The Rose City meteorite is a high iron chondrite and was selected for this study because it offered an opportunity to characterize a meteorite representing the highest grade or level of shock metamorphism (as indicated by vaporization of the silicates and metals). It is a

meteorite that apparently has undergone multiple impact events similar to the lunar breccias. Finally, because shock (impact) metamorphism is a heterogeneous process, within this one meteorite it is possible to go from lithologies representing the highest degrees of shock metamorphism such as shock-melted silicate veins depleted in metal and sulfide, to lithologies within the clasts in which mainly comminution and a much smaller amount of shock-melting and volatilization occurred.

The samples used in this study were loaned by Carleton B. Moore at Arizona State University, Tempe, Arizona.

Nomenclature and Classification of Ordinary Chondrites

Chondrite¹ is the name given by Gustav Rose in 1864 to stony meteorites that contain small (up to several millimeters in diameter) spheroidal or ellipsoidal bodies (chondrules). Today, meteorites are classified as chondritic on the chemical basis of having non-volatile element abundances similar to those found in the sun. This is considered to be a "primitive" or undifferentiated composition relative to terrestrial rocks. In chondrites lithophile, chalcophile and siderophile elements occur intimately mixed, but in terrestrial rocks these groups of elements have been separated by processes of differentiation. Table 1 shows a chemical analysis of the Rose City chondrite. Note that iron occurs in three different forms: oxidized, in silicates (olivine, pyroxene) and reduced, in sulfides and metal (troilite, kamacite).

¹For further reading on the nature of chondrites readers are referred to the following: Sorby, 1877; Tschermak, 1883; Mason, 1962; Ramdohr, 1963; Wasson, 1974.

TABLE 1: Chemical analysis of the Rose City meteorite by Whitfield (in Hovey, 1922).

SiO ₂	43.71 wt.%
MgO	26.97
FeO	15.09
Al ₂ O ₃	3.44
CaO	3.14
Na ₂ O	1.13
Cr ₂ O ₃	0.61
P ₂ O ₅	.25
MnO	.36
K ₂ O	0.18
Fe	17.25
NiO	.57
CoO	.08
SO ₃	.68
FeS	3.88

Total	100.09
-------	--------

In spite of the general undifferentiated nature of chondrites, there are chemical differences among them that can be used to divide the chondrites into five groups. The abundance of Fe (shown by the Fe/Si ratio) and its distribution between phases (best illustrated by its oxidation state, given by the Fe metal/total Fe ratio) was first used by Urey and Craig (1953) to distinguish between the chondrite groups. Figure 1 (from Wood, 1968) shows the differences in total iron abundances versus oxidation states, and the relationship of the high iron (H) chondrites to the other groups on the basis of these differences. The other chemical groups of chondrites are named as follows: the enstatite chondrites (E) after their most abundant constituent mineral; the carbonaceous chondrites (C) named by Tschermak in 1883; the low iron group (L) named because of their lower total iron content; and the very low iron group (LL) distinguished only recently as a separate group from the L's by Keil and Fredriksson (1964)². The H, L, and LL groups account for 78% of observed meteorite falls and hence are referred to as the ordinary chondrites.

Mineralogically the chondrites contain predominantly Fe- and Mg-rich silicates with smaller amounts of feldspar, diopside, iron-nickel metal and troilite. Table 2 shows the mineral composition of the Rose City chondrite, including the relative mineral proportions. The minerals are present in essentially two forms: chondrules and matrix, the latter being everything interstitial to the chondrules. The

²A good general discussion on the classification of chondrites is given by Van Schmus (1969).

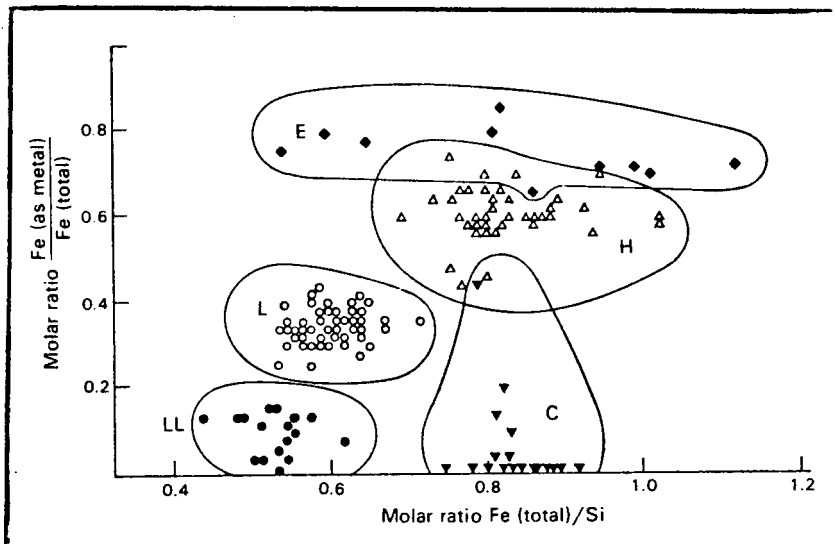


FIGURE 1: The five chemical groups of chondrites illustrated by their differences in Fe metal/total Fe. (From Wood, 1968).

TABLE 2: Mineral content of the Rose City meteorite.

Olivine	}	78.87
Pyroxene (Bronzite)		
Feldspar		
Apatite		
Chromite		
Troilite		3.88
Nickel-iron		17.25

minerals composing the chondrules, predominantly olivine and pyroxene, essentially are identical with the minerals found in the matrix. From one chemical group to another there is a range in composition of the olivines and pyroxenes, but within each group the composition is remarkably uniform. Table 3 summarizes some useful chemical and mineralogical criteria for distinguishing among the chondritic groups.

Within each chemical group there are textural and mineralogical differences which have been described in detail by Van Schmus and Wood (1967) and are summarized in Table 4. Van Schmus and Wood assigned petrologic types to the textural and mineralogical range within each chemical group of the chondrites. Their underlying premise is that thermal metamorphism has occurred, but the heat source is not specified. Ordinary chondrites show a range in texture from a distinct chondrule-in-matrix association, to textures where the fine-grained matrix has increased in grain size (recrystallized) to form a coarse-grained matrix such that the chondrules can no longer be distinguished easily from the matrix. Mineralogical changes occur with the textural changes such that heterogeneous olivine and pyroxene crystals show increasing homogenization or "equilibration". Clinopyroxenes are a disequilibrium product and occur in the unequilibrated chondrites. Inhomogeneous olivines and pyroxenes, and glass also are present in unequilibrated or unrecrystallized ordinary chondrites. Homogeneous orthopyroxenes are found in the equilibrated chondrites along with homogeneous olivines and no glass. According to the classification of Van Schmus and Wood, Type 3 indicates unrecrystallized distinct chondrule-in-matrix texture,

TABLE 3: Summary of the Fe, Mg and Si distributions in the 5 chemical groups of chondritic meteorites (from Van Schmus and Wood, 1967).

Group	Fe/SiO ₂	Fe ^o /Fe total	Olivine Fa (mol.%)	SiO ₂ /MgO
E	0.77	0.80	0	1.90
	±0.30	±0.10	-	±0.15
C	0.77	-	-	1.42
	±0.07	-	-	±0.05
H	0.77	0.63	18	1.55
	±0.07	±0.07	± 2	±0.05
L	0.55	0.33	24	1.59
	±0.05	±0.07	± 2	±0.05
LL	0.49	0.08	29	1.58
	±0.03	±0.07	± 2	±0.05

TABLE 4: Summary of the petrologic differences which occur within each chemical group of chondrites (from Wasson, 1974).

	Petrologic type					
	1	2	3	4	5	6
I. Homogeneity of olivine and pyroxene compositions	—	Greater than 5% mean deviations		Less than 5% mean deviations to uniform	Uniform	
II. Structural state of low-Ca pyroxene	—	Predominantly monoclinic		Abundant monoclinic crystals	Orthorhombic	
III. Degree of development of secondary feldspar	—	Absent		Predominantly as microcrystalline aggregates	Clear, interstitial grains	
IV. Igneous glass	—	Clear and isotropic primary glass; variable abundance		Turbid if present	Absent	
V. Metallic minerals (maximum Ni content)	—	Taenite absent or very minor (<20%)	Kamacite and taenite present (>20%)			
VI. Average Ni content of sulfide minerals	—	>0.5%	<0.5%			
VII. Overall texture	No chondrules	Very sharply defined chondrules		Well-defined chondrules	Chondrules readily delineated	Poorly defined chondrules
VIII. Texture of matrix	All fine-grained, opaque	Much opaque matrix	Opaque matrix	Transparent microcrystalline matrix	Recrystallized matrix	
IX. Bulk carbon content	3-5%	0.8-2.6%	0.2-1%	<0.2%		
X. Bulk water content	18-22%	2-16%	0.3-3%	<1.5%		

Types 4 and 5 represent increasing matrix grain size and homogenization of the constituent minerals, and Type 6 indicates the most mineralogically equilibrated and recrystallized texturally. Table 5 shows the Van Schmus and Wood (1967) classification scheme which uses both chemical and petrologic criteria to classify the chondrites. The number in each box is the number of examples of each meteorite type now known.

Shock Metamorphism in Chondrites

Most meteorites show some evidence of shock or impact metamorphism superimposed on the thermal metamorphism described above. This is consistent with evidence such as meteorite orbital determinations (Anders and Mellick, 1969) and earth-based asteroidal studies (Bowell and Zellner, 1973), which suggest many meteorites are asteroidal in origin. Multiple impact histories might be involved in the removal of meteoritic material from asteroidal parent bodies, eroding the material to the typical sizes of meteorites, and in deflecting these fragments into earth-crossing orbits. In addition, Taylor and Heymann (1969) present evidence that shock-induced reheating occurred on the parent meteorite bodies prior to the ejection of the chondrites from their parent bodies. Large scale impact events on the parent meteorite bodies are highly probable on the basis of what is now known about the early impact history of the moon, and the earth-based observations that all observable solid bodies in the solar system bear craters supposedly from numerous impact events.

There are many petrologic features associated with shock metamorphism in meteorites. Blackening, veining, and brecciation are the

TABLE 5: Classification of the chondrites from Van Schmus and Wood (1967).

		<u>Petrologic Type</u>					
		1	2	3	4	5	6
Chemical Group	E	E1	E2	E3	E4	E5	E6
		—	—	1*	3	2	6
	C	C1	C2	C3	C4	C5	C6
		5	18	9	1	—	—
	H	H1	H2	H3	H4	H5	H6
	—	—	6	23	53	32	
L	L1	L2	L3	L4	L5	L6	
	—	—	9	11	28	117	
LL	LL1	LL2	LL3	LL4	LL5	LL6	
	—	—	6	1	7	20	

*Number of examples of each meteorite type now known is given in its box.

result of shock or impact events (Fredriksson et al., 1963; Binns, 1967; Heymann, 1967). Mineralogical changes occur as the result of shock metamorphism and include the following: plagioclase is transformed to maskelynite at a minimum shock pressure of 300 kb and plagioclase and pyroxene are shock-melted at 450 kb (Stoffler, 1972); orthopyroxene can be transformed to clinopyroxene (Wlotzka, 1969); olivine becomes finely polycrystalline at shock pressures above approximately 130 kb (Fredriksson et al., 1963); metal and sulfide are melted (Begemann and Wlotzka, 1969); and recrystallization of kamacite occurs at 750 kb and forms martensite (Taylor and Heymann, 1969). A comprehensive survey of the shock processes and effects in natural materials, including terrestrial, lunar and meteoritic rocks is presented by Stoffler (1972). In an earlier paper, Stoffler (1971) presents a classification for shocked rocks based on the evidence of progressive shock metamorphism and defines six stages or zones of increasing shock metamorphism. Stage VI is where the highest pressure and temperature conditions occur at or near the point of impact. Temperatures exceed the boiling point of the rock melt and produce a vapor phase, which upon cooling will yield condensation products if the latter are contained. Stoffler admits this stage is theoretical in large part, but it is based on the fact that appreciable rock volumes are vaporized and condensed during impact processes (Butkovich, 1968).

Description of the Rose City Meteorite

The Rose City meteorite was observed to fall on October 17, 1921 at approximately 11 pm near the town of Rose City, Michigan. Three

meteorite fragments, weighing 6.4, 3.2 and 1.5 kilograms respectively, fell on the property of Mr. George Hall, the largest piece of which made a two foot deep hole in the ground. Grass embedded in the meteorite crust was not singed, indicating the meteorite had free fallen for some distance and was cold upon impact. Alteration of some of the metal and silicate phases has occurred during the meteorite's 54-year residence on the earth. The alteration is a consequence of the water vapor in the earth's atmosphere, varying laboratory conditions, and handling of individual samples (such as sawing, thin sectioning, etc.). Many meteorites contain the hygroscopic mineral lawrencite (FeCl_2) in minor amounts which decomposes into $\text{Fe}(\text{OH})_3$ and HCl upon contact with air.

Chemical analyses performed by Whitfield (Hovey, 1922) found the Rose City meteorite to contain 17.25% metal and 27.4% total iron. A second bulk chemical analysis was performed by Mason and Wiik (1966) which found a much higher metal content (28.6%) and a higher total iron content (36.40%). In their report, however, Mason and Wiik pointed out that the Rose City meteorite is a brecciated and inhomogeneous meteorite and that their sample could have been from a metal-rich part. Table 6 compares the H-group averages with the values determined by analyses of the Rose City meteorite. It is a high iron (H) group meteorite based on the bulk chemical analysis of Whitfield, and the olivine and pyroxene compositions determined by Mason and Wiik. Electron microprobe analyses performed by this investigator are listed in Appendix A and agree with the findings of Mason and Wiik (1966) of olivine compositions of Fa_{20}

TABLE 6: Typical H-group chemical averages compared with the Rose City meteorite analyses.

	H-group Average*	Rose City Meteorite Analyses**
Silicates	77.95 wt%	78.87 wt%***
Metal	16.80 wt%	17.25 wt%***
Fe ^o /Fe	0.63 ± 0.07	0.63
Olivine	Fa _{19.3}	Fa ₁₉
Pyroxene	Fs _{16.8}	Fs ₁₅

*Reported in Van Schmus (1969)

**Reported in Mason and Wiik (1966)

***Reported in Hovey (1922)

and pyroxene compositions of Fs_{15} . Both ortho- and clino-pyroxene was reported by Mason and Wiik, determined by x-ray diffraction methods.

Megascopically the Rose City meteorite is a breccia with centimeter- and greater-sized clasts. Figure 2 illustrates the clastic nature and inhomogeneity of this meteorite. The petrologic assignment of Type 6 is given to the Rose City meteorite by this investigator because the clasts composing the main mass of this meteorite appear to be of this type, with evidence of shock metamorphism superimposed upon the clast lithology. Petrographically, the clasts appear to be composed of coarse, but broken and partially melted crystals of olivine and pyroxene with a few discernable chondrules. Features in the Rose City meteorite normally found in the lower petrologic types, such as glass and a fine-grained matrix, are interpreted as being the result of shock-melting and recrystallization of the "original" Type 6 lithology. Many of the anomalous Type 6 textures are similar to those found in the Ramsdorf meteorite, described by Begemann and Wlotzka (1969), and interpreted by them as due to shock-induced thermal metamorphism. Large olivine and pyroxene crystals have undergone shock as evidenced by fracturing and partial melting of the grains, but where preserved, crystals and crystal fragments are homogeneous as determined by microprobe analyses by this investigator. This indicates that the Rose City meteorite was "equilibrated" before the major impact event. It is important to establish the pre-shocked petrologic type of the Rose City meteorite in order to determine which characteristics, both chemical and textural, are associated with the shock metamorphic process. The Rose City meteorite clasts are distinguished readily by

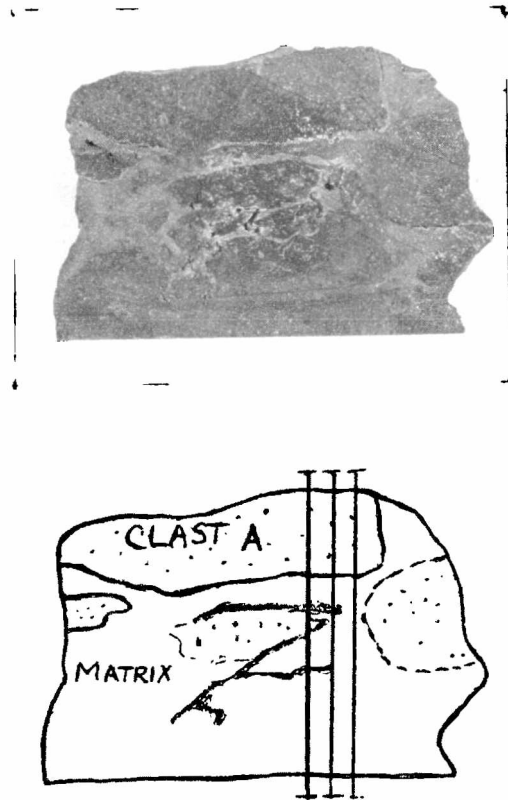


FIGURE 2: Photograph of section of Rose City meteorite from which the samples used in this study were obtained. Dimensions are 33 mm x 60 mm. Lower drawing: solid outlines of clasts (spotted) indicate metal; dashed outline indicates clast without metal band.

their coarser crystallinity, their irregular-shaped but randomly-distributed patches of metal, and the fact that many of them are "outlined" by a band of metal and sulfide.

Between the clasts there are largely shock-melted areas that are considered to be the matrix of the Rose City meteorite in this study. This use of the term "matrix" is different in connotation from what is generally referred to as matrix in most chondrites (usually the interstitial material between chondrules. The matrix is very complex and contains a variety of lithologies. Glassy to microcrystalline veins of what is interpreted as being shock-melted and partially recrystallized silicates occur in the matrix. Shock metamorphism produces disequilibrium clinopyroxene (Wlotzka, 1969) and this is the probable origin of the clinobronzite reported by Mason and Wiik (1966) in the Rose City meteorite because clinobronzite would not be found in an equilibrated chondrite. The silicate veins are depleted in metal and sulfide. The matrix also contains bands of metal and sulfide with a globular texture interpreted by Gegemann and Wlotzka (1969) as being the result of shock-melting. Apparently the silicate and metal-sulfide formed immiscible liquids which segregated before solidifying. There are numerous areas within the matrix in which the metal has been melted entirely, and much of the silicate portion melted to form a glass, but instead of separating, the metal is dispersed through the glass in discrete globules. There are partially-melted clasts, evident in thin section, but which do not have an iron-nickel rim. Taylor and Heymann (1969) used two criteria, the polycrystallinity of the olivine and the form of the iron-

nickel (martensite), as indicators of shock intensity. Their x-ray diffraction measurements show the Rose City meteorite to be moderately shocked on the basis of the polycrystallinity or mosaicism of the olivine. The iron-nickel present is predominantly martensite which indicated a very strongly reheated meteorite.

There are numerous cavities and vesicles within the clasts and matrix, interpreted by this investigator as being formed by volatilization of silicates, metal and sulfides, the result of the high temperatures and pressures reached during the impact event. Post-shock residual temperatures of the silicates for lesser-shocked meteorites (showing much less shock-melting, veining, etc.), such as the Ramsdorf and Orvinio chondrites, have been estimated in the range of 1200°C to 1350°C (Heymann, 1967; Begemann and Wlotzka, 1969). These temperatures correspond to a shock pressure on the order of at least 800 kb (McQueen et al., 1967). The Rose City meteorite must have undergone much higher temperatures, sufficient to have caused volatilization of even the higher temperature silicate, metal and sulfide phases. Studies of terrestrial impact samples have found temperatures of 1500° to 1700°C to be reasonable (El Goresy, 1965; Hörz, 1965) for such melting. Experimental shock studies by Gibbons et al. (1975) suggest temperatures in excess of 3000°C occur locally in shock-produced liquids. The cavities within the Rose City meteorite were considered to be logical sites for deposition from the vapor phases produced by shock-melting and volatilization by this investigator.

According to D. Bogard (unpublished manuscript) the Rose City meteorite underwent extensive shock-melting and volatilization approximately 400 m.y. ago, a conclusion based on rare gas release patterns. Hintenberger et al. (1965) reported that the Rose City meteorite has a U, Th-He age of 0.4 b.y. which represents the last major heating event. Taylor and Heymann (1969), in their investigation into the shock and reheating effects in ordinary chondrites, concluded that the shock and reheating seen in such meteorites occurred during impact events on the parent bodies rather than by the later impacts that ejected the meteorites from the parent bodies. They based this conclusion on the fact that all cosmic radiation ages (ejection ages) for the bronzite (H group) meteorites are shorter than 100 m.y., much less than the U, Th-He ages. Therefore, the above evidence indicates that the Rose City meteorite underwent extensive shock metamorphism in an impact event on its parent body. The degassing documented by Bogard (unpublished manuscript) indicates extensive volatilization, and a study of the vapor phase products retained may give some insight into the complicated processes operating during and after impact events on the parent bodies. The possibility exists that impact metamorphism is the source of the thermal metamorphism in many of the ordinary chondrites.

Impact-Generated Lunar and Terrestrial Analogs to Shocked Meteorites

Lunar breccias and meteorites show many features interpreted as the result of complex and repeated impact processes on the parent bodies (Urey, 1958; Fredriksson and Keil, 1963; Kurat et al., 1969; King et al., 1972; Warner et al., 1974). Based largely on petrologic studies, Wahl

(1952) proposed meteoritic breccias be divided into two categories: (1) monomict breccias in which the xenoliths are of the same material as the surrounding, finer-grained host; and (2) polymict breccias in which the xenoliths are not closely related to the interstitial host, and in which additional foreign fragments are sometimes found. Monomict breccias exist in the lunar rocks, an example being anorthosite 15415, described by James (1972), another example being dunite 72415, described by Albee et al. (1972). One meteoritic analog to the lunar monomict breccias is the Johnstown bronzite achondrite (Mason, 1963). The majority of the lunar highland samples are polymict breccias (Warner et al., 1973; Warner, 1972), as are the majority of the chondrites. Kurat et al. (1974) described lunar polymict breccia 14318 as having a chondritic texture. There are many meteoritic polymict breccias described, especially among the achondrites (Duke and Silver, 1967). Among the chondrites, polymict breccias have been documented by Dodd (1975), Van Schmus (1967), Wilkening and Clayton (1974) and many others.

Impact-generated silicate spherules from terrestrial and lunar samples have been studied and found to be analogous to meteoritic chondrules (King et al., 1972; Kurat et al., 1972; Nelen et al., 1972).

McKay et al. (1972) found vugs with well-developed crystals of plagioclase, pyroxene, ilmenite, apatite, whitlockite, iron, nickel-iron and troilite extending into the cavities of lunar rocks. These features were interpreted as formed by deposition from a high temperature vapor phase associated with hot ejecta blankets deposited by major cratering events.

Laboratory Work

The scanning electron microscope used in this study is a Jeolco JSM-U3 which generally was operated at an accelerating voltage of 25 KV. A lower voltage of 15 KV was used when a greater depth of field to increase apparent surface texture was desired. The SEM, with attached Nuclear Diodes EDX (energy dispersive x-ray analyzer) capable of yielding semi-quantitative chemical analyses, was used to characterize in situ morphology, mineral associations and mineral chemistry of the vapor phase products within the vugs and vesicles exposed on the sawn surface of the meteorite samples.

The samples were initially cleaned in a sonic bath of quadruple-distilled freon for 20 seconds, air-blown dry, and coated with gold by a Technic's Hummer (which sputters a hundred angstrom thick layer of gold onto the sample in an argon atmosphere). The prepared samples were mounted on brass SEM studs with Duco cement. To increase conductivity and lower background scattering, the brass SEM mounts were painted with carbon. Finally, several thin lines of silver paint were drawn from the sample to the carbon-coated brass mount.

Standard petrographic polished thin sections were made of the surfaces studied by the SEM. The porous samples were first vacuum-impregnated with epoxy in an attempt to preserve fine, delicate crystals within the cavities, as well as to minimize plucking during the thin sectioning process. Figure 2 illustrates where the two columns studied were taken from the Arizona State University Rose City meteorite sample (top photograph). The largest clast in the sample was designated Clast A for this work. The thickness of the original slab was approxi-

mately 6 mm, and this is the "working" surface studied with the SEM and made into a polished thin section. The thin section was thicker than the standard thickness of 30 micrometers because the large amount of metal in the sample has the tendency to peel away from the glass slide. A Zeiss camera-microscope Ultraphot II was used for the petrography portion of the study.

Microprobe analyses were collected with an ARL electron microprobe, under operating conditions of an accelerating voltage of 15 KV and sample current of 0.02 microamperes. Three elements were analyzed for simultaneously and the standards used were the same as those used for lunar samples analyzed in the microprobe laboratory at JSC.

Previous Work

Vapor Phase in Lunar Rocks

Carter and MacGregor (1970) showed a SEM photograph of pyroxene and plagioclase crystals lining a vug in an Apollo 11 basalt; Evans (1970) described a euhedral troilite crystal in a vug of an Apollo basalt; Gay et al. (1970) reported on an amphibole they found in a basalt vug. Charles et al. (1971) discussed the latter occurrence and suggested that chlorine may be an important constituent of the amphibole. Jedwab (1971) found ilmenite crystals in basalt vugs. He considered the layer-by-layer growth (growth steps) common on many crystals, to be characteristic of slow deposition rates at low supersaturations, and assumed the crystals in vugs to be vapor-derived. Skinner and Winchell (1972) describe what they consider to be vapor-phase-grown plagioclase needles in vugs and vesicles of Apollo 12 basalts.

McKay et al. (1972) were the first to report on the occurrence of well-formed crystals projecting into vug interiors in the highly re-crystallized lunar breccias. They documented subhedral to euhedral crystals of plagioclase, pyroxene, ilmenite, apatite, whitlockite, iron, nickel-iron and troilite that project into vug open spaces of lunar breccias and interpreted them to be vapor phase crystallization products. They considered the same argument for vapor phase used by Skinner and Winchell (1972) to be applicable to lunar breccias. That is, if vesicles or cavities were closed, it was not possible for a melt to drain away. Therefore, the vesicles were vapor formed, and projecting crystals are vapor deposited. Possible vapor components include oxides, halides, sulfides, alkali metals and iron. They interpreted these as formed by

the deposition from a hot vapor phase associated with the thermal metamorphism and subsequent cooling of the Fra Mauro Formation. The Fra Mauro Formation is interpreted to be the ejecta blanket emplaced by the Imbrium impact event, and contains a variety of petrologic rock types texturally similar in process of formation to terrestrial pyroclastic ash flows (Warner, 1972; King et al., 1972).

More recent work on vapor-derived crystals in lunar breccias is reported by Clanton et al. (1973) who discuss iron crystals in lunar breccias, Carter (1973) who raises the possibility of VLS (Vapor-Liquid-Solid) type of whisker structures in lunar breccia 15015,36, and Carter et al. (1975) on the morphology and chemistry of chalcopyrite, chromite, copper, iron-nickel, pentlandite and troilite in Apollo 17 breccias.

Criteria for Identification of Vapor-Derived Crystals

In this study the following guidelines were used to distinguish vapor-grown crystals from melt-derived crystals. Growth steps on crystals are indicative of crystallization from low supersaturations, which represents the vapor or solution phase (Sunagawa, 1967). Crystallization from a melt phase indicates high supersaturations by comparison. Lack of glassy or amorphous coatings on euhedral crystals, especially doubly-terminated crystals, in cavities is indicative of a vapor phase origin as opposed to a melt origin (McKay et al., 1972). The presence of vugs and vesicles, which are themselves products of volatilization, is indicative of the formation of a vapor phase and the containment of a vapor phase.

In addition to crystal surface morphology, crystal associations within cavities may be indicative of formation from a vapor phase. Crystals which are flush with the vug wall are interpreted as being crystallized from a melt phase, but crystals that project into the vug interior, especially from a crystalline substrate, are interpreted as being crystallized from the vapor phase (McKay et al., 1972). Crystals in vug interiors which have a substantially different orientation from the crystals composing the vug walls are considered to have a different origin from the vug wall crystals, and this different origin is interpreted to be from the vapor phase (this work). Finally, crystals which appear to coarsen towards the vug interior are interpreted to have crystallized at least in part, from the vapor phase contained in the vug.

Vapor Phase in Terrestrial Pyroclastic Ash Flows

Impact ejecta blankets are considered to simulate terrestrial pyroclastic ash flows, both in emplacement processes and cooling histories (McKay et al., 1972; Anderson et al., 1972).

Briefly, ash flows are a turbulent mixture of gas and pyroclastic material at very high temperatures which have been explosively ejected from a volcanic vent and travel along the ground surface by the process of fluidization - solids suspended in a gas. The deposit that results from this eruption essentially is unsorted, nonbedded, tens of feet thick, and is called an ash flow tuff. If the temperature of emplacement is high enough for welding to occur, at least four distinct zones may be formed. Zones of no welding usually are found on the top and

the bottom of the flow. These zones will contain some incipiently welded tuff (a sticking together of glassy fragments at their points of contact). Such zones are important because they show the original character of the pyroclastic material. Similarly, the unwelded zone in an ejecta blanket would reflect the nature of the soil and bedrock, albeit comminuted in some measure, of the impact "surface" (sampling to whatever depth the impact penetrated). A zone of partial welding beneath the zones of no welding contains incipient welding and welding in which nearly all pore space is gone. This is the most diverse zone. A zone of dense welding produces a glass or vitrophyre in which there usually is no pore space, except that of a vesicular nature resulting from trapped gas.

Crystallization of the glass may occur during the cooling of the ash flow (ejecta blanket), and devitrification and vapor phase crystallization are the most common mechanisms. Devitrification occurs in the glass phase, and vapor phase crystallization involves growth of crystals into pore space by the movement of vapors and transfer of material. Without pore space this cannot occur and therefore, in a densely welded tuff, or in the zone of dense welding where there has not been extensive gas trapped, devitrification is the dominant process of crystallization. The crystallized part of the zone of dense welding is referred to as the devitrified zone. A crystalline porous zone containing crystal growths in pore spaces is the vapor phase zone.

An ash flow containing hot gas or emplaced at temperatures high enough to crystallize on cooling should give off gas at its surface,

thereby altering the surficial and upper parts of the deposit. Smith (1960), Scott (1966) and Sheridan (1970) characterize ash flows and their deposits.

There is one major difference that prevents the terrestrial ash flow deposits from being nearly perfect analogs for both lunar and meteorite impact breccias: water plays an important role in transport of chemical species in terrestrial examples, whereas lunar and meteoritic breccias were formed in essentially anhydrous systems. Hence, other volatiles were the transport media in the extraterrestrial cases studied to date.

Vapor Phase in Meteorites

The porosity of meteorites, and ordinary chondrites in particular, has been noted by several workers (Alexeyeva, 1958; Engelhardt, 1963), but not studied in any detail. Stacey et al. (1961) found a negative correlation between porosity and magnetic properties suggesting that porosity was associated with the original aggregation of the chondrites. The porosity generally decreases from low petrologic types (3, 4) to high petrologic types (5, 6). Increasing degrees of shock (short of shock melting) will have the effect of lowering porosity by compaction, regardless of petrologic type. Weathering of many chondrite finds has increased porosity because of the removal of iron by leaching. Compaction from "mild" shock collision events and weathering superimpose porosity trends without any relationship to petrologic type. In addition, plucking during the thin sectioning process may occur and has made many workers wary of seriously considering cavities as indigenous to the meteorites.

In spite of all of the above, M. Christophe-Levy (1971) reported the occurrence of drusy crystals in apparently natural voids of chondrites.

The Rose City meteorite is one of the most highly shocked ordinary chondrites, evident even in hand specimen because of its clastic nature and shock-melted veins of silicate and metal. Also apparent in hand specimen are irregular vugs and cavities, formed largely by the vaporization of material from the high temperatures and pressures attained at impact. The clasts as well as the matrix contain large irregular cavities, which is atypical of equilibrated high iron chondrites. This indicates that although these clasts were not assimilated into a melt such that the metal and sulfide separated from the silicate phases, there was melting and even volatilization within the clasts. The possibility also exists that some vapor phases were driven into the clasts from those parts (shock melted veins) which attained higher pressures and temperatures than the clasts.

CHAPTER TWO

PETROGRAPHY OF THE ROSE CITY METEORITE

Clast Lithology

This study centered around the two columns (Figure 2) which sampled most, if not all, of the lithologies present in the Rose City meteorite. The column that was ultimately thin sectioned weighed 2.7 grams and measured 6 x 33 x 3.5 mm. Clast A was the largest clast of the least-shocked lithology. A transmitted light photograph of the thin section made through Clast A is shown in Figure 3. White areas are vugs, light gray areas are silicates, dark gray areas are fine-grained to glassy silicates and black areas are opaque minerals. One preserved chondrule is visible at the upper left edge of the thin section. The silicate crystals are highly fractured and, in places, melted along these fractures. The opaque phases show a moderate amount of coalescing into irregular and elongate patches. Branching black veins of melted opaques and silicates extend from the top center edge of the thin section.

The principal minerals are olivine, pyroxene and low-nickel iron (Kamacite, 4-7% Ni). Troilite and feldspar are present, with minor amounts of accessory minerals including, chromite, ilmenite, apatite and whitlockite. The olivine and pyroxene, where preserved, are unzoned and of uniform composition (Fa_{20}) as determined by multiple spot microprobe analyses on clear fragments performed by this investigator. This investigator also found $FeSiO_3$ to be in the 15 - 16 mole per cent range in those matrix crystals large enough and well-preserved-enough for

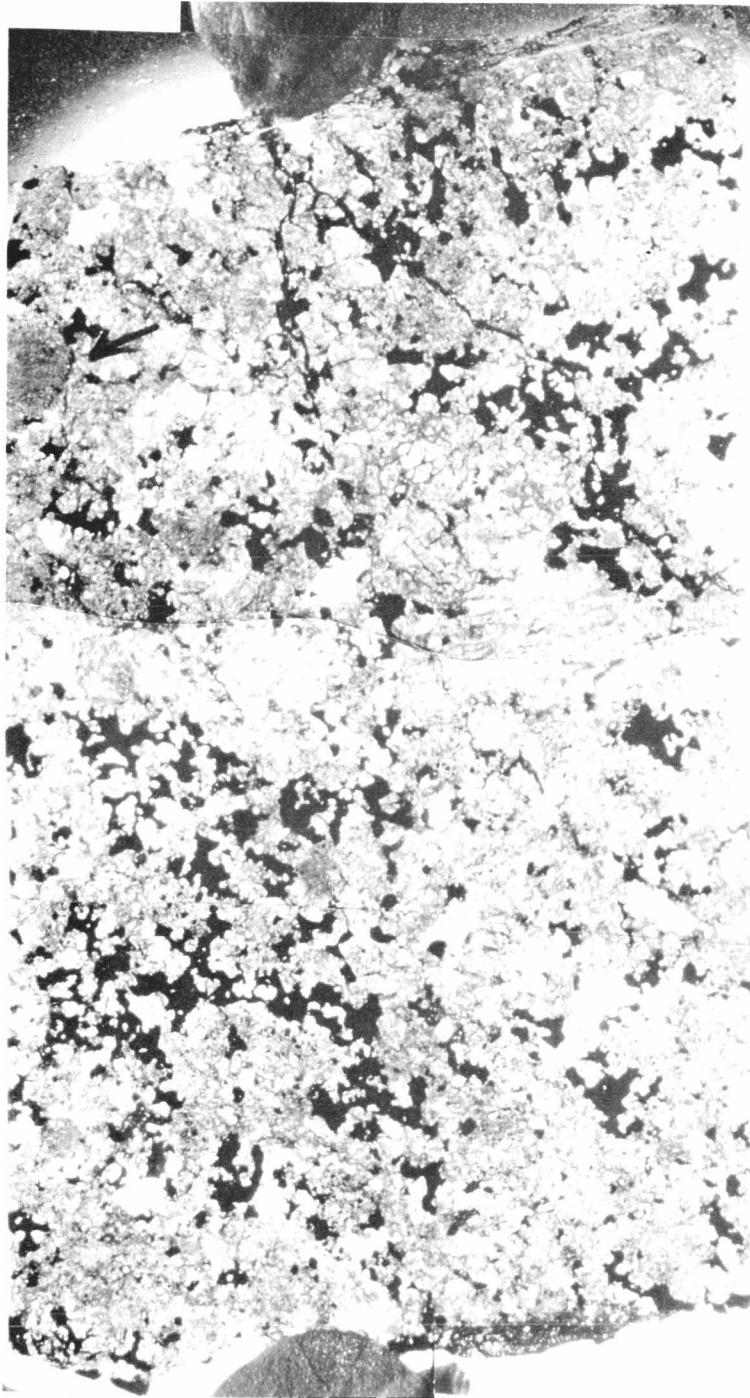


FIGURE 3: Transmitted light photograph of clast A lithology. Width (short dimension) across section is 5.6 mm.

microprobe analyses. Table 7A and 7B present representative olivine and pyroxene analyses of these silicates.

X-ray work by Mason and Wiik showed both an ortho- and clinobronzite to be present, with the latter being the dominant phase. This is contrary evidence to the Rose City meteorite originally being an equilibrated chondrite (Van Schmus and Wood, 1967). Because previously-cited parameters indicate an equilibrated preshocked meteorite, it is the shock metamorphism that probably is the source of the high temperature, disequilibrium clinopyroxenes, not the original lithology.

The plagioclase which occurred in interstitial arrangement to the olivines and pyroxenes were too small (submicron) for probe analyses. They tend to be radiating blades, and have a mean refractive index of 1.54 corresponding to a composition of An_{15} (Mason and Wiik, 1966).

Figure 4 illustrates the form of the opaque minerals in more detail. The highly interstitial nature of the metal and sulfide is evident by the very rounded forms. The fact that the metal and sulfide has actually been molten is evidenced by the spheres, slightly above center. The sphere on the left has a "quarter-moon" of sulfide, indicating the immiscibility of the metal and sulfide.

Figure 5 shows the occurrence of sulfide and metal grains in cavities in the clast lithology. The opaques have rounded and irregular boundaries where in contact with the matrix silicates, but exhibit angular or polygonal forms where they extend into open spaces. This is considered due to (1) their ability to crystallize in their normal habits where free to do so, and (2) vapor phase deposition (layer-by-layer deposition in planes). There is a general tendency for the

TABLE 7A: Representative microprobe analyses of Rose City meteorite clast silicates

	Olivine in Matrix	Olivine in Vug	Pyroxene in Matrix	Pyroxene in Vug
SiO ₂	40.066	39.085	57.832	57.979
Al ₂ O ₃	0.000	0.000	0.101	0.189
Cr ₂ O ₃	0.040	0.057	0.103	0.124
FeO	17.312	19.025	10.827	10.922
MgO	42.343	40.629	30.668	30.975
CaO	0.066	0.115	0.884	0.829
TOTAL	99.828	98.909	100.406	101.018

TABLE 7B: Representative microprobe analyses of Rose City matrix silicates

	Olivine Mineral Clast	Recrystallized Olivine Clast	Olivine in Chondrule
SiO ₂	39.070	39.089	39.106
Al ₂ O ₃	0.029	0.006	0.000
Cr ₂ O ₃	0.009	0.036	0.046
FeO	17.387	16.957	17.389
MgO	43.116	42.832	43.055
CaO	0.022	0.043	0.053
TOTAL	99.629	98.964	99.648

	Pyroxene Clasts in Matrix			Pyroxene in Chondrules
FeO	11.222	9.266	4.518	10.493
CaO	0.106	4.386	19.626	0.807
MgO	29.059	24.725	17.487	30.600
TOTAL	40.387	38.377	41.631	41.900

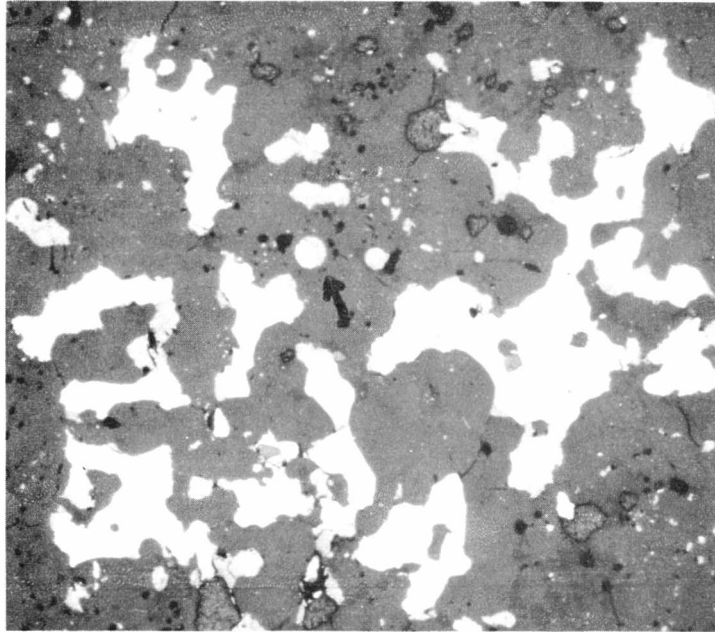


FIGURE 4: Metal (white), sulfide (light gray), silicate (dark-gray). Sphere in center of photograph is 6 μm in diameter.

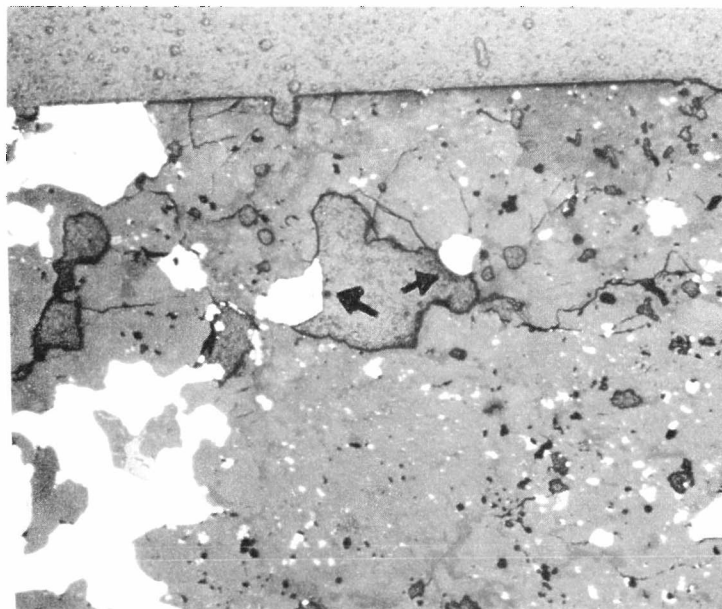


FIGURE 5: Large subhedral (white) crystal (left side of yug) is troilite, round-appearing grain (right side) is iron. Larger crystal is 14 μm across.

sulfide grains to have more pronounced crystal faces and the metals grains to be more subdued, within cavities where each was free to grow. This could be a function of the different abilities or rates at which the troilite versus metal would crystallize from a melt or vapor phase, or it could reflect the different susceptibilities of the sulfide versus the metal to alteration. This photograph also illustrates the heterogeneity of the opaque distribution on a small scale (tens of micrometers) within the clast lithology.

Figure 6A is a transmitted light photograph of the branching dark gray to black glassy veins. In Figure 6B, reflected light, it is seen that tiny droplets of metal and sulfide are concentrated in these shock-melted veins relative to the surrounding gray silicate areas. Dark gray patches in the silicate areas of Figure 6B indicate silicate melting also, obviously not always associated with concentrations of opaques.

Near the chondrule in Figure 3 is a vug with silicate crystals lining part of the vug wall, Figure 7. Several small silicate crystals, on the order of 5 microns in diameter, (bronzite crystals by electron microprobe analysis, see Table 6B) are attached to a portion of the vug wall. The wall itself is a preserved, if somewhat fractured, bronzite crystal. The small crystals apparently have not crystallized from a glass melt, nor is there evidence of any glass around these crystals (see arrows). The opposite wall of the vug is a sulfide extension of a low-nickel iron (lighter opaque) grain in the matrix. The metal and sulfide show an immiscible relationship based on their rounded boundary.

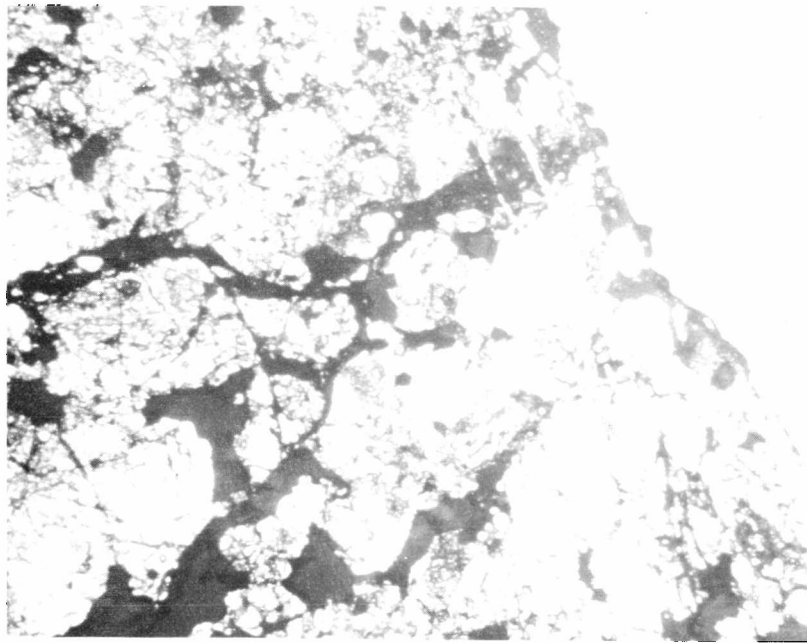


FIGURE 6A: Black shock veins (transmitted light). 175 μm across field of view.

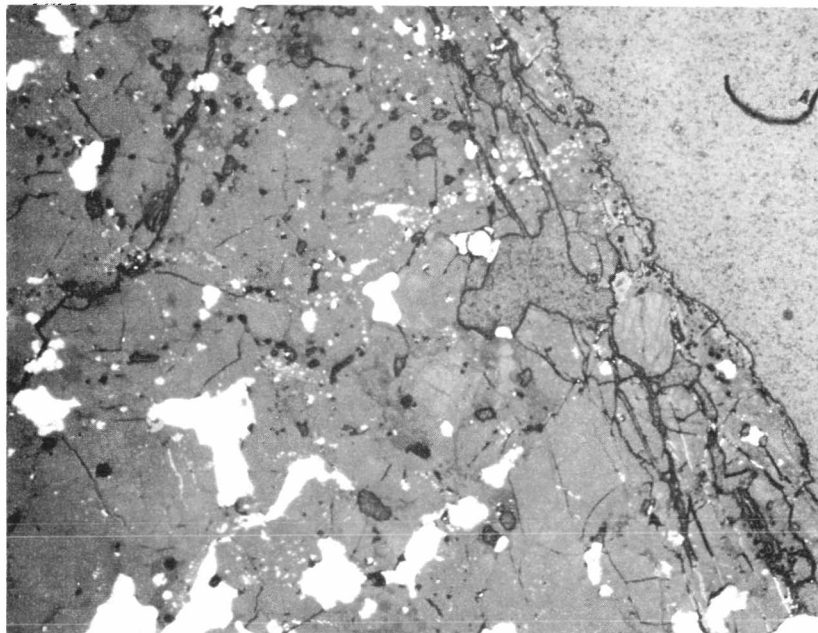


FIGURE 6B: Reflected light, same area. Note concentration of metal and sulfide spheres in the shock veins.



FIGURE 7: Width of vug is $13.5\ \mu\text{m}$. Note micron-sized crystals on vug wall which is a coarse-grained matrix silicate. Transmitted light.

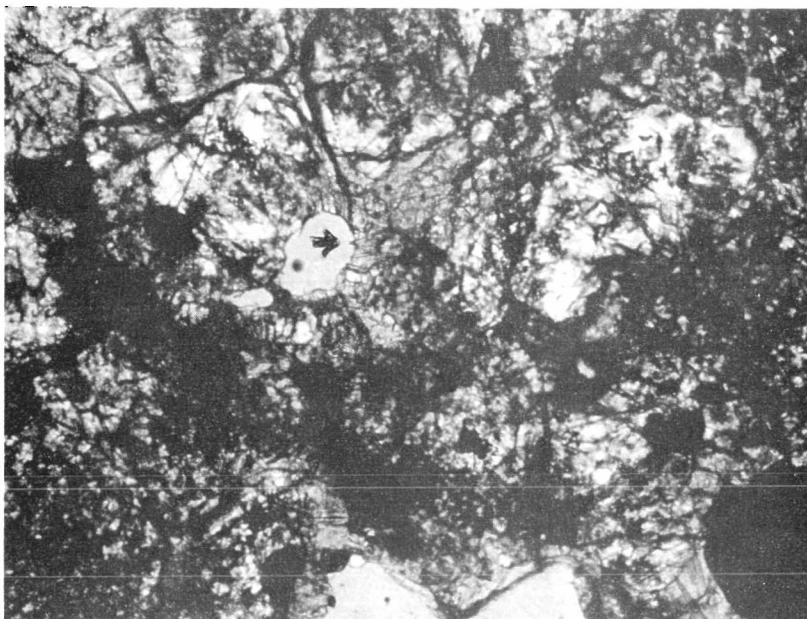


FIGURE 8: Glass-lined vesicle, $5\ \mu\text{m}$ long dimension, with submicron silicate crystals projecting from glass into vesicle interior. Transmitted light.

Figure 8 shows a glass-lined vesicle to the left of center. This is noteworthy because tiny, submicron crystals project from the glass into the vug interior. Not all crystals projecting into cavities are interpreted as vapor-deposited, even though the cavity or vesicle indicates a vapor phase. In this example the dominant process of crystallization is from a melt phase.

Figure 9 is a large irregular vug which is lined, in part, by equant, high magnesium olivine crystals of Fa_{22} (microprobe analyses performed by this investigator). The largest, round-appearing crystal is about 4 microns in diameter. These small sizes are close to the limits of resolution of the electron microprobe, but consistent analyses indicated these are olivines, slightly enriched in iron relative to matrix olivines which are Fa_{20} (see Table 6A). Combined with the SEM part of this study, these olivines are interpreted as vapor condensed by this investigator. The upper crystal appears to be doubly terminated (see arrow). The rounder crystals could have condensed as silicate droplets that crystallized upon cooling. According to H. S. Yoder (pers. communication, 1974), high Mg-olivines cannot be quenched to a glass.

Figure 10 is a transmitted light photograph of an unusual shaped calcium phosphate occurrence of whitlockite with about 2% Na and no F or Cl. The irregular shape does not give the appearance of being a vapor deposit. The opposite wall of this cavity is a very fine-grained (sub-micron) gray material, glassy in part. Probe analyses indicate this glassy area is composed of Na, K, Al (minor constituents) and Ca, P and



FIGURE 9: Olivine crystals (2-3 μm in diameter) lining irregular vug 40 μm in length. Note doubly-terminated crystal at top of vug, next to round (black) opaque.



FIGURE 10: Calcium phosphate mineral projecting into cavity is about 13 μm in diameter.

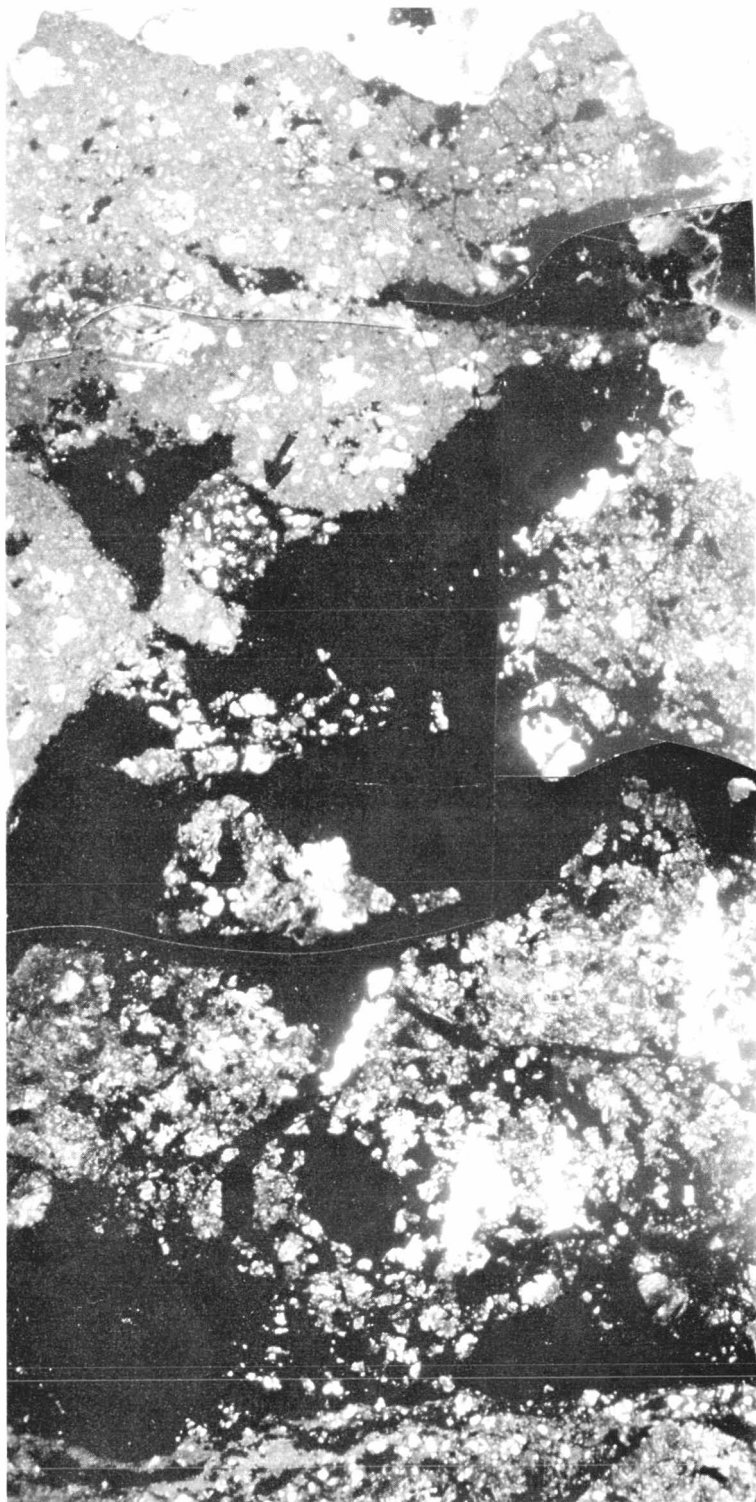
Si (major constituents). Both EDX and microprobe analyses indicated the presence of a new phase composed of Si, Ca and P. Quantitative analyses were not performed on this phase.

Matrix Lithology

The mineralogy is essentially the same as for the clast lithology, but the textural associations indicate the effects of a very high level of shock metamorphism. Figures 11A, B and C illustrate the range in matrix lithology, with Figures 11A and C being the top and bottom halves of the matrix section, respectively, and Figure 11B being a low magnification photograph of the total section through the matrix. The heterogeneous occurrence of metal in the Rose City meteorite is well-illustrated by these photographs.

The top part of Figure 11A (gray areas) illustrates the shock-melted, recrystallized, metal-depleted, silicate matrix lithology. Note the numerous, unassimilated mineral fragments (white). On a finer scale, not seen at this low magnification, there are numerous (~30%) small vesicles on the order of 15 - 20 μm in diameter. Also in Figure 11A are the bands of metal-sulfide (black) and large, irregular vugs and cavities (very bright white areas). The interbanding of the silicate/metal veins indicate movement in the molten state was required to go from the silicate/metal relationship in the clasts to this. Assuming this material was similar to Clast A lithology before the impact event, this structure is interpreted as resulting from the melting of some clast material with the silicate and metal-sulfide forming an immiscible liquid which segregated and solidified in this form. In the upper,

A x 18



B x 6

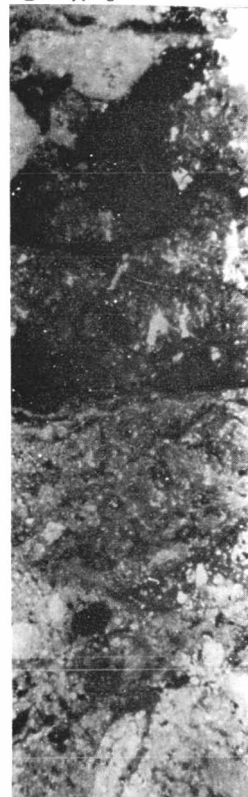


FIGURE 11A, B: Large photograph is top half of matrix lithology, entire section through matrix is shown in the smaller photograph. Transmitted light. Width of both sections are 5.6 mm.

C x 18

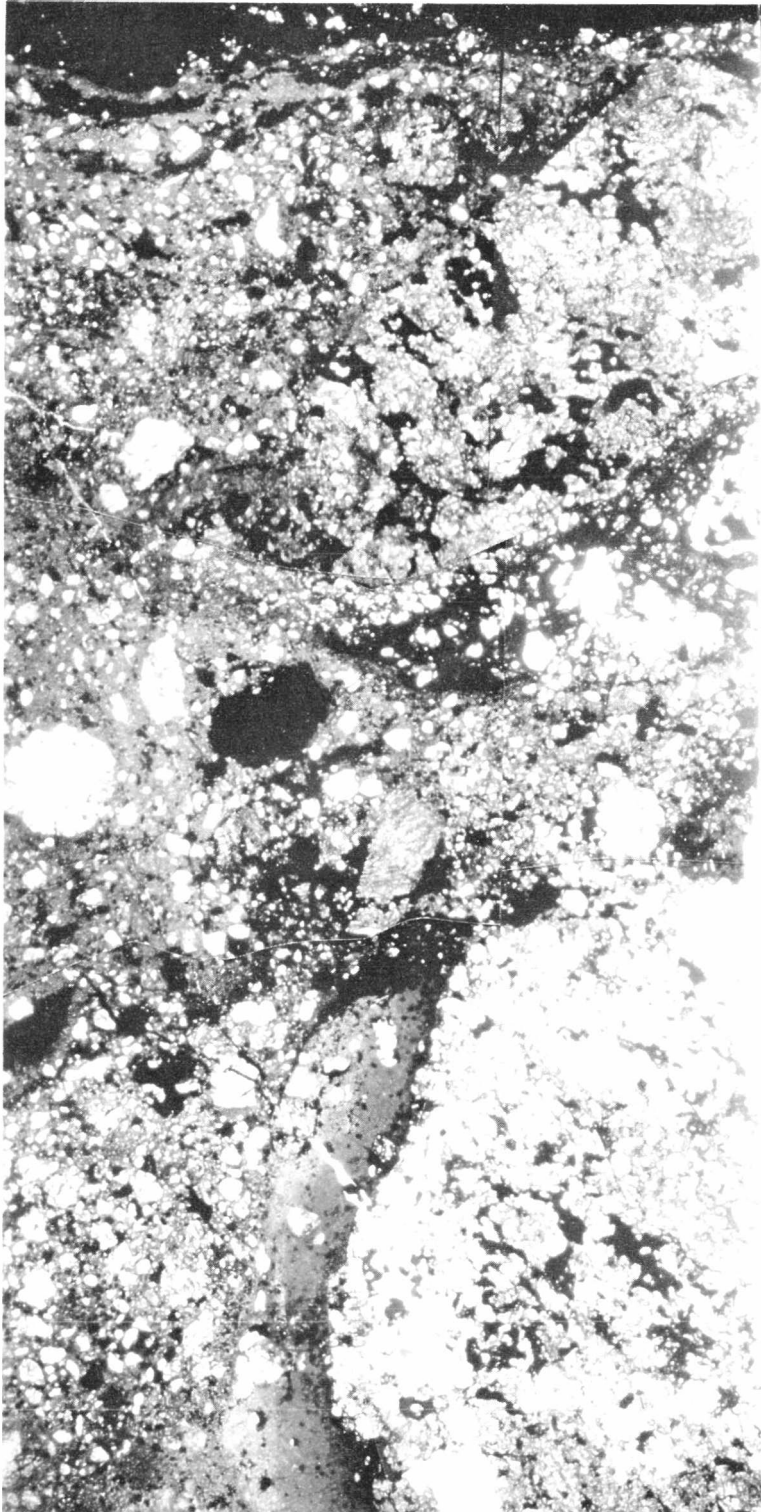


FIGURE 11C: Lower portion of matrix lithology. Transmitted light. Width of thin section is 5.6 μm .

middle-left side of the thin section (Figure 11A), there is an apparently newly formed chondrule, rimmed by opaques, with a porphyritic igneous texture of coarse olivine and pyroxene crystals in a glassy to microcrystalline matrix. This is very similar to the dark-zoned chondrules described by Van Schmus (1969) and interpreted by Dodd and Van Schmus (1971) to be produced by shock. The dark-zoned chondrule in this thin section appears to be closely associated with the shock-melted matrix lithology: the chondrule occurs between the metal-sulfide veins and the shock-melted silicate veins. It has an accretionary exterior structure. The glass is interpreted as being shock-melted silicates which did not recrystallize, and the "phenocrysts" of pyroxene and olivine in the glass are interpreted as being preserved mineral clasts.

The lower half of the thin section is illustrated in Figure 11C. Several olivine chondrules (white) have been preserved on the basis of their coarse grain size. Clast lithology has been preserved, upper-right, bottom-right, but is not rimmed by metal. A glassy vein extends about a third of the way up from the bottom of the thin section. Even in the most highly shock-melted areas, there are numerous mineral clasts preserved.

Figure 12A is a reflected light photograph of the metal-sulfide-rich area, showing the globular texture of the metal in the sulfide. A vug in the center of the photograph extends between the right and left opaque mineral areas. On the upper wall of the vug is a small crystal of low-nickel iron. It is totally on the edge of the silicates forming the vug wall. Figure 12B is a transmitted light photograph of this vug.

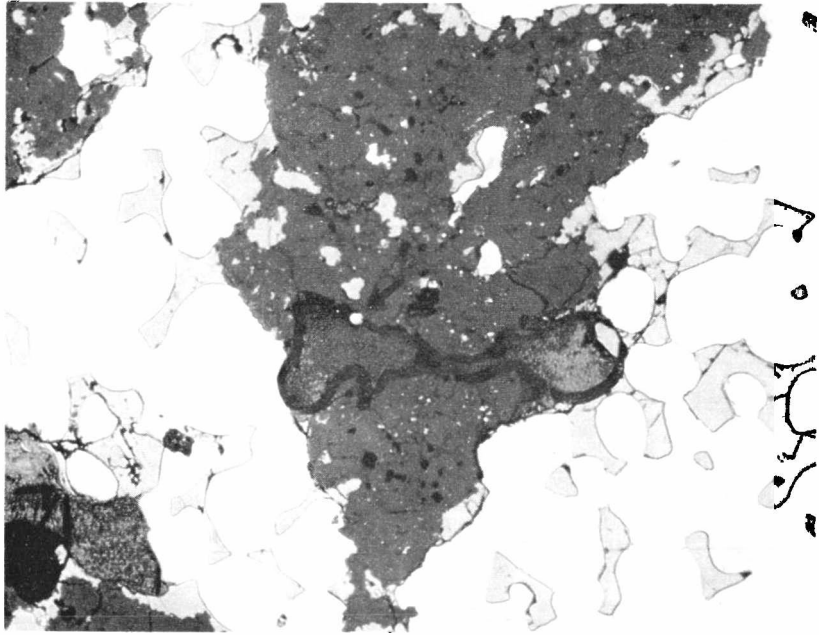


FIGURE 12A: Metal (white) sulfide (light gray) area within Rose City matrix. Irregular vug between two metal areas is 70 μm long. Note metal grain on vug wall. Reflected light.



FIGURE 12B: Transmitted light of same vug. Iron sphere on cavity wall is 4 μm in diameter.

The metal grain appears embedded in the silicates in this photo because the wall of the vug apparently curves under the iron grain with depth in the thin section. Other lithologies in the matrix include the following: clasts discontinuously surrounded by metal-sulfide (Figure 13); glassy veins depleted in metal except for aligned spheres of metal and sulfide (Figure 14); shock-melted areas without segregation of silicate and metal or recrystallization of silicates (Figures 15A and 15B). The latter area contains large mineral fragments which have not been assimilated, but between these fragments are areas where the metal is finely-dispersed as droplets within a silicate glass (Figure 15A). The lower photograph is in cross-polarized light illustrating the lack of recrystallization in this area. The area above the glassy area is shock-melted, but largely recrystallized by comparison.

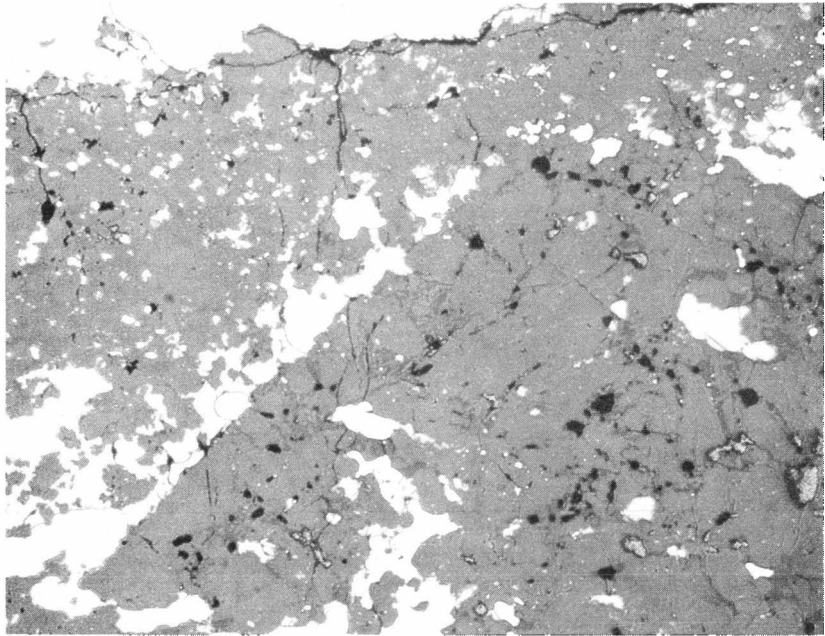


FIGURE 13: Reflected light photo showing metal (white) and sulfide (light gray) outlining partially-melted clast lithology, right side of photo. Field of view, 176 μm across.

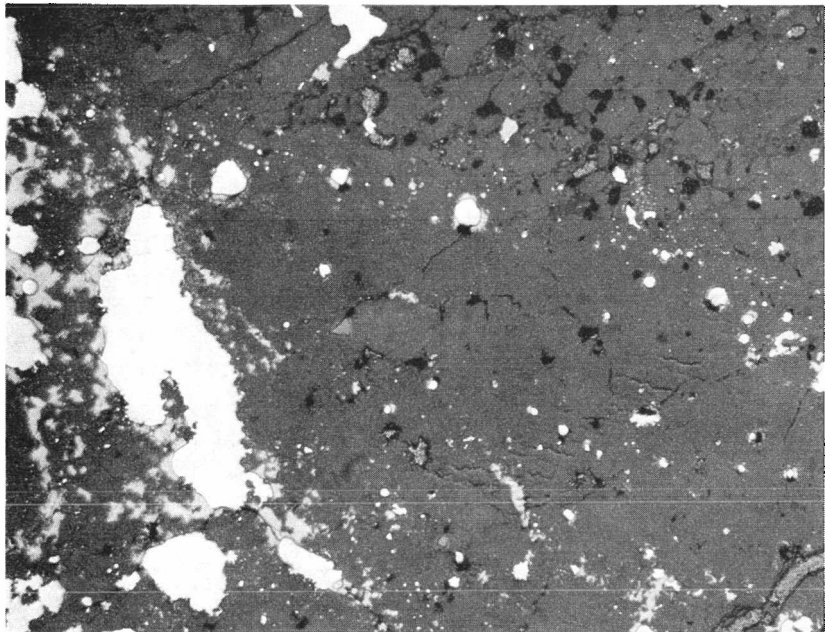


FIGURE 14: Reflected light photograph of portion of matrix glassy vein with streams of metal and sulfide spheres. Field of view is 178 μm across.

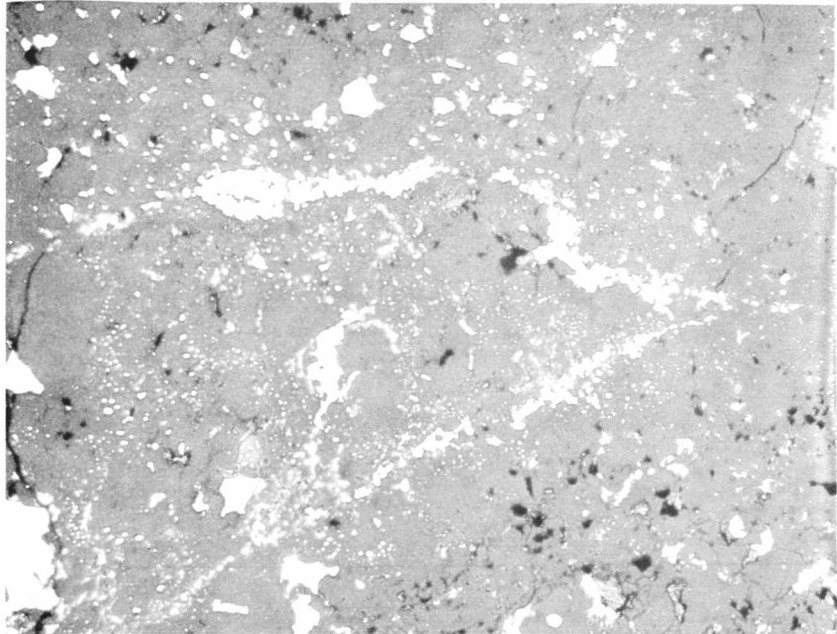


FIGURE 15A: Reflected light photograph of melted silicate area with melted metal outlining it. Field of view is 177 μm .

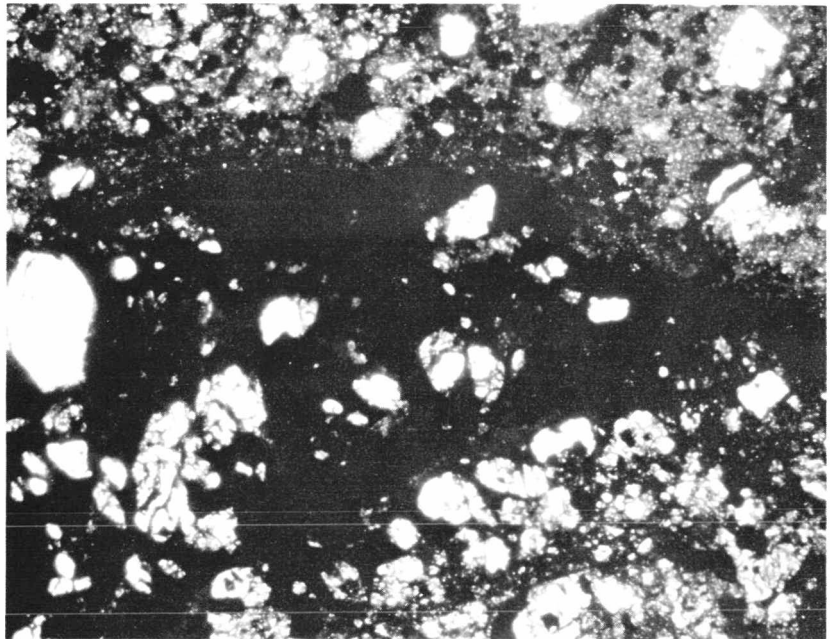


FIGURE 15B: Transmitted light photograph of same area. There are still large clasts, but glass has not recrystallized as it has in the shock-melted area above.

CHAPTER THREE

SCANNING ELECTRON MICROSCOPE STUDY OF THE ROSE CITY METEORITE

Vug Morphology and Vug Mineralogy in Clast Lithology

The clasts in the Rose City meteorite, especially those which are surrounded by metal-sulfide bands, appear to be equilibrated H6 chondrites according to the Van Schmus and Wood classification (1967). These clasts show textural evidence of shock (as do many high iron group chondrites), such as black shock veins, crushed olivine and pyroxene crystals, interstitial melting and discrete metal and sulfide spheres.

The most unusual feature in the clast lithology, if the original pre-impact lithology is considered to be approximately that of an H-6 chondrite, is the great amount of porosity, or vugs. Figure 16A is a low magnification SEM photograph of a typical area of Clast A. The striations are saw marks, most obvious in the metal grains. Vugs range in size from smaller spherical, more vesicle-like vugs (10 - 20 μm diameter) to large irregular-shaped vugs (200 - 300 μm diameter). In the clasts most examples of vapor phase crystallization occur in the larger, more irregular vugs. There is a tendency for non-random distribution of vugs because the larger ones tend to occur in alignments, and the vesicle-like ones tend to form clusters. Some of both types of vugs have glassy linings with what appear to be divitrification crystals of feldspar (acicular crystals) or pyroxene or olivine (equant crystals). Most vugs have microcrystalline walls (submicron-sized grains) and some vugs abut coarse-grained crystals.

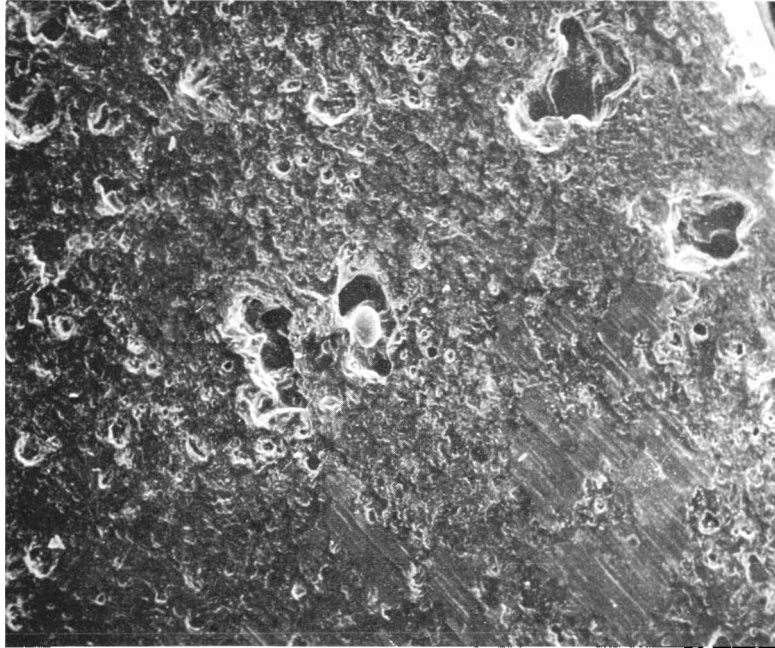


FIGURE 16A: Low magnification SEM photograph of Clast A illustrating large, irregular vugs. Center vug is $220\ \mu\text{m}$ in length, contains troilite crystal, $75\ \mu\text{m}$ long. Note abundance of small ($15 - 20\ \mu\text{m}$) vesicular-type vugs. Saw marks are most obvious on metal grains.

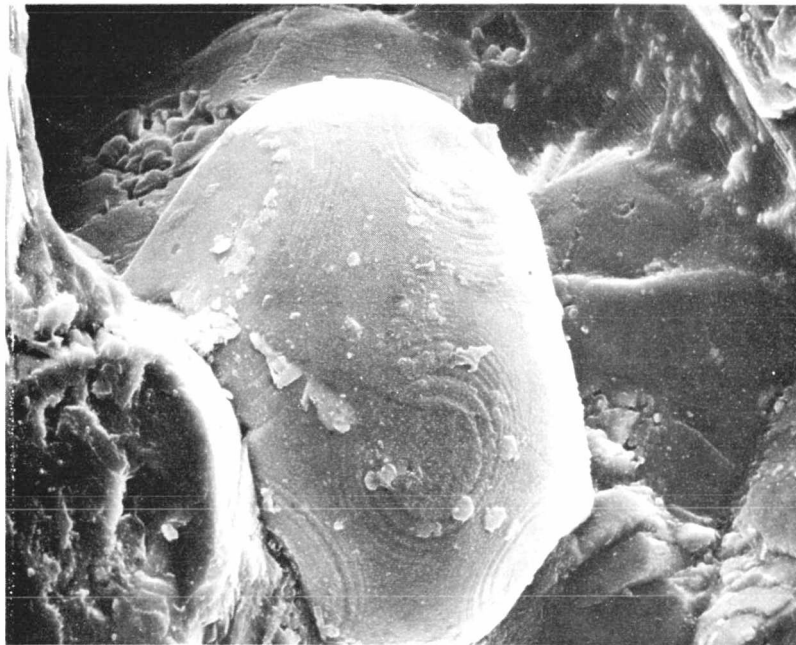


FIGURE 16B: Troilite crystal, $75\ \mu\text{m}$ long, with growth steps on numerous crystal faces. Highly distorted crystal, but first and second order hexagonal prisms and (probably) first and second order dipyrramids are present.

The origins of the vugs are interpreted to be two-fold: (1) the smaller vesicular ones are considered to be formed at the time of the shock metamorphism mainly by melting and volatilization in place; (2) the large, irregular vugs are interpreted to be formed by volatilization of material in place, and in addition, by volatilization of material in the matrix that was then driven into the clasts. The clasts experienced lower overall temperatures and pressures than the shock-melted matrix (as evidenced by their coherent nature).

Figure 16B is a troilite crystal attached to the wall of a large irregular vug (also seen in the center of Figure 16A). The walls have the appearance of being partly devitrified. The troilite crystal itself has a distorted form, with numerous growth steps on the crystal faces present. Crystal faces present are hexagonal prisms and perhaps, first and second order dipramids. Figure 16C is a higher magnification photograph of one set of growth steps. Two other features are apparent: micromounds and skeletal hexagonal crystals. EDX analyses showed no difference between these secondary features and the substrate. One explanation is that one or both are late phase vapor phase deposits onto the troilite crystal. A more likely explanation is that these are weathering products from the addition of terrestrial water. Rose City meteorite shows a moderate amount of weathering in thin section as evidenced by red alteration products around some of the opaque minerals.

Figure 17A is an example of a lunar troilite crystal with growth steps. Figure 17B shows the entire euhedral lunar troilite crystal. In general all lunar crystals have much cleaner, smoother features than any comparable meteoritic example. The basic reason for this difference

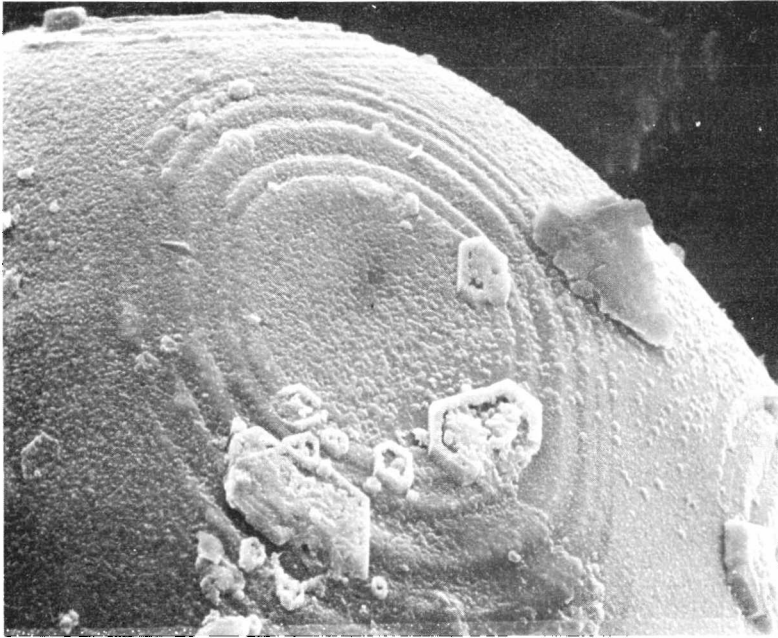


FIGURE 16C: Troilite growth steps with micromounds and hexagonal skeletal crystals. 40 μm across field of view.

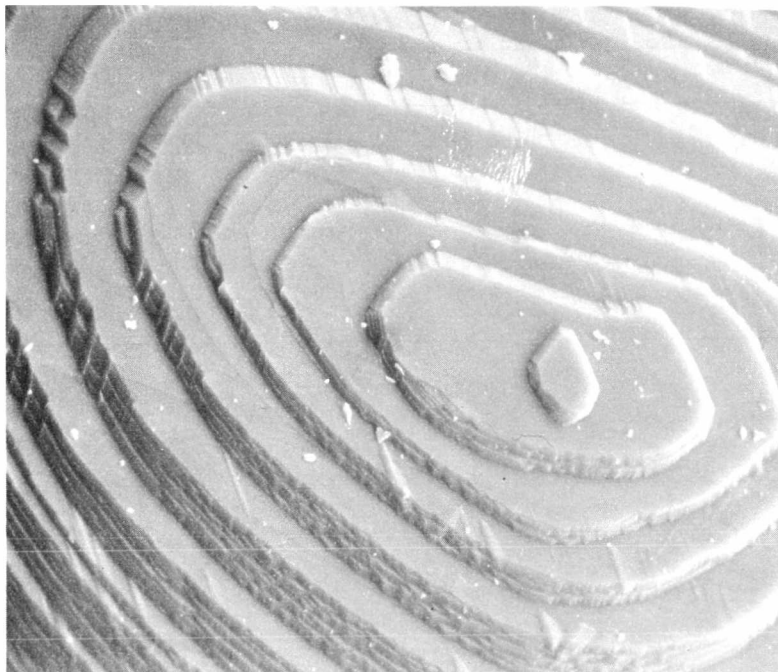


FIGURE 17A: Lunar troilite growth steps. Field of view is 116 μm . Note absence of mounds, crystals, overgrowths of any type.

is interpreted as due to the pristine state in which the lunar samples have been maintained, versus meteorites which spend finite time exposed on the earth's surface. Even meteorites observed to fall undergo vagaries of weathering until collected.

The origin of both the lunar troilite and meteoritic troilite is proposed to be vapor phase, because of the vug association and growth steps (McKay et al., 1972), but another possible mechanism could be that each was an immiscible sulfide liquid droplet in the silicate liquid which found its way to the vug wall interior before solidification, and crystallized there upon cooling.

Iron-nickel crystals have bunched growth steps similar to troilite grains as is seen in Figure 18 where an Fe-Ni crystal apparently is bridging an irregular vug. There is metal at the sawed surface in the lower right hand corner of the photograph and the grain might be attached to metal in the matrix on the unseen side. From what can be observed however, the grain appears to be attached to silicate walls.

Metal and sulfide grains projecting into vugs could have one of two associations: (1) they could be attached to a larger metal or sulfide grain in the silicate matrix (which does not preclude their possessing bunched growth steps on the free-standing faces where they could have been exposed to vapors for deposition); and (2) grains could be attached to the walls of vugs as discrete individuals, formed from (a) the vapor phase trapped in that particular cavity, (b) crystallized from an immiscible droplet of metal or sulfide on the silicate wall; or (c) by a prolonged movement of vapors through interconnected cavities and pore spaces.

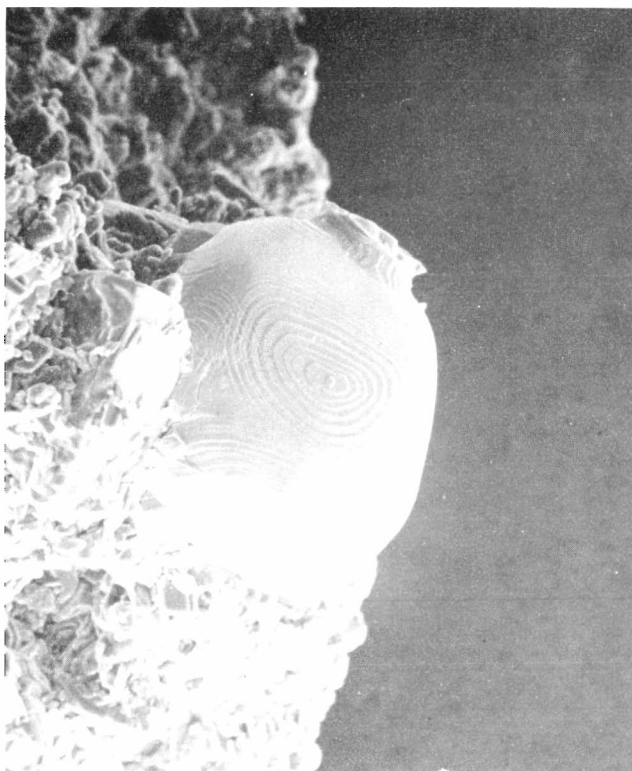


FIGURE 17B: Lunar troilite crystal, 75 μm in length. Very clean surface.

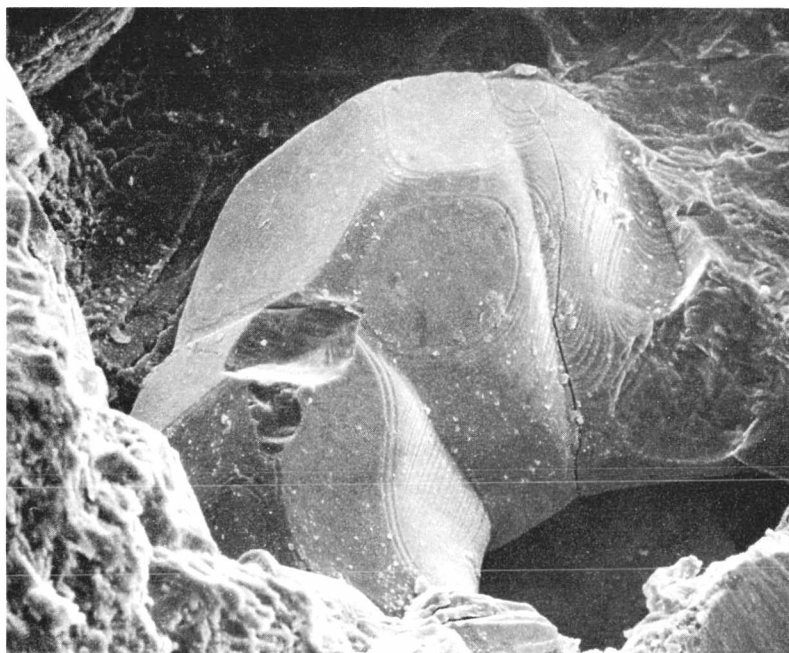


FIGURE 18: Iron crystal, approximately 100 x 108 μm bridging open space in irregular vug.

This particular iron-nickel crystal appears to have been deposited from two sides of the vug interior, joining in the center, similar to cave formations of stalagmites and stalactites which have grown together to form columns. The extension into the center of the vug, and the surface growth steps indicate formation from the vapor phase.

Calcium phosphate minerals occur in both the clast and the matrix lithologies. Figure 19 illustrates an unusual occurrence of probable whitlockite. Both EDX and probe analyses showed about 2% sodium, with essentially no chlorine and perhaps, a trace of fluorine, in addition to calcium and phosphorus. It is definitely not euhedral in form or free-standing. This association of calcium phosphate merges with the silicate matrix wall of the vug and has an interlocking granular texture. This crystal(s) has none of the characteristics that are associated with vapor phase crystallization cited previously. This occurrence might be the result of selective volatilization or leaching, whatever process formed the vug itself, which left the more resistant calcium phosphate mineral in place.

Silicates are a common constituent of both vug types in the clasts. The ellipsoidal vug in Figure 20 contains only silicates: the walls predominantly are crystalline with little, if any, glass present; the large crystals are equant, low silicon relative to iron plus magnesium, and contain no calcium. These crystals, because of the chemistry and form probably are olivines. They are interpreted as being vapor-derived because of their euhedral crystal form, lack of glass association, and large size relative to the substrate crystals.

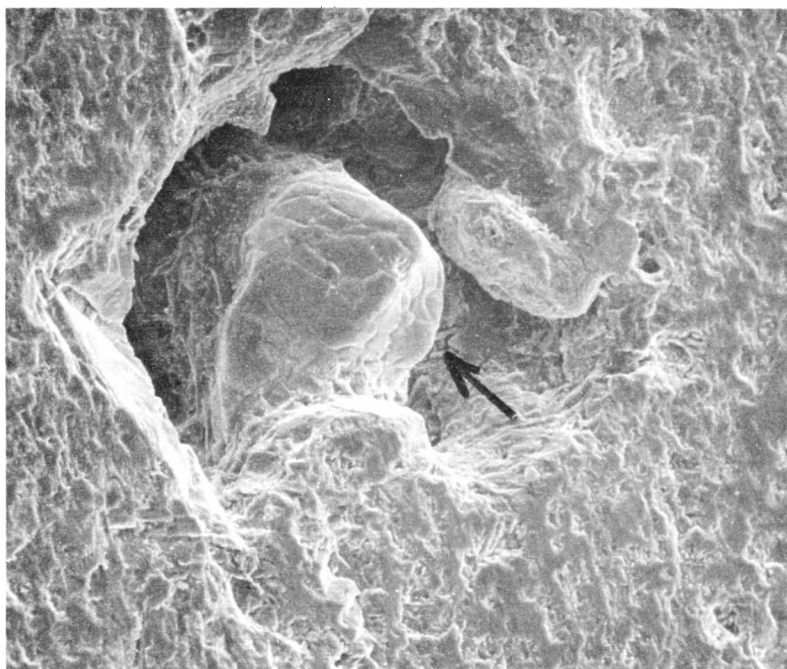


FIGURE 19: Irregular mass in cavity is a calcium phosphate mineral. Diameter of grain(s) is 97 μm . See Figure 10 for thin section photograph of this mineral.

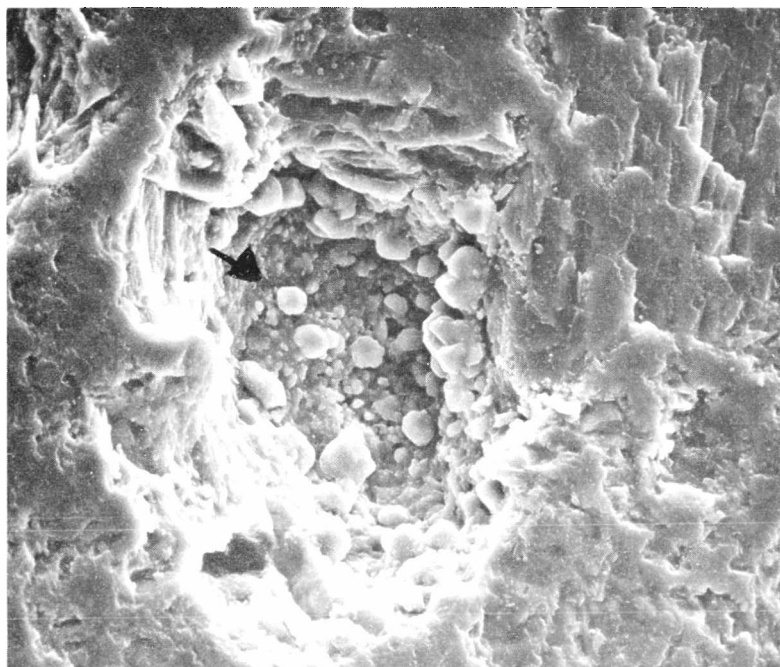


FIGURE 20: Irregular vug, 83 x 116 μm . Porous vug walls of 1 - 2 μm crystals in a glassy or microcrystalline matrix. Larger (7 - 8 μm) iron-magnesium silicate crystals are attached to the vug walls.

The last example of silicate deposits in clast vugs is shown in Figure 21A. The vug walls show range in texture and chemistry. The upper left corner shows a glassy substrate with elongate, needle-like crystals of feldspar, typical of rapid cooling. The central portion of the vug wall is mostly crystalline with the crystals appearing more equant, and typical of pyroxene or olivine. There is an iron-nickel grain on the left side with bunched growth steps which may or may not be attached to a large iron-nickel grain in the matrix. The "coarse" (10 - 12 μm long) silicate crystals in the center are low calcium iron-magnesium silicates. The silicon to iron plus magnesium ratio is much higher than for the olivine crystals, and the presence of calcium indicates these crystals are pyroxenes. Table 7A, B shows the typical microprobe analyses for vug occurrences of olivine and pyroxene vapor-derived crystals. No difference is observed between the vapor-grown pyroxene crystals and the matrix pyroxenes. A slight iron enrichment is apparent in the vapor-derived olivine crystals compared with the matrix olivines. The substrate is predominantly crystalline, superficially porous and somewhat glassy between grains. The substrate chemistry is similar to the coarser crystals containing Fe, Mg, Ca, and Si as major elements, with a minor amount of Al. The coarse crystals have well-formed faces, and do not appear to have any glassy rim or coating as do the substrate crystals (Figure 21B). It is suggested that these coarse crystals are vapor grown. Two other possibilities exist: they could have been formed long after the initial shock melting by recrystallization of material similar to the vug wall substrate during slow cooling from high temperatures; or they could have been formed from a melt which

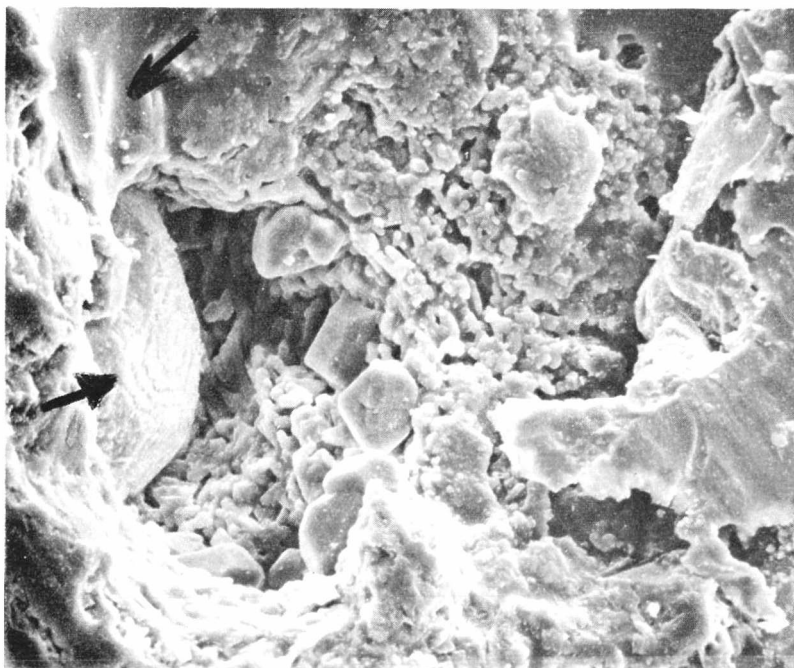


FIGURE 21A: Irregular vug with a range in vug wall texture from glassy (upper left) to crystalline. Vapor deposited crystals include iron crystal (left) with growth steps, and silicate minerals (center). Iron crystal is 45 μm top to bottom for scale.

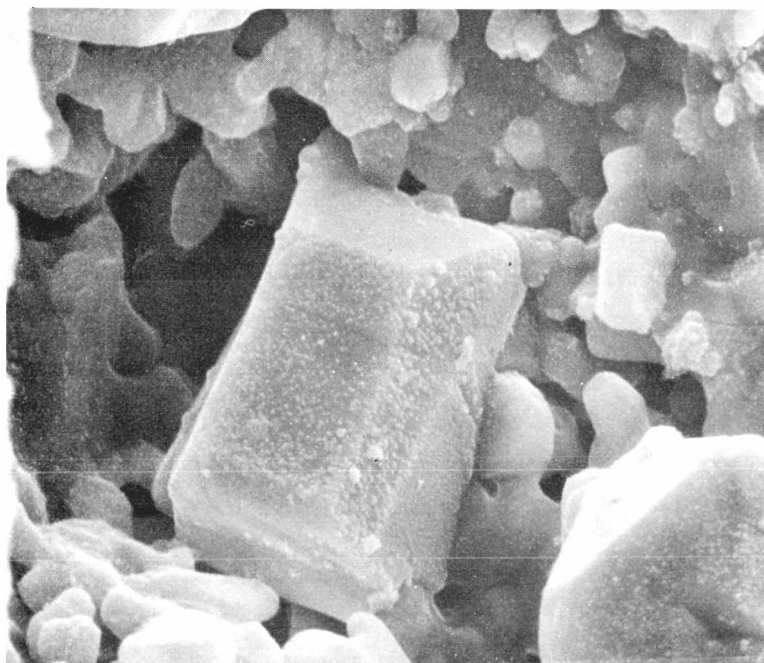


FIGURE 21B: High magnification of silicate crystal, 11 μm long.

subsequently drained away, leaving the cavity behind. The first possibility is unlikely because of the dichotomy between the large crystals and the substrate - if there was significant recrystallization there should be a gradation from fine to coarser grains. The vug wall shows a gradation from glassy to crystalline, but the coarse pyroxene grains do not appear to be an extension of this coarsening, but are separate entities from the wall association. There is nearly an order of magnitude difference between the vug wall grain sizes and the coarse crystal grain sizes.

The second possibility is more likely because of the apparent porosity of the substrate, which may have allowed the liquid to move to another area. However, neither the iron grain nor the silicate grain has any glassy coatings, and there is no evidence of a melt phase which filled this cavity. It is assumed this vug, and others similar to it, were formed by a gas phase and that the most probable origin of the coarse-grained crystals (sulfide, metal, silicate) is from the vapor phase.

In Figure 21A, the metal grain could be totally vapor-deposited, or layers could have been vapor-deposited on a pre-existing metal grain.

Vug Morphology and Vug Mineralogy in Matrix Lithology

The matrix of Rose City is very complex and reflects the heterogeneity of the shock metamorphic process. As Gibbons et al. (1975) have pointed out, "in any shocked rock, including "whole rock" melts, temperatures may vary by hundreds of degrees over distances measured in microns." The matrix of Rose City is a classic example of this heterogeneity:

glass veins with metal and sulfide droplets surround clasts of the original lithology; whole chondrules as well as numerous chondrule and mineral clasts are preserved in areas of extensive (50 - 60%) shock melting; bands of metal-sulfide occur next to metal-depleted silicate areas of a high (35 - 40%) clastic nature. In addition, there is a surprisingly high level of porosity (~30%) in the recrystallized shock-melted, metal-depleted areas. Large cavities are associated with the metal-rich areas, generally at the boundaries between the metal and the silicates. Large, irregular vugs are associated with the clasts where metal segregation is incipient.

The vug and vesicle distributions are considered to be the result of several processes, reflecting the uneven distribution of high temperatures and high pressures attained during shock metamorphism. The view is taken that the clasts which are more or less coherent entities, represent "static" shock metamorphism. That is, there has been fracturing, comminution, vitrification, minor flow with some vesiculation, and some aggregation of metal along grain boundaries as well as some mixing of metal and sulfide phases. The coarser, irregular vugs in these clasts are interpreted as originating in part, in the higher pressure and subsequently high temperature matrix areas where the high pressure literally drove volatilized material into the "cooler" and lower pressure clast areas.

The matrix proper, is considered to represent "dynamic" shock metamorphism because of the evidence for flow and plastic deformation. The matrix possesses characteristics of the higher classes of progressive shock metamorphism such as shock glass (devitrified or recrystallized

in part), flow features (metal bands) and vesicles. The glasses represent a "whole silicate melt" as opposed to a "whole rock" melt because ordinary meteorites contain a very high metal content and the metal forms an immiscible liquid within the silicate melt.

The next series of SEM photographs illustrates the vugs and vug minerals in partially melted clasts in the matrix. These clasts are not bounded by metal, but there is more segregation of metal from silicate than in the clast lithology proper.

Figure 22A illustrates an irregular vug with a nearly pure iron crystal deposited in it. Figure 22B shows the crystal's relationship to the glassy or microcrystalline substrate: the crystal appears somewhat corroded, but there is no evidence of a connecting melt phase between the metal and silicate. The crystal is about 20 microns across, and upon close examination it shows growth steps at intersections of octahedral and dodecahedral forms. Figure 23 illustrates common crystal forms, and some possible combinations.

Metal and sulfide occurrences in vugs are not always discrete crystals as Figure 24, a stereo pair of an iron crystal with a small amount ($\sim 1 - 2\%$) of copper, shows. There appears to be a separation between the metal crystal and the silicate substrate. Growth steps on the two faces exposed appear to be of the cubic form and are evidence of vapor phase deposition.

A troilite crystal appears to have been just exposed by the saw cut in Figure 25A. The cavity itself appears to enlarge on the opposite side of the sulfide crystal. Figure 25B is a higher magnification stereo pair of photographs of the growth steps which occur where there is open

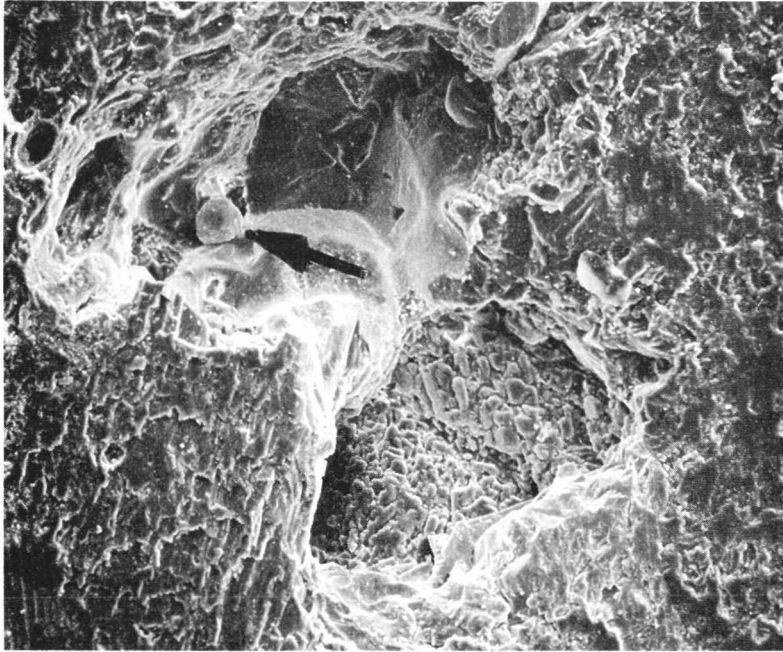


FIGURE 22A: Irregular cavity in non-metal-rimmed clast lithology. Microcrystalline to crystalline vug wall. Note iron crystal on left side of vug. Field of view 418 μm .

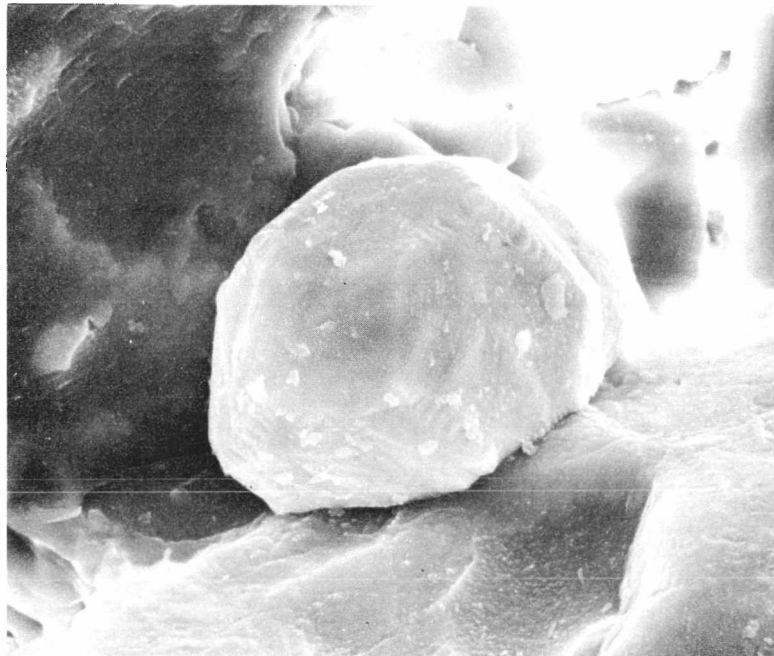


FIGURE 22B: Corroded-appearing iron crystal, 20 x 22 μm in size. Crystal forms present include the cube, tetrahedron, octahedron and dodecahedron.

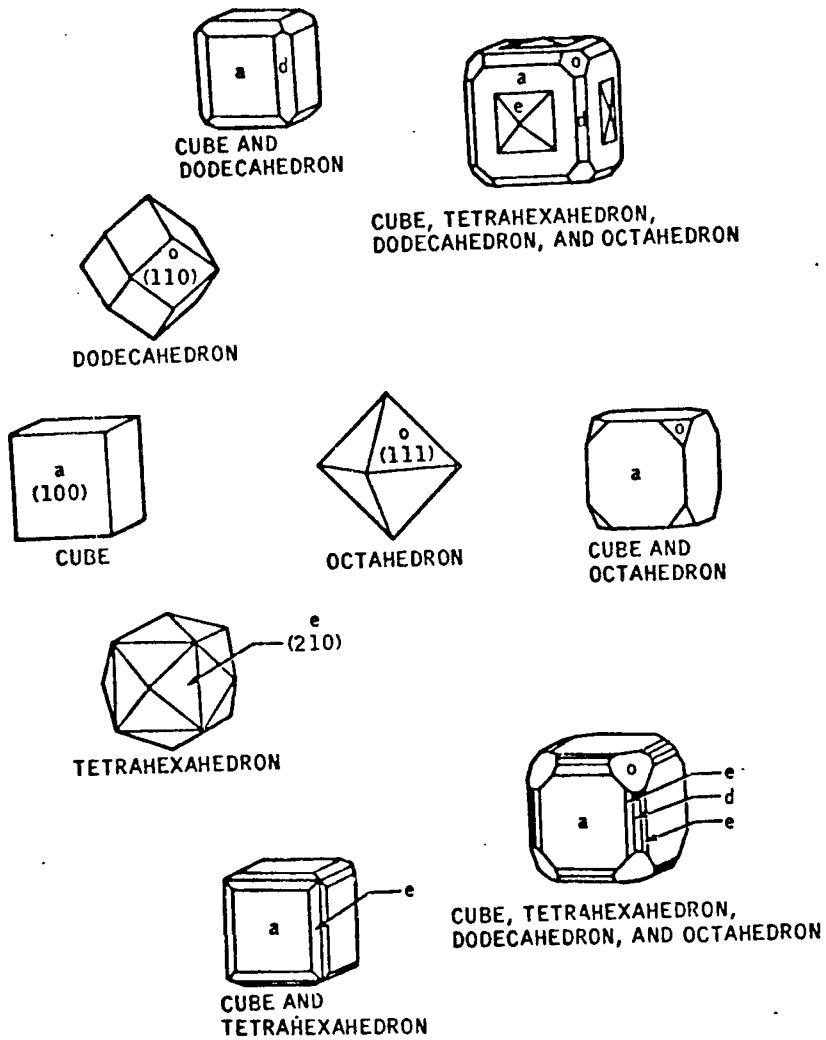


FIGURE 23: Common crystal forms.

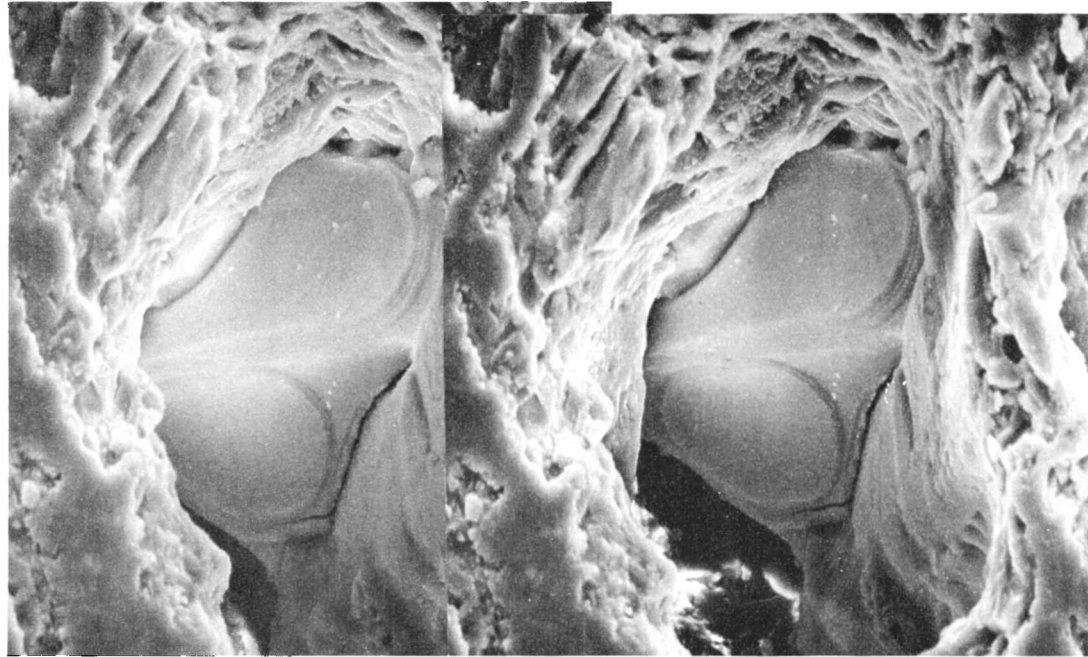


FIGURE 24: Stereo view of iron crystal with growth steps on (probable) cubic faces. Longest dimension of crystal is 28 μm . Small amount ($\sim 1\%$) Cu may be present, EDX analysis.

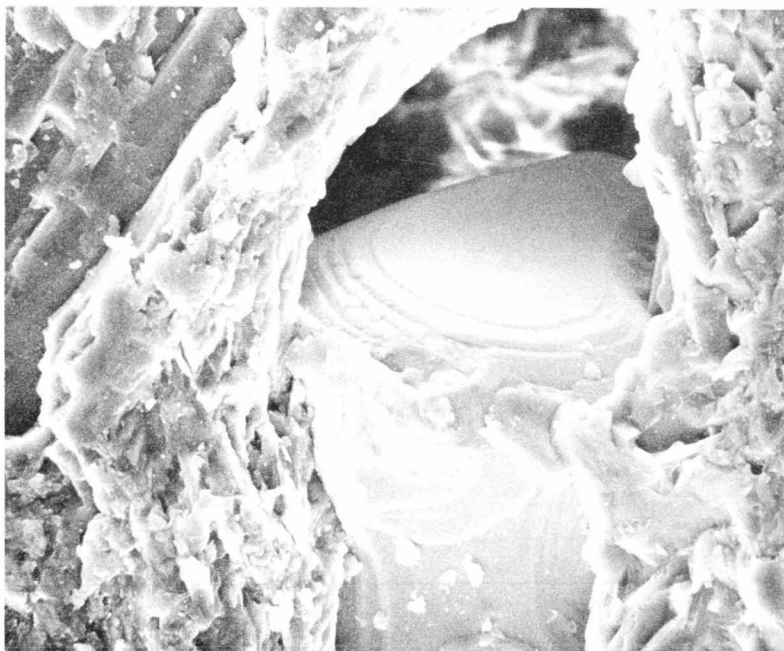


FIGURE 25A: Troilite crystal, barely exposed by sawing, 70 μm across grain.

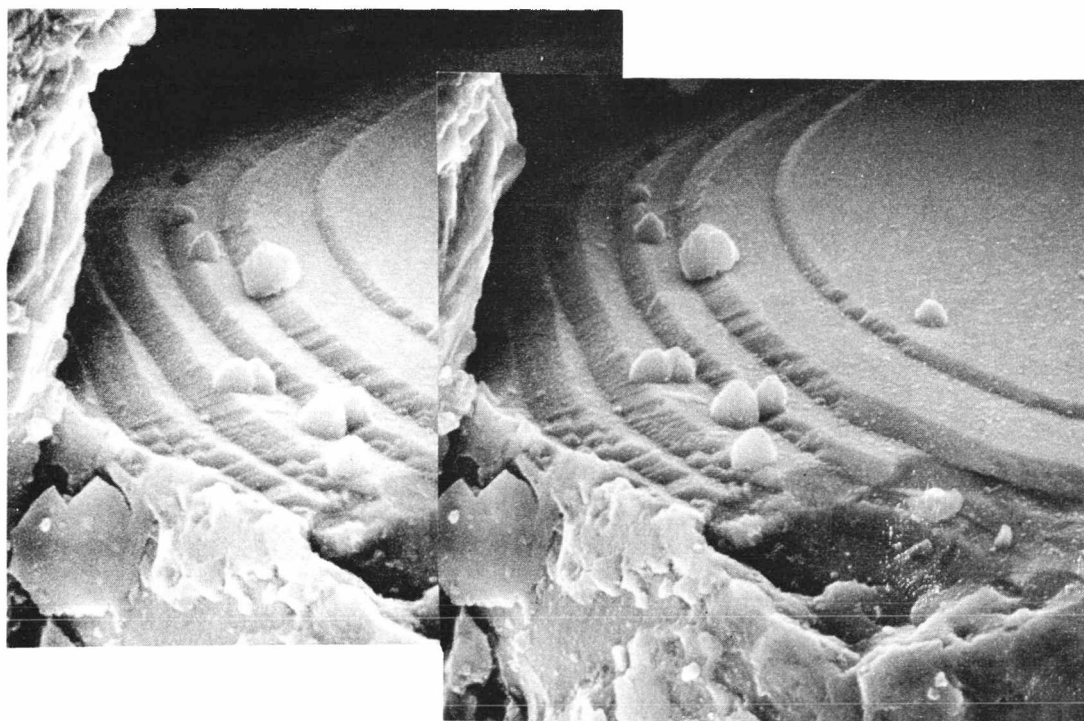


FIGURE 25B: Stereo pair of growth steps on troilite crystal. 27 μm across field of view, right photograph. Note relatively clean surface, similarity to lunar troilite.

space. This is a "clean" troilite crystal with few micromounds on its surface. The growth steps are very similar to the lunar example in Figure 17A and are strong evidence for formation from the vapor phase.

The next series of figures represents an unusual but not uncommon occurrence in the Rose City meteorite. Figure 26A shows two irregular cavities. An iron crystal with a small amount of sulfur appears in the upper cavity. The sulfur could come from a coating of troilite over the iron crystal which also occurs in lunar breccias (McKay et al., 1972). The crystals in the lower vug (Figures 26B, C) appear to be crystallizing from a melt because the crystals are embedded in a glassy interstitial phase. There is a range in size and form from large, irregular crystals, to smaller, well-formed crystals, to skeletal crystals. The crystal chemistry varies with these forms. The largest irregular crystals and the skeletal crystals are composed of calcium, phosphorous and silicon; the smaller, equant crystals, Figure 26C, are composed only of calcium and phosphorous as major elements. This is essentially the same chemistry as the interstitial glass, but the glass contains a small amount of potassium, aluminum, magnesium, iron and a trace of sodium, in addition.

This association is very unusual because there appears to be a phospho-silicate of unknown form lining the wall of this vug. The irregular shapes of the larger crystals may represent a distorted crystal form which is trying to accommodate phosphorous in a silicate structure (or perhaps vice versa). These crystals appear to come predominantly from a melt phase although some interaction from a vapor phase is not improbable. The equant crystals are probably apatite or

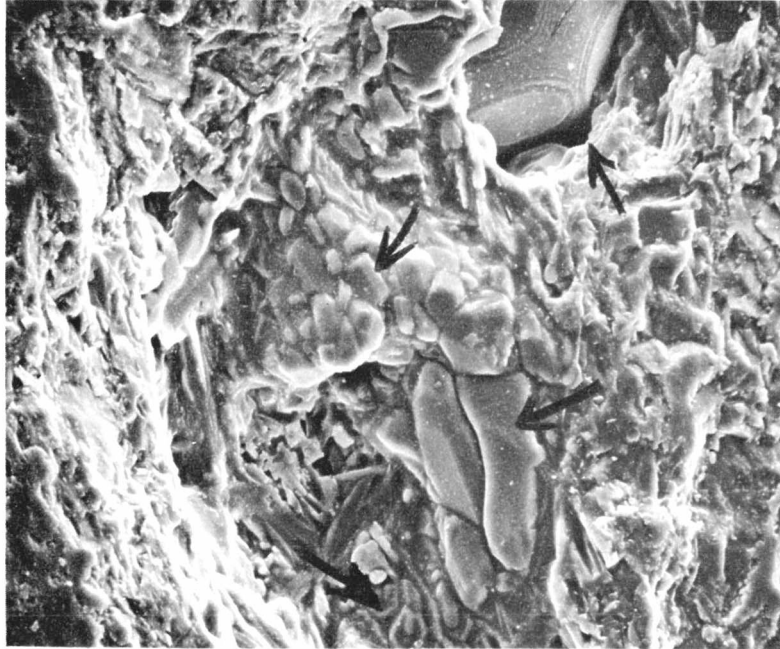


FIGURE 26A: The two vugs in this photograph contain different mineralogies. Upper, right-hand vug contains iron crystal with (possibly) a sulfide coating and a small amount of copper present (EDX analysis). The predominant minerals in the lower, larger cavity are forms of calcium phosphate. Field of view, 140 μm .

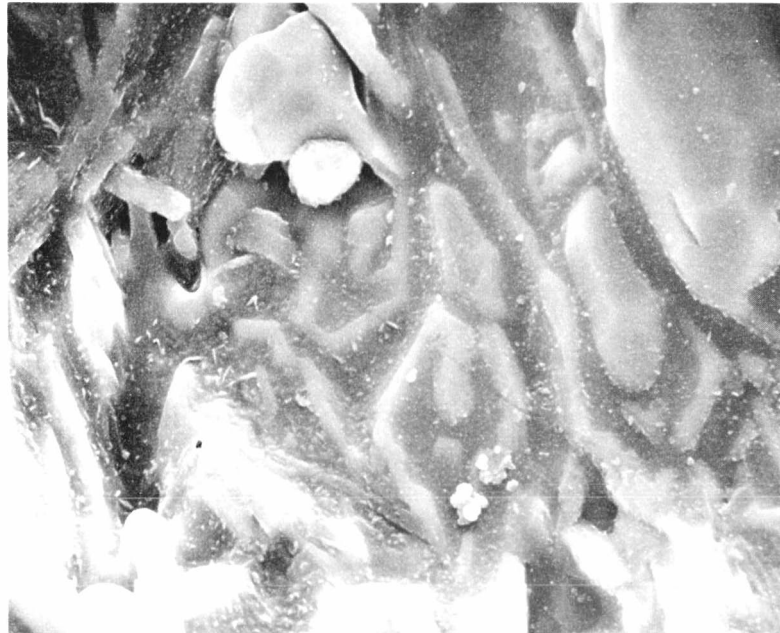


FIGURE 26B: The large crystals and the skeletal crystals in this photograph (field of view, 35 μm) contain Ca, P and Si as major elements (EDX analysis).

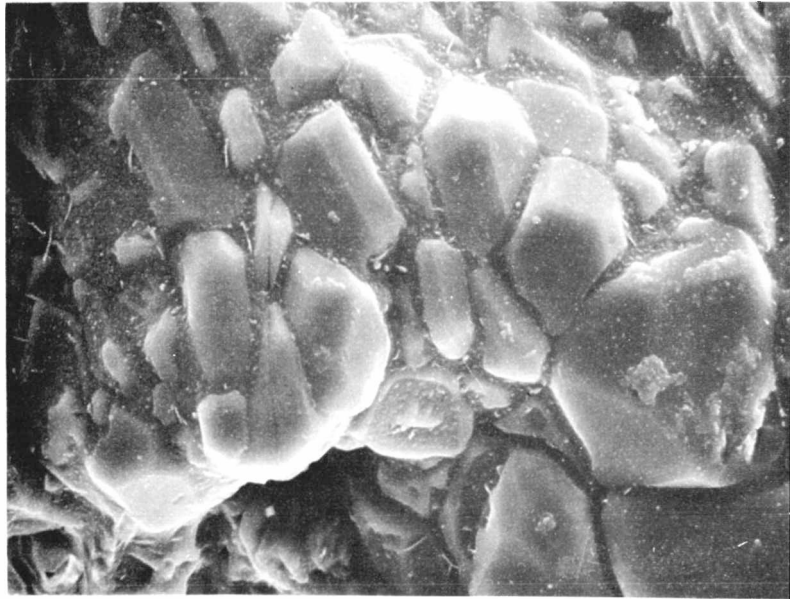


FIGURE 26C: The majority of crystals in this photograph contain Ca and P only, by EDX analysis. This suggests these crystals are apatite or whitlockite. Field of view, 50 μm .

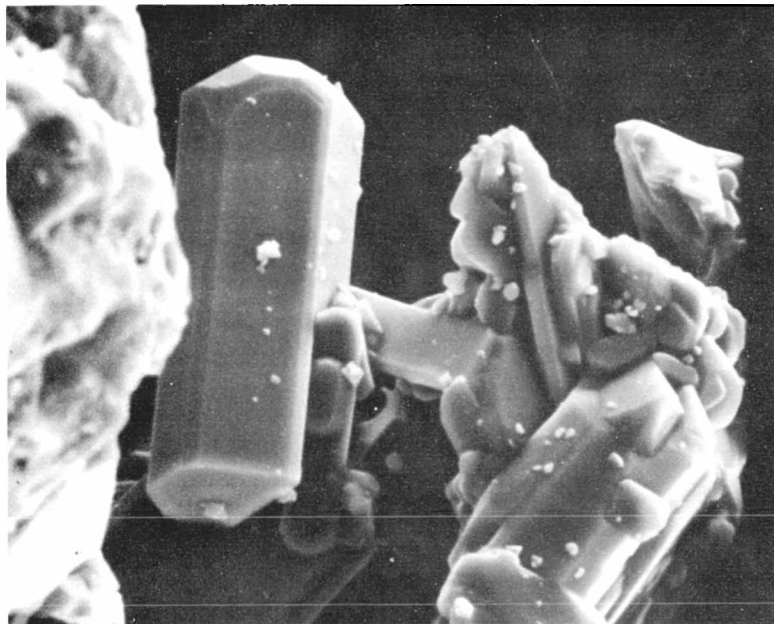


FIGURE 27: Lunar apatite crystal, projecting into void space within a vuggy breccia. Crystal is 17 μm long (courtesy D. S. McKay).

whitlockite. The skeletal crystals also could be the unknown phospho-silicate. They are too small (1 - 2 μm on a side) to do an accurate EDX analysis.

W. J. Walton (1972), (unpublished doctoral dissertation), reported the occurrence of a new Ca-P-Si phase in the system whitlockite-forsterite but was not able to identify it. The apparent phospho-silicate in this meteorite could be a natural occurrence of this phase. The exact chemical composition was not determined by Walton but the morphology was determined by petrographic study. The phospho-silicate phase occurred as simple diamond-shaped rhombs, sometimes truncated at the acute ends. This form is very similar to the skeletal crystals in Figure 26B.

Figure 27 is an example of lunar apatite. The form is quite different from the forms documented in the Rose City meteorite. No evidence of chlorine in greater than trace amounts has been found either by EDX or electron microprobe analysis in any phosphorous-bearing minerals in the Rose City meteorite by this investigator. Several per cent sodium has been found in most of the pure calcium-phosphates and therefore, whitlockite, rather than apatite, is apparently the common phosphate mineral in the Rose City meteorite. If apatite occurred originally in the pre-shocked, pre-metamorphosed Rose City meteorite, the chlorine was lost most efficiently during the subsequent heating events.

Another occurrence of iron plus silicate phases in one vug is seen in Figure 28A. The iron grain fills up most of the cavity and has growth

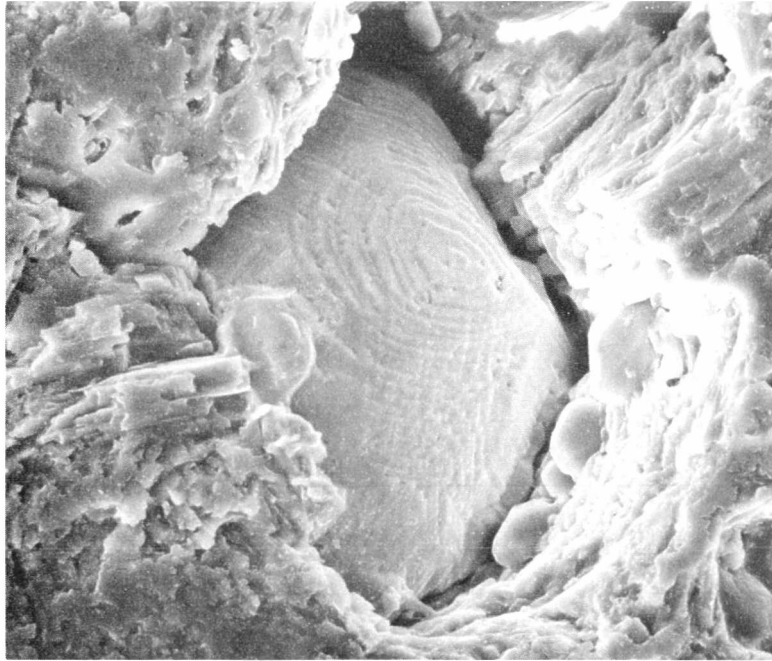


FIGURE 28A: Fe-Ni crystal fills most of this cavity. Low-Ca pyroxenes are attached to finer-grained cavity wall. Note that the long axis of the elongate matrix crystals tend to be perpendicular to the cavity wall. Field of view, 175 μm .

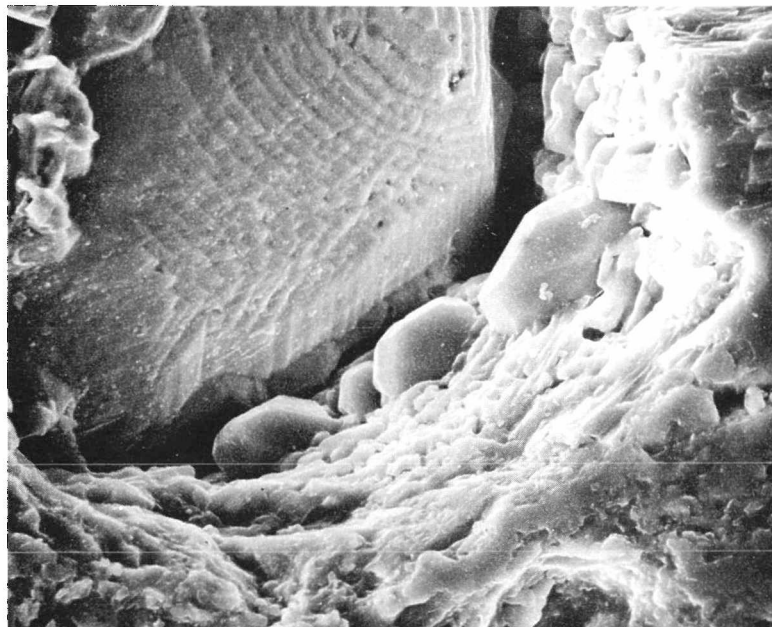


FIGURE 28B: Low-Ca crystals, 23 to 25 μm in length, appear to be attached to the vug wall parallel to their long axes.

steps only on a portion of the exposed free area. The nickel content is equivalent to that of kamacite, more than 5%, and is probably an extension of a kamacite grain in the matrix. The growth steps may represent vapor deposition on the preexisting metal grain. Probably volatilization around the metal grain, formed the vug and deposited the low-calcium, iron-magnesium silicates on the vug wall, Figure 28B. The latter are seen on the lower right side as stubby well-formed crystals with their long axes parallel to the vug wall. On the upper right and middle left the elongate matrix crystals are perpendicular to the cavity wall.

A different vug type and metal grain association is seen in Figure 29A. This appears to be a vesicle, formed in situ, by shock-melting and volatilization of a small portion of clast material. The vesicle wall is glassy with few crystals. The low nickel-iron (1 - 2%) grain is attached to the glassy wall and the crystal form, seen in more detail in Figure 29B, is either ill-formed, or superficially corroded or weathered. Figure 29C shows a lunar iron crystal (with a troilite coating) on a glassy substrate which has well-formed crystal faces and some growth steps. The meteoritic example shows similar features, except the crystal faces are more subdued. This either represents a trapped gas of Fe and Ni of a fractionally volatilized metal grain (because of the low Ni content), or an immiscible metal droplet in the silicate melt which migrated to the vesicle wall and subsequently crystallized there.

Figure 29D shows a chromite crystal apparently crystallizing, at least in part, from a silicate melt. All crystals on cavity walls are not necessarily exclusively vapor-deposited.

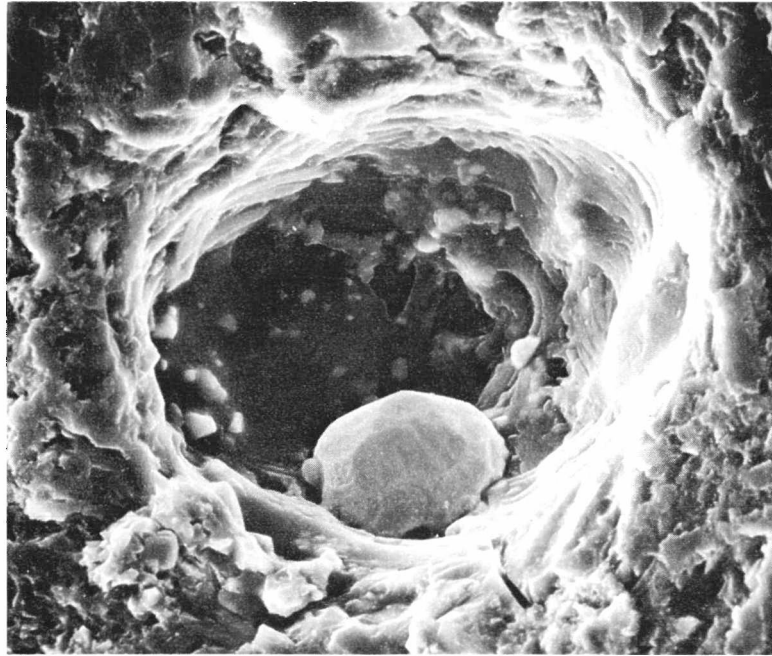


FIGURE 29A: Glass-lined vesicle (85 μm in diameter) contains an iron-nickel crystal, approximately 30 μm in diameter.

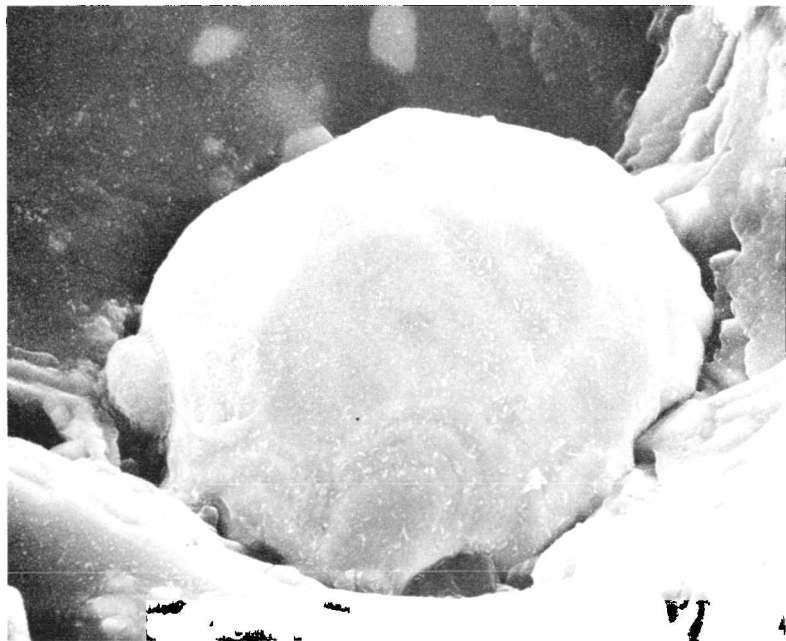


FIGURE 29B: High magnification photograph of iron-nickel crystal in Figure 29A (30 μm diameter). Note subdued crystal faces.

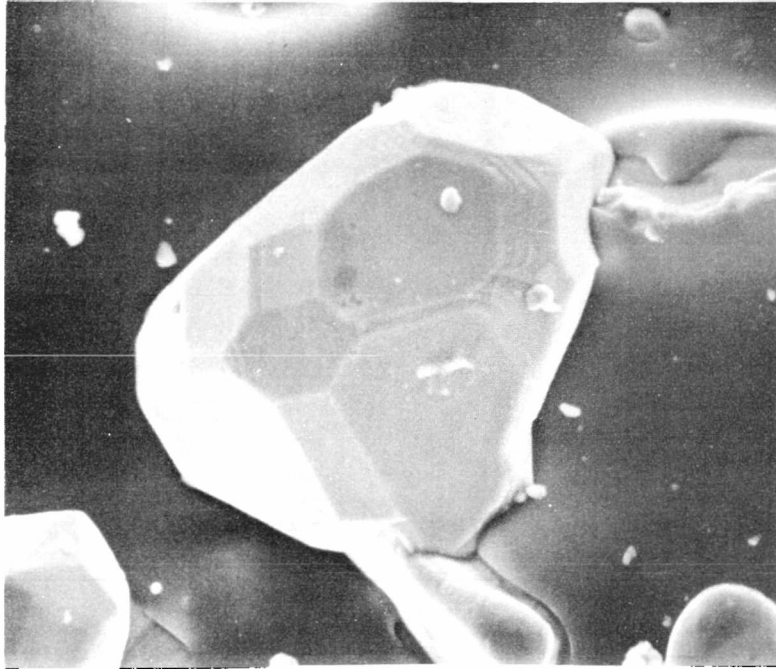


FIGURE 29C: Lunar iron crystal with a troilite coating on a glassy substrate. Crystal is 14 μm in diameter (courtesy U. S. Clanton).

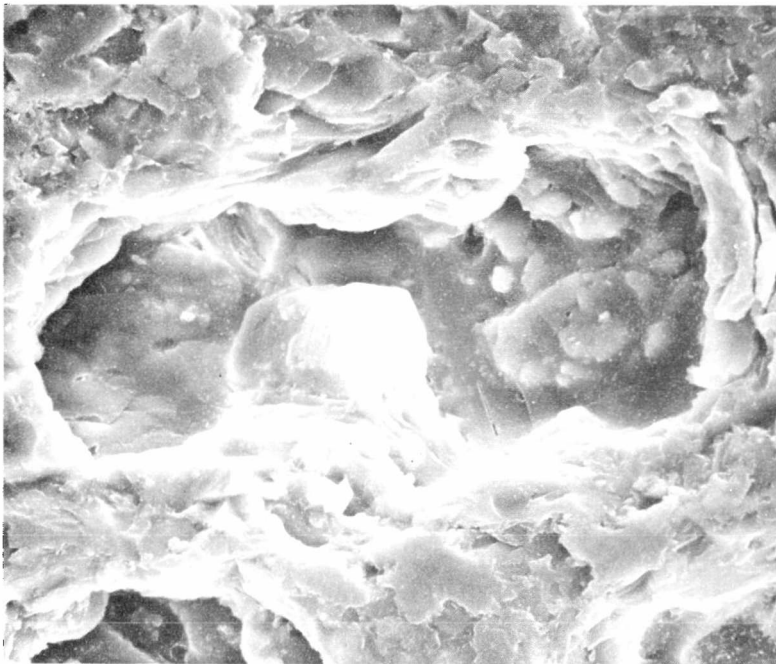


FIGURE 29D: The crystal in the center of glass-walled vug/vesicle is Fe chromite with <1% Ti. The crystal is approximately 10 μm in diameter.

Figure 30A is a stereo pair showing the silicate wall texture, bunched growth steps and projecting crystals. The small projecting equant crystals are a high calcium, magnesium-iron silicate, probably diopside, which is a minor mineral in most meteorites. This represents the only occurrence found in this study of the Rose City meteorite. Most of the crystals lining the vug walls are low-Ca pyroxenes. Figure 30B is of growth steps on a low calcium lunar pyroxene crystal.

The next series of SEM photographs illustrates the crystal morphologies and associations in the shock-melted, recrystallized silicate veins. These are the areas depleted in metal and sulfide phases, and this is reflected by the rare occurrence of metal or sulfide minerals in these vugs. These areas contain a high percentage of silicate mineral clasts (30 - 40%) which were not entirely consumed by the shock-melting. Most of the mineral clasts show evidence of shock or high temperatures in thin section, such as mosaicism, wavy extinction and fracturing. The shock-melted veins are surprisingly porous (~25 - 30%), indicating much vesiculation. Vesicles may have been high temperature areas for a longer period of time during the initial rapid quenching. Clasts would be just the opposite, representing "cold" areas in the melt, favoring rapid cooling and quenching in the surrounding melt.

In thin section the average crystal diameter in the shock melt veins is on the order of 0.5 to 1.0 μm . The major mineral constituents appear to be a low-calcium, iron-magnesium silicate, probably clino-bronzite, and high magnesium olivine which both form equant crystals. The interstitial melt is enriched in Na, Ca, K and Al with respect to the pyroxene composition. In some areas the "melt" shows a quench feldspar texture of radiating bladed crystals.

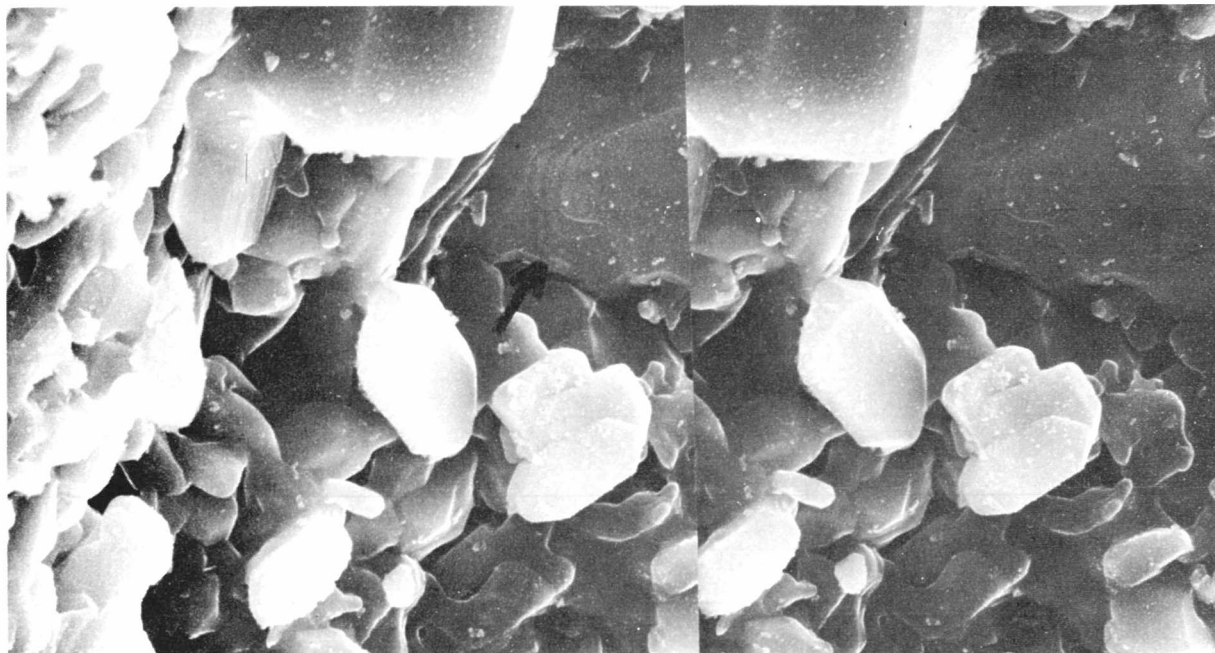


FIGURE 30A: Stereo pair of 7 - 8 μm doubly-terminated high-Ca silicates (probably diopside). Note growth steps in background silicate.

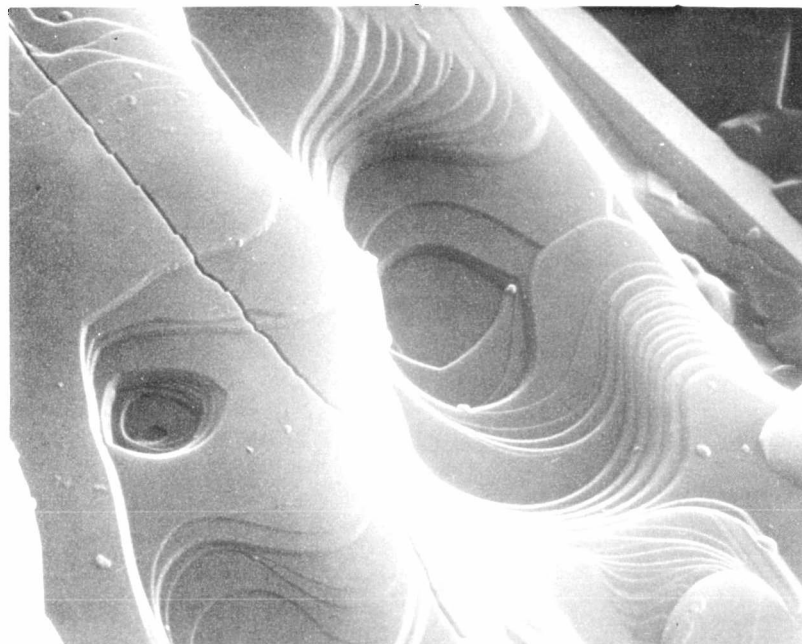


FIGURE 30B: Growth steps on low-Ca silicate crystal in lunar breccia. Field of view approximately 30 μm (courtesy D. S. McKay).

Figure 31A shows several relatively large (11 x 20 μm), euhedral low-Ca silicate crystals in a vug in the shock melted silicate vein (bottom, Figure 11C). Figure 31C is a stereo pair and illustrates the euhedral nature of these crystals. They are considerably coarser-grained than the average 1 - 2 μm matrix grains. Morphologically, as well as chemically, these appear to be bronzite because of the chemistry and blunt termination. The lunar recrystallized breccias contain low-Ca pyroxenes of similar composition and form (blunt terminations), and Figure 31B shows lunar pyroxenes (8 microns long) projecting into free space within an Apollo 14 breccia.

The vug association in Figure 32A is predominantly crystalline with euhedral to subhedral crystals intergrown or perched on each other. The chemistry indicates most of these are Mg-rich olivines by EDX analyses. Figure 32B shows an equant crystal with a button form on one face. The button is higher in Al and Si than the rest of the crystal. Figure 32C is a high magnification photograph of the euhedral, doubly-terminated crystal, 2 x 4.5 μm in size.

On many crystals there are small mounds (\sim 1 micron) which appear on most surfaces in a random fashion. These micro-mounds are too small to distinguish their chemistry from the substrate chemistry. They could represent a final vapor phase condensation; a weathering product; or a weathering product of a final stage vapor deposit.

Figure 33 shows a doubly-terminated euhedral crystal in a predominantly crystalline vug. Crystal growth features are quite pronounced including button features on two crystal faces. The "micro-mound" deposits appear to be restricted to certain faces, and the button growths.

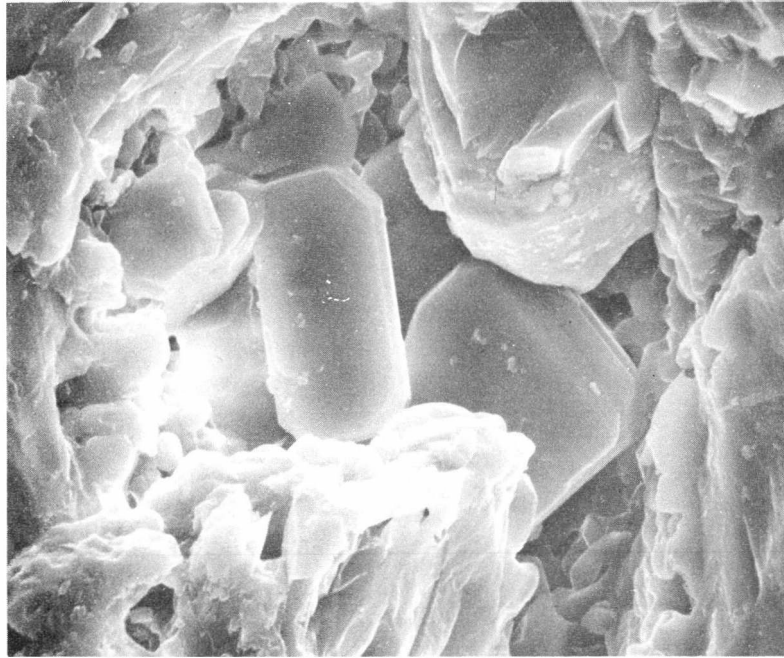


FIGURE 31A: Low Ca, Fe-Mg silicate crystals in irregular cavity. Elongate crystal is $11 \times 20 \mu\text{m}$.

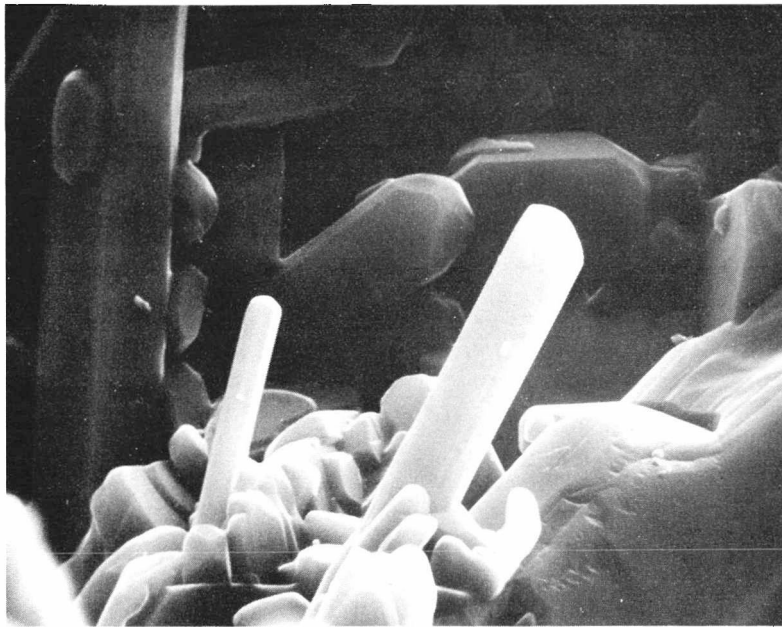


FIGURE 31B: Low Ca pyroxene crystals in recrystallized lunar breccia. Length of foreground crystal is $8 \mu\text{m}$ (courtesy D. S. McKay).

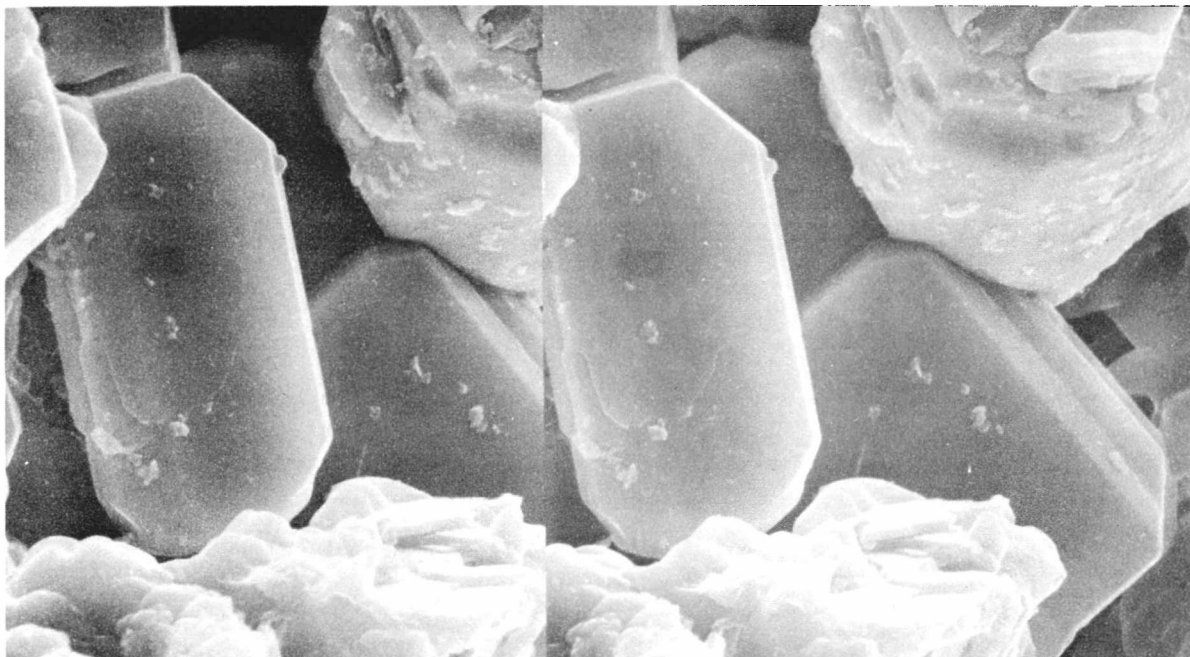


FIGURE 31C: Stereo pair of silicates in Figure 31A (left crystal is 20 μm in length).

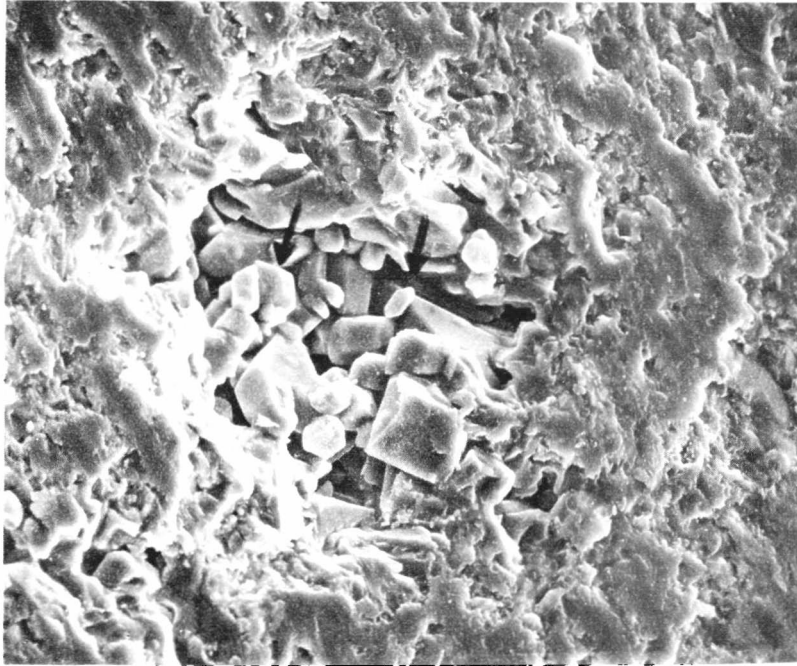


FIGURE 32A: Small vug in recrystallized matrix lithology. Note numerous crystals within the cavity. Field of view, 50 μm .



FIGURE 32B: Equant crystal, center of photograph. High Mg, Fe silicate (EDX analysis). Probably olivine because of high Fe+Mg/Si ratio. Field of view, 15 μm .

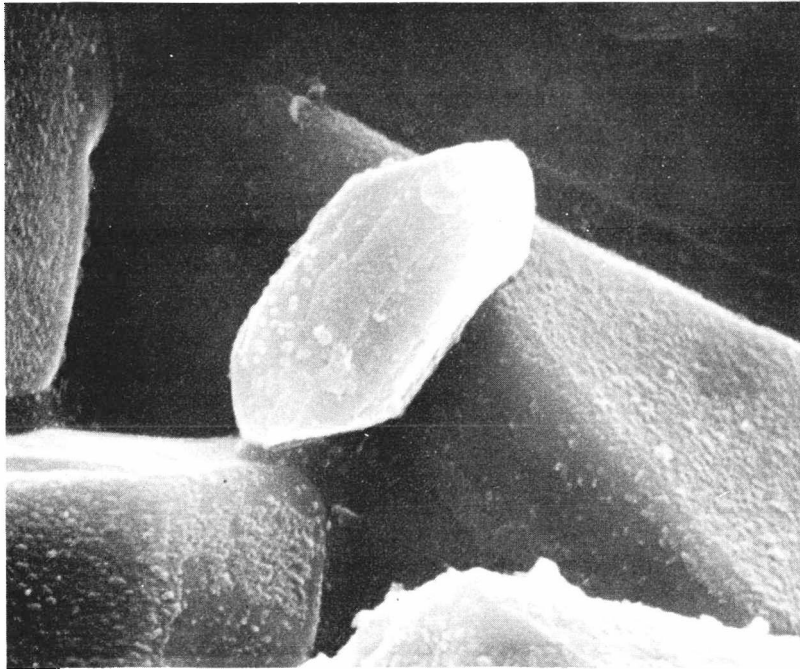


FIGURE 32C: Doubly-terminated crystal is $2 \times 4.5 \mu\text{m}$ in size.

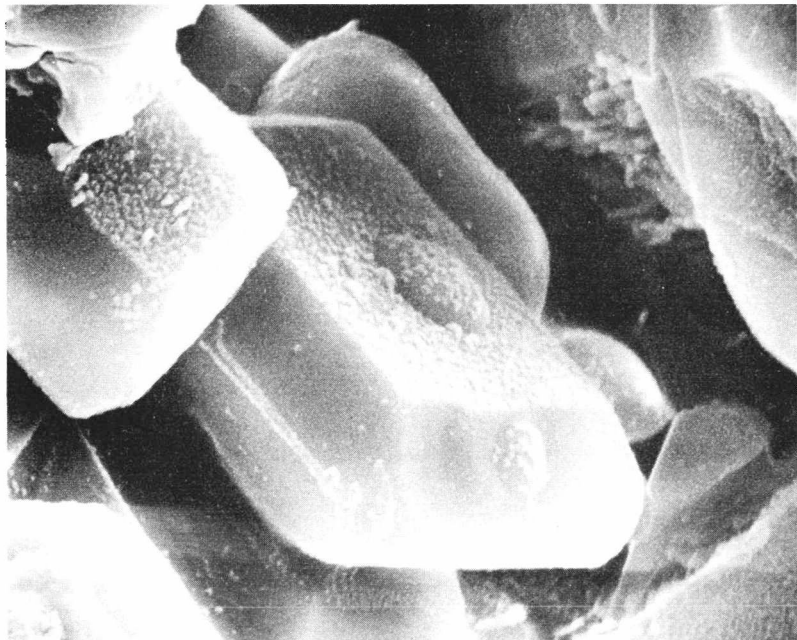


FIGURE 33: Note detail of crystal growth features, micromounds, button features. Center crystal is $3.3 \times 5.8 \mu\text{m}$.

This is in contrast to Figure 32B where the button growth on the equant crystal has fewer micro-mounds than the surrounding crystal face. These crystals, like those in Figure 32B, C appear very similar to euhedral olivine crystals.

The button forms appear to be related to the crystal growth and are not randomly deposited on the crystal surface. EDX analysis shows a distinct difference in chemistry between the crystal proper and the button: the button forms are consistently more silicon-rich with lesser amounts of iron and magnesium, several percent aluminum, and traces of sodium and potassium. The button features may be inclusions of glass (material that condensed as glassy amorphous droplets rather than crystallizing) in the vapor deposited crystals. This difference in morphology could reflect the differences in chemistry. Enstatite can be quenched to form a glass but forsteritic olivine cannot be quenched to form a glass, rather it appears to always crystallize.

Jedwab (1972) presented SEM photographs of very similar occurrences on ilmenite and pyroxene crystals in Apollo 12 lunar vesicular basalts. He documented examples of what he terms "globular overgrowths" on free growing crystals in vugs of lunar basalts. Jedwab observed different temporal relationships between his ilmenite crystals and the overgrowths. He found blebs which were deposited during the growth of the ilmenite but partially covered by growth steps, and other blebs which were deposited randomly after the supporting crystal was formed. He observed, and this study also shows, that the silicate globules tend to form and be larger on basal faces and also to be located at the centers of these faces, especially where the macroscopic symmetry is well-developed.

Both Jedwab and this worker (see Figure 33) noted the orderliness of the globules, as if there were crystallographic factors aiding the growth of the globular or button overgrowths.

The next two vug examples contain more of a glass phase. In Figure 34 the wall of the vug is amorphous-appearing in part and crystalline in part: The crystals appear to be crystallizing from the glass phase on the vug wall, but the crystals become coarser towards the vug interior. Most of the projecting crystals have a glassy neck or rim, but the coarsening of the crystals into the open vug interior is interpreted as the result of their growing, at least in part, in contact with a vapor phase.

One must always keep in mind the limitation of the SEM in that it reproduces surface morphology (and chemistry when that alters the conducting properties) and therefore the interpretation of material as amorphous or glassy versus crystalline is subjective without petrographic studies. Areas which may appear glassy compared to obviously crystalline material, may be microcrystalline, i.e., crystalline on a scale too small to be discerned by SEM techniques. Figure 8 illustrates the case of a glass-encased vesicle with several elongate crystals which project several (~ 5) micrometers into the glassy matrix, and the same (apparent) crystal would project a very short distance into the void space of the vesicle itself. In these cases one could envision the crystal forming from the melt phase and merely extending into the cavity because of lack of resistance. On the other hand, a vapor phase present in the cavity may have been a necessary condition for the crystal to continue (begin?) growth into the interior space of the vug.

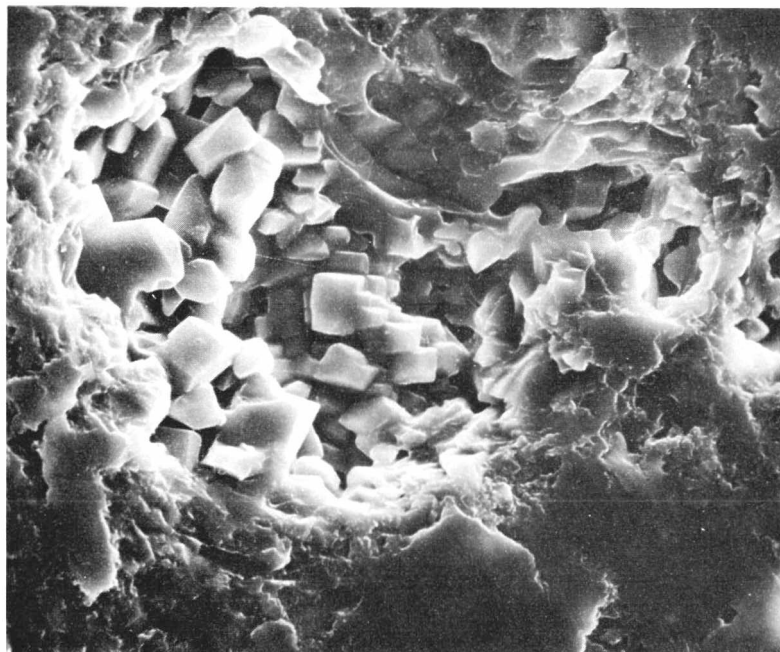


FIGURE 34: Elongate vesicle/vug, 100 μm across, in recrystallized silicate vein lithology. Note crystals coarsen towards interior of cavity.

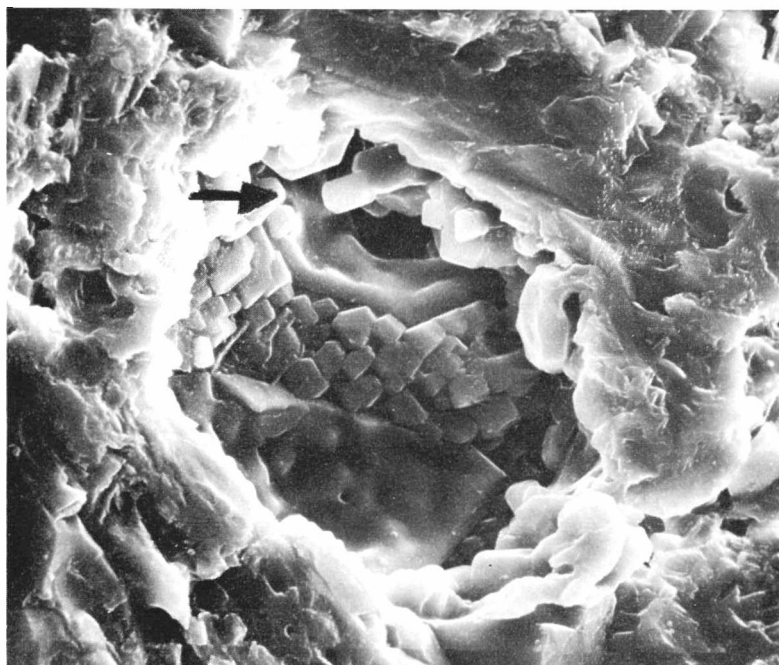


FIGURE 35: Spherical vesicle/vug in recrystallized matrix. Note the glassy surface; crystals flush with a section of the cavity wall; crystals projecting into the interior of the cavity (top of vug). Field of view, 250 μm .

Figure 35 shows a vesicle-like cavity which appears to be largely glass-lined. The crystals in the center are more-or-less flush with the glass and wall of the vesicle. These crystals show no growth steps and little tendency to project. The chemistry of the crystals versus the apparent glassy phase is very similar, both containing Mg, Fe and Si as the only detectable elements. The crystalline areas appear to be enriched in Fe. Figure 35 illustrates one crystal projecting from another crystal into the vesicle interior. This is interpreted as vapor-deposited.

Within the metal-rich areas in the matrix were found the most unusual vug mineral associations. There appears to be a combination of processes associated with the shock metamorphism which lead to these mineral assemblages, including crystallization from a vapor phase and from the melt. In Figure 36A an interconnected series of irregular cavities are shown. The top portion of the SEM photo, and the cavity, is a metal area, and the remaining sides of the cavity are bounded by shock-melted silicate areas. Figure 36B is of the upper right part of the vug.

The grain with the well-formed growth steps is nearly pure iron. The more corroded crystal to the right is composed of iron-nickel (nickel ~5 - 10%). Even more corroded, or alternatively, skeletal in form, is the grain just below the iron-nickel grain. Figure 36C is a close-up of this grain which, by EDX analysis, is composed of predominantly chromium and iron in roughly equal amounts and is probably chromite.

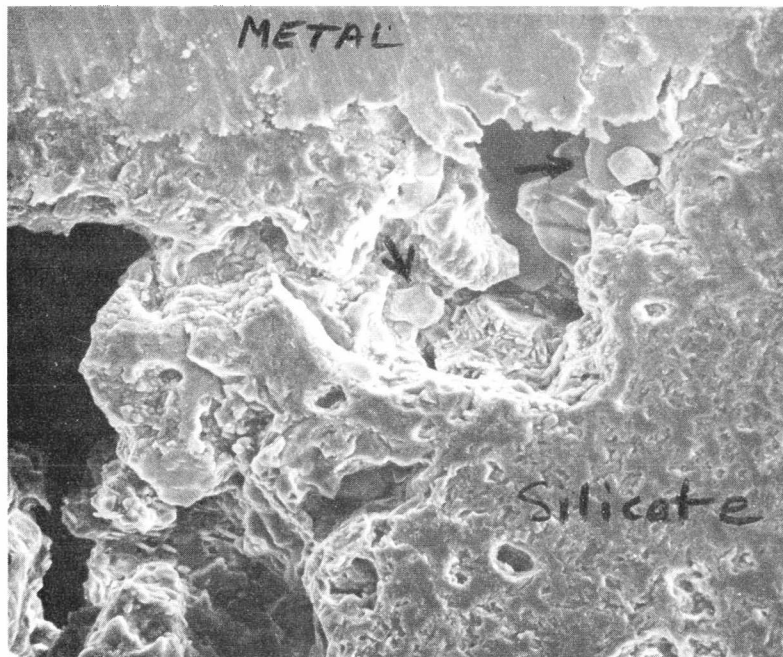


FIGURE 36A: Irregular vug between metal area (top of photograph) and recrystallized silicate area. Field of view, 540 μm .

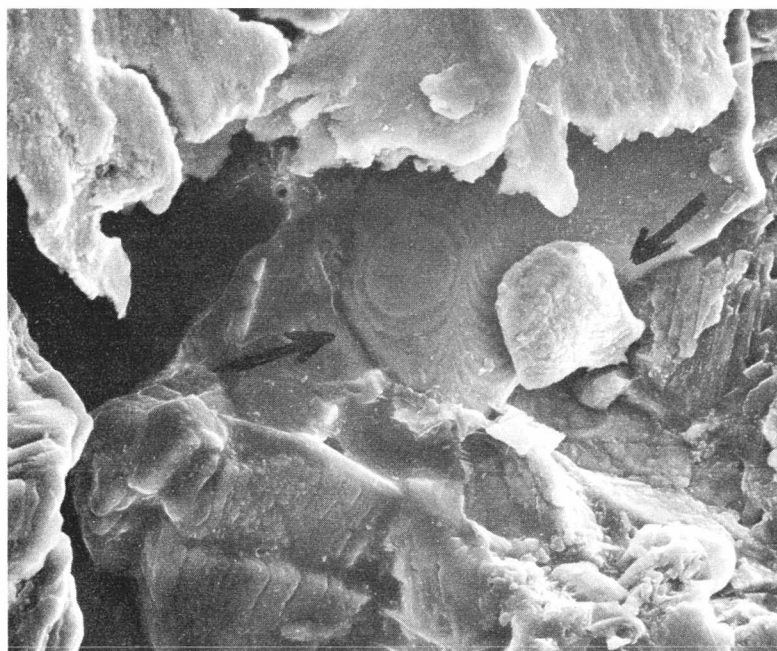


FIGURE 36B: Iron-nickel grain, to the right of center, is highly corroded-appearing, but a faint octahedral form is suggested. Growth steps in background are on a pure Fe grain. Field of view, 175 μm .



FIGURE 36C: The grain in the center is composed of Fe and Cr (EDX) and is 16 μm in diameter.

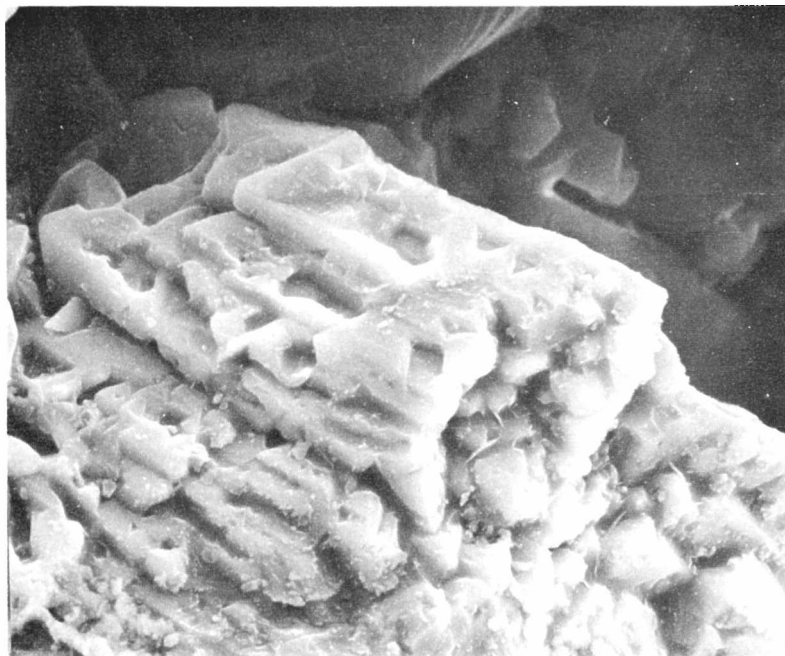


FIGURE 36D: This mass of what appears to be skeletal crystals in a glassy matrix is another form of chromium and iron (chromite?). Field of view, 50 μm .

Figure 36D shows a skeletal arrangement of chromite crystals (Cr, Fe) in the center of the vug, Figure 36A. These crystals appear to be crystallizing predominantly from the melt phase.

Figure 36E is a high magnification photo of well-formed crystals of calcium phosphate which occur beneath the chromite crystal in Figure 36C. Because there was no Cl or F detected, these are probably whitlockite crystals. Figure 36F shows a lunar example of whitlockite with a very similar form. Figure 36G is a calcium phosphate mineral association just above the skeletal chromite crystals. Lack of detectable Cl or F, and equant as opposed to elongate crystal habit, indicates these are whitlockite crystals. The next photograph, Figure 36H, documents another occurrence of the unusual "phospho-silicate" within the same vugs, which has been found to be a relatively common minor constituent in mineral assemblages in many of the vugs of the Rose City meteorite. Figure 36H shows a needle-like crystal, 3 x 8 μm , apparently crystallizing in part from a silicate melt. The major elements by EDX analyses are Ca, Si and P with minor Mg, Fe, Al and Na. Hexagonal prism faces are suggested.

Figure 36I is of a twinned and distorted iron crystal (center, 36A) with minor amounts of chromium and nickel. An axis of 4-fold symmetry is indicated on the photo. Cubic, tetrahedral, and octahedral forms are present. Figure 36J is a lunar iron crystal with similar forms.

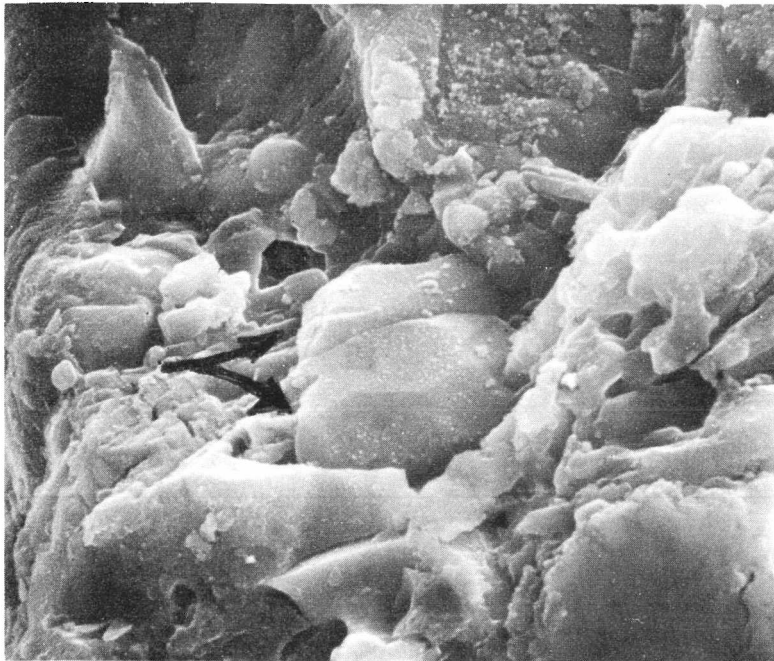


FIGURE 36E: Stubby crystals of calcium phosphate, 10 μm in diameter. No chlorine or fluorine was detected (EDX), therefore these crystals probably are whitlockite.

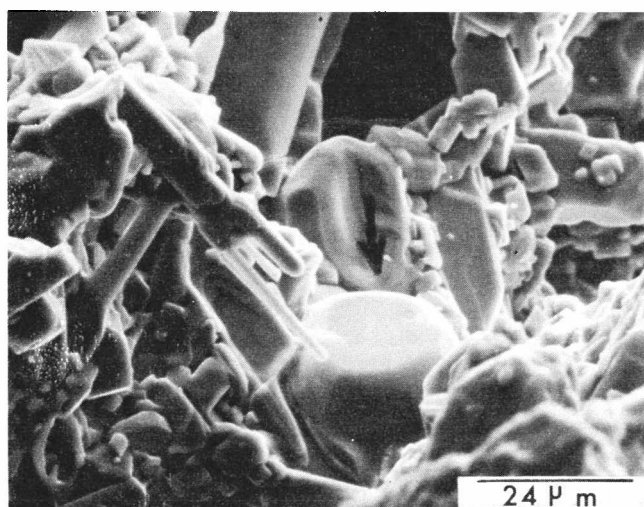


FIGURE 36F: Lunar whitlockite crystal (courtesy D. S. McKay).

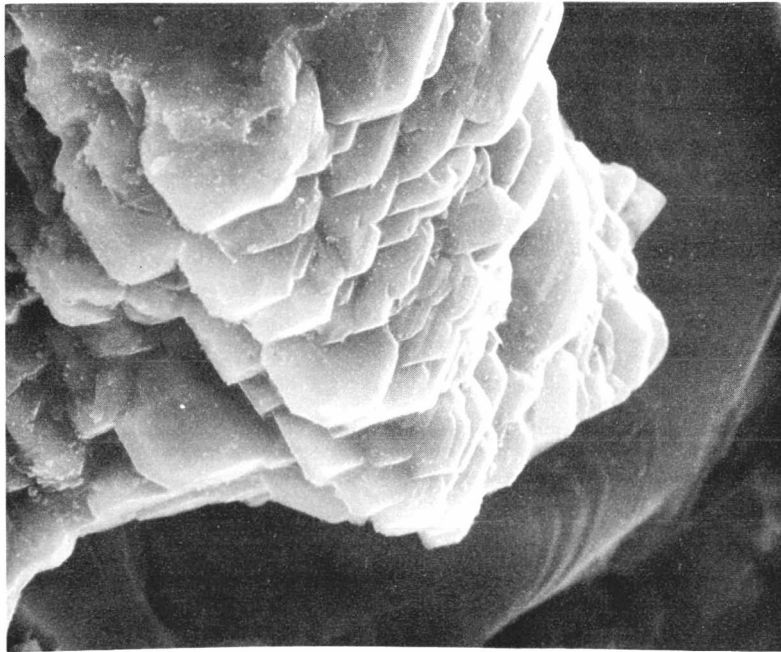


FIGURE 36G: Calcium phosphate mineral association. Field of view, 50 μm .



FIGURE 36H: Needle-like crystal is a Ca- P- Si-bearing mineral, measures 3 x 8 μm .

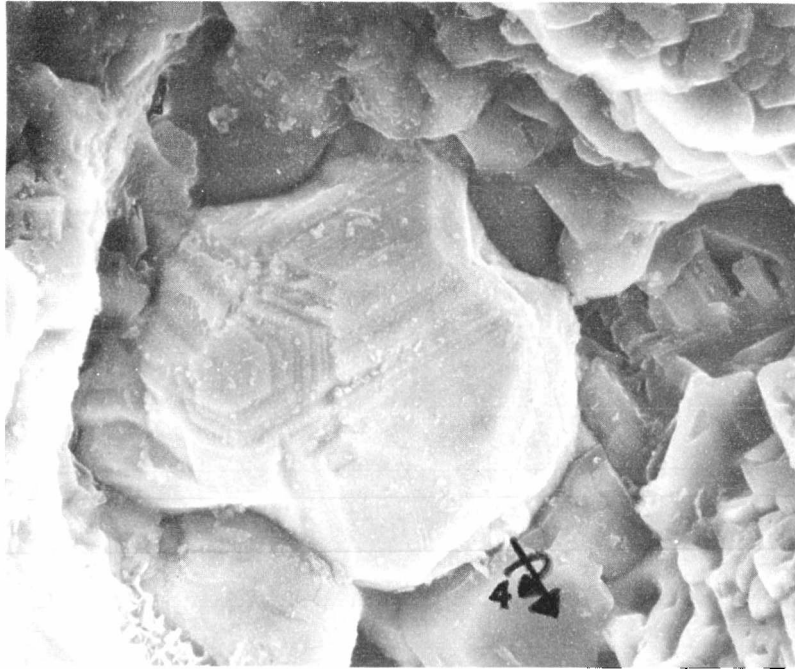


FIGURE 36I: Rose City meteorite - twinned iron crystal with 1 - 2% Ni and Cr. Diameter of crystal is 50 μm . Right side of crystal has cubic and tetrahexahedral forms.

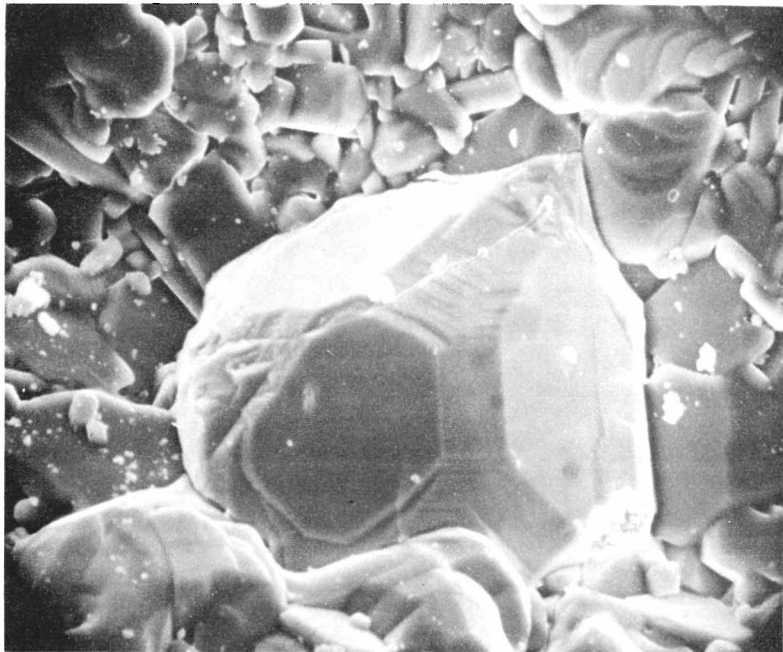


FIGURE 36J: Lunar iron crystal, approximately 30 μm in diameter. No detectable nickel.

CHAPTER FOUR

ALTERATION PRODUCTS IN THE ROSE CITY METEORITE

Weathering or terrestrial alteration can cause substantial changes in the composition of meteorites. Weathered, porous chondrites can have minor and trace element relative abundances quite different from unweathered specimens of the same chemical group and petrologic type. Wasson (1974) observed the trend that lower Mg and Si values were obtained from the bulk analyses of the more weathered specimens. For this reason it is important to determine the extent of alteration that has occurred in any meteorite prior to its analysis. The scanning electron microscope provides a particularly sensitive method for the detection of alteration products.

The Rose City meteorite is a very porous chondrite as has been shown previously. Over the years, exposure of the Rose City meteorite to the humid, oxygen-rich atmosphere has caused some alteration to occur as indicated by red or "rusty" discolorations around some of the metal-rich areas. The largest cavities in the Rose City meteorite occur in the matrix, around the bands of metal and sulfide which have segregated from the shock-melted silicate veins. These cavities are debris-filled, but show no signs of crystals projecting into the open spaces and are interpreted as tension cracks or cavities that have formed along some metal-silicate contacts. This general matrix area, probably because of the large cavities and passageways, is the location of the most obvious alteration products. However, both large irregular cavities and the smaller vesicular-type cavities show evidence of weathering which is interpreted as terrestrial in origin.

In hand specimen, the original sample of the Rose City meteorite (Figure 2) showed yellow-brown and red surficial coatings on the metal in the matrix lithology. Binocular microscope observation of the columns used in this study indicated similar surficial alteration of some of the veins of metal. Thin section study revealed deep red and yellow to orange-red rims on some areas. The observations made with the SEM show Fe forms with habits ranging from platy (most common) to botryoidal. Spheres covered with pointed crystal termination and internal radial structure also were seen. These features all best fit the properties of hematite and goethite, and it is concluded that these are the most probable alteration products.

In lunar samples goethite is the common alteration product found. The water in its structure is terrestrial in origin (Epstein and Taylor, 1971). The goethite in lunar samples is associated with meteoritic Fe-Ni spherules, troilite and several other minor sulfide and sulfate minerals (Taylor, 1975).

Figure 37A is of a large vug with numerous spheres on the walls. The vug itself is within a silicate area and is not obviously adjacent to a metal-rich vein. Figure 37B is a closer view of the spheres within the vug and shows the surface texture of the spheres to be "dog-tooth" crystals. The floor of the vug next to the spheres has a fuzzy or spongy surface, apparently from small intersecting blades of probably hematite. EDX analyses indicated Fe as the major element but the SEM with the EDX cannot distinguish between hematite and goethite. These spheres are probably iron/iron-nickel/iron-sulfide crystals which were originally deposited on the vug walls during the shock metamorphism. Alternatively

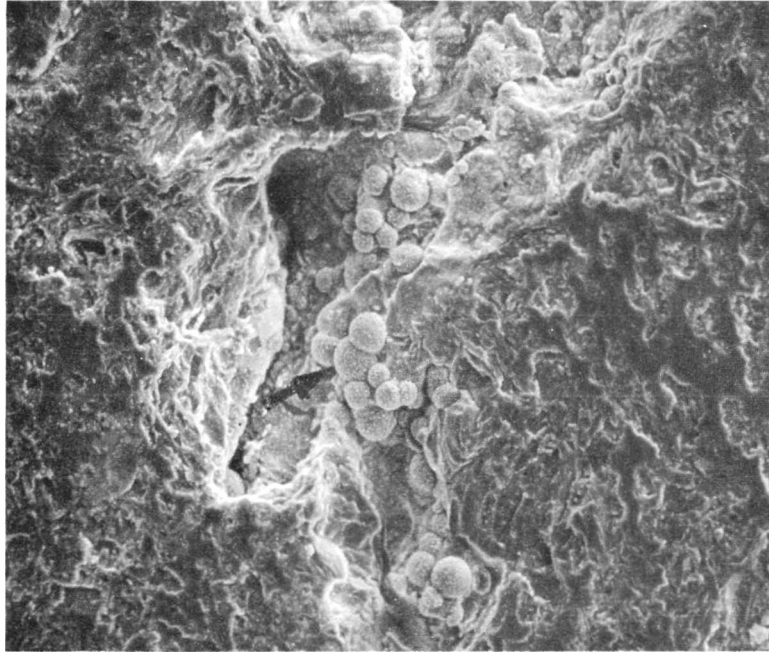


FIGURE 37A: Weathering products of iron in Rose City vug. Largest sphere is 20 μm in diameter. Fe is the only detectable element.



FIGURE 37B: Note floor of cavity is covered with bladed forms of oxidized iron. Largest sphere is 20 μm .

they could have been leached from the metal rich areas and deposited here after the meteorite fell to earth.

The next figures, 38A and B, show a smaller vug with iron spheres of a different form. Again, iron is the major detectable element, and it is assumed that the iron is mainly hematite because of the botryoidal form. A small, vesicle-like cavity in Figure 39 which appears to have glassy to devitrified walls, contains a bladed form of hematite or goethite. These weathering products are not random, but are localized, even within the small area of this vesicular-type vug. Perhaps there were one or more iron grains, similar to Figure 29A which have subsequently been oxidized.

Figure 40A shows an association of intergrown iron blades in the Rose City meteorite. Figure 40B is a lunar example of "iron-weathering". Lawrencite (FeCl_2), is a metastable mineral, common as a minor constituent of meteorites, which decomposes upon contact with water vapor. Although very little chlorine was detected in Rose City (nothing above trace amounts, even in the phosphate minerals), this is one possible source of these alteration products. Petrographic work showed the lunar alteration products to be goethite and lepidocrocite.

Within one of the larger vugs in the matrix, there was an iron crystal with a minor amount of nickel which displayed a cubic form. Figure 41A is a stereo pair of this crystal. There are several subhedral to euhedral low calcium, iron-magnesium silicates next to the iron crystal. In Figure 41B, a closer view of the surface reveals a fuzzy or spongy appearance to the surface of this grain. It appears as if the iron grain has been etched or suffered some degree of leaching. It has a quite

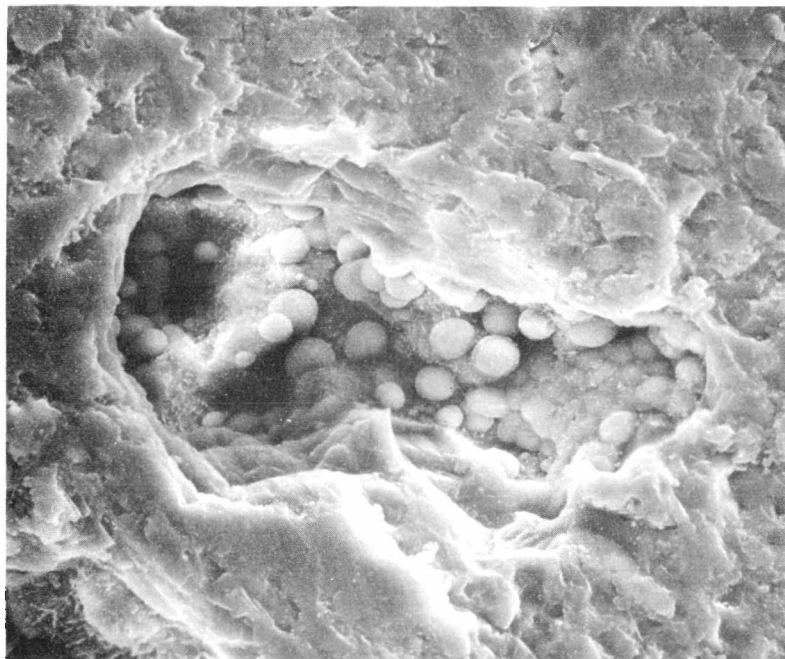


FIGURE 38A: Another form of iron spheres. Length of vug, approximately 65 μm .

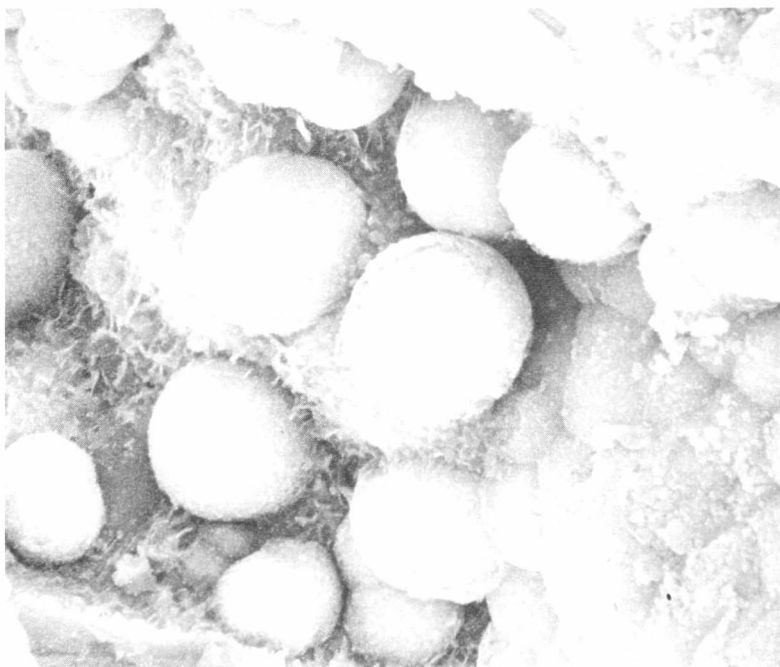


FIGURE 38B: Spheres are Fe (EDX analysis), 7 - 8 μm in diameter. Several appear to have shells or a coating on their surfaces.



FIGURE 39: Iron weathering products in partially glass-lined, partially-devitrified vesicle. Field of view 62 μm .



FIGURE 40A: Bladed iron alteration product in Rose City meteorite. Field of view, 25 μm .

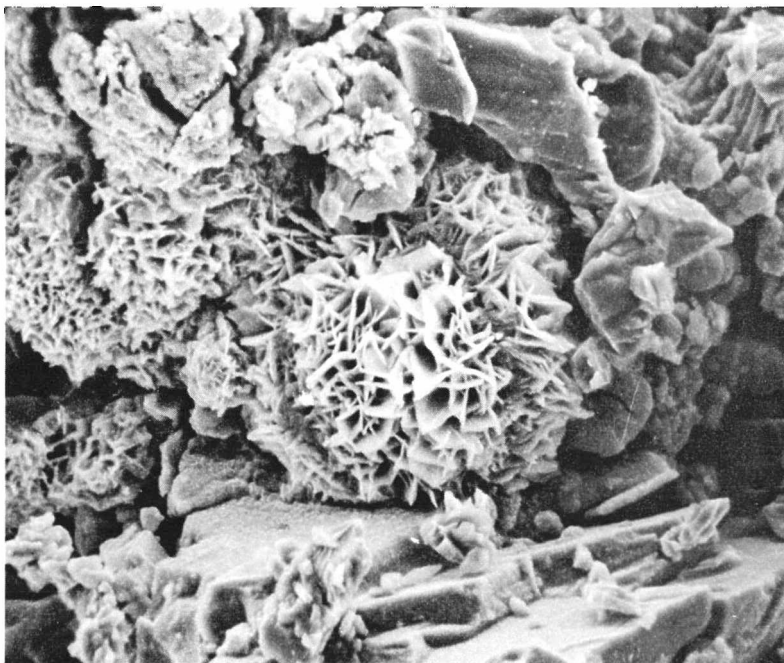


FIGURE 40B: Rosette of iron alteration product in lunar breccia. Rosette is 7 μm in diameter (courtesy U. S. Clanton).

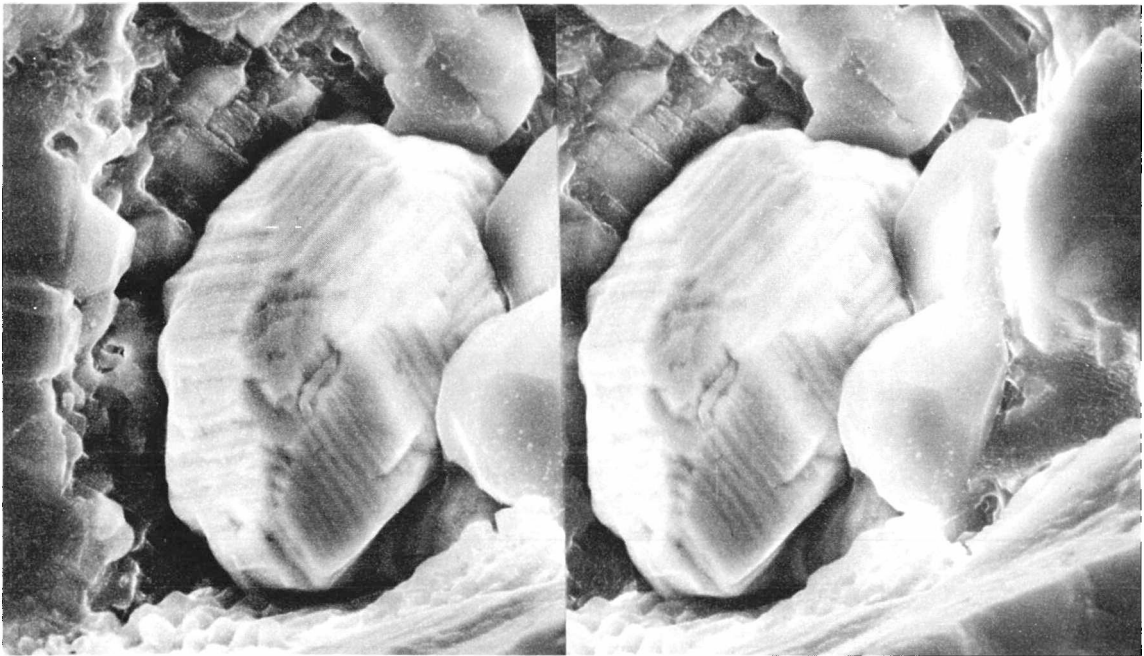


FIGURE 41A: Stereo pair of cubic iron crystal, 22 x 30 μm .



FIGURE 41B: High magnification of cubic iron crystal. Growth steps are evident. "Fuzzy" texture of surface attributed to etching, alteration of iron by weathering. Field of view 15 μm .

different appearance from the silicate crystals next to it, and from previous iron and iron sulfide crystals with well-defined growth layers. This unusual surface texture is interpreted as being the result of a leaching (weathering) process acting upon an original iron grain in this cavity. This occurrence could indicate the source of some of the weathering products in other vugs if one assumes, as seems logical, that the large cavities are interconnected and there has been some movement of water (water vapor) within Rose City meteorite.

CHAPTER FIVE

Summary

A handicap in this type of study is the limited experimental work with vapor phase crystallization, as well as the necessary documentation of the characteristics (on the detailed scale provided by the SEM) of crystals grown from a vapor phase versus crystals grown entirely from a melt. The existence of vapor-formed vugs and vesicles, crystals projecting into space, bunched growth steps, and a source and containment of a vapor phase are all indications of crystallization from a vapor phase.

Vugs are an important feature of the highly shocked Rose City meteorite and lunar breccias. In the cavities of both types of samples, euhedral crystals of metals, sulfides, silicates and phosphates are interpreted as vapor-deposited. In this study, iron, iron-nickel, troilite, low Ca and high Ca pyroxene, olivine and whitlockite were found in vugs of the Rose City meteorite and are interpreted as vapor phase in origin. Evidence of a new phospho-silicate phase in the Rose City meteorite also was found.

The temperatures reached locally (during an impact event of sufficient energy) would be in excess of 1800 - 1900°C - great enough to vaporize virtually anything present in the meteorite. In these local areas the vapor phase will contain essentially all chemical species present in the original lithology. If local vaporization occurs only within an olivine chondrule and no vapor movement occurs, the vapor phase constituents will be limited to the olivine composition and one would naturally expect olivine as a vapor phase product. For reasons given

before (segregation of metal and silicate, apparent movement of volatiles into unmobilized clasts) there appears to have been a fair amount of mixing, both in the melt and vapor phases. Therefore, in some vugs one would expect to find more than one mineral species and this is generally the case.

Based on crystal morphology and EDX Mg + Fe/Si ratios, the two dominant silicates deposited from the vapor phase in the Rose City meteorite are magnesium-rich olivines and low calcium pyroxenes. The silicates in the vugs and vesicles are generally in the range of 5 to 15 μm in size, a size that limits the accuracy of probe analyses. Attempts were made, and the olivine crystals lining vug walls appear to be slightly enriched in Fe (Fa_{22}) relative to matrix olivines (Fa_{20}). There is no detectable difference between the Clast A preserved pyroxenes and the Clast A vapor-deposited pyroxenes, both containing a ferrosilite component of 15 mole per cent and CaO content less than 1 per cent. Microprobe analyses of the silicates are presented in Appendix A. In the matrix the pyroxenes yielded highly variable analyses from grain to grain, and within single grains. The CaO content was found to have a wide range, from <1% to 20%. The highest CaO values occur at pyroxene contacts with silicate glass. Begemann and Wlotzka (1969) found a similar phenomenon in the Ramsdorf meteorite and attributed it to a reaction of the Ca-poor orthopyroxene with plagioclase and small amounts of indigenous Ca-rich clinopyroxene. This would appear to be a reasonable explanation in the Rose City meteorite, also.

In addition, the vug silicates in the matrix lithology commonly bear the Al-Si-rich "button" features observed in numerous SEM photographs. These are interpreted as being condensed glass blebs incorporated into the vapor-deposited olivine and pyroxenes during and after the latter's crystallization. These glass inclusions would handicap accurate probe analyses of the individual silicates in the matrix lithology. Even the olivine crystal compositions in the vugs of the matrix are slightly more variable than for those in the matrix lithology. The unusual button features and associated non-olivine, non-pyroxene chemistry were not observed in the clast lithology. The button features only occur in the matrix lithologies with the greatest amount of evident melting and glass. In view of this observation, one interpretation of their origin is that they are melted (possibly vaporized) high silica components of the meteorite which formed molten spheres or mounds that subsequently quenched to an amorphous phase deposited simultaneously with the vapor phase components in the vugs and vesicles.

EDX analyses of the surfaces of iron crystals in vugs (in both matrix and clast lithologies) show a general depletion in Ni (Ni \approx 1 - 2%), relative to the interiors of grains, where microprobe analyses indicate variable nickel contents, with an average of 10% Ni. The Ni content of the troilite crystals in vugs is on the order of 0.1 - 0.2% by microprobe analyses. See Appendix A for microprobe analyses of the iron-nickel and sulfide phases.

Both EDX and microprobe analyses detected no fluorine and only trace amounts of chlorine in the calcium phosphate minerals. The bulk chemical

analysis of the Rose City meteorite by Mason and Wiik showed no chlorine in detectable amounts.

Discussion

The well formed crystals in the cavities in lunar breccias are interpreted as crystallizing during the thermal metamorphism of a hot ejecta blanket (McKay et al., 1972) emplaced by a large scale impact on the moon. The similar features in the cavities of the Rose City meteorite are interpreted as being formed during thermal metamorphism associated with a violent impact and subsequent ejecta blanket deposition on the Rose City meteorite parent body (this work). Thermal regimes in impact melts have been studied and are summarized by Simonds (1975). Two stages of cooling appear to occur. There is an initial rapid equilibration between clasts and matrix on the order of seconds, in which the extremely high temperatures attained in the impact event are lowered to the neighborhood of 1200° to 1400°C. Cooling at this point will either cease or be significantly slowed because the initiation of crystallization will release the latent heat of fusion. This apparently will buffer the melt's temperature through the crystallization range. The second stage of cooling as the heat is transferred to the surroundings will be orders of magnitude slower - months or years depending on all of the variables such as position in the melt sheet or ejecta blanket, the range of clast sizes, the values of thermal diffusivity, the differences in heat capacity between melt and clasts, and the latent heats of fusion. Recrystallization can occur during the second stage of cooling. Growth steps and

crystal faces will form on silicates, metals and sulfides within the vugs and vesicles where the condensed droplets and vapors have been entrapped.

Impact and shock metamorphism result in redistribution and loss of the volatile mineral species, as well as the more refractory elements in the more violent events. These processes affect the elemental distributions of the ordinary chondrites and need to be sorted out from elemental trends which are the result of the original accretional processes.

Taylor and Heymann (1969) showed a direct correlation between reheating and shock events in some chondrites and concluded that the reheating observed in chondrites is primarily due to shock. In their 1971 paper they presented evidence for two-stages of cooling in the postshock thermal histories of reheated chondrites.

If impact or shock-metamorphism is the origin of the thermal metamorphism indicated by the petrologic grades observed in the ordinary chondrites, how would the original mineralogy and chemistry be affected? In a very good summary paper on metamorphism in ordinary chondrites, Dodd (1969) points out that for the major, non-volatile elements, there is no systematic difference between Types 3-6 with the possible exception of total iron which increases from H3 to H5, and decreases from H5 to H6. Let us assume the petrologic grades represent different positions within one ejecta blanket on a parent meteorite body (Figure 42). Iron can be volatilized as evidenced by this study, and therefore some Fe could be transported a certain distance before deposition. For the high iron

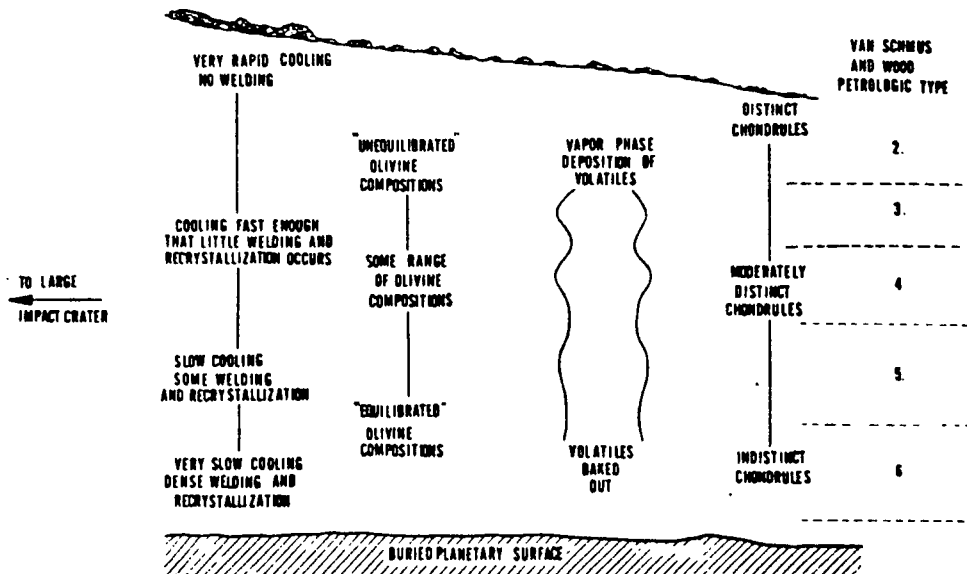


FIGURE 42: Schematic diagram of impact-emplaced ejecta blanket (from King, et al., 1972). Possible relationships to the petrologic types of Van Schmus and Wood (1967) are indicated. The Rose City meteorite would represent a sample of the fall-back melt sheet (in or very near to the impact crater) at the base of this ejecta blanket.

chondrites, another observed trend is for the metallic nickel-iron to increase from H3 to H5, but decrease slightly from H5 to H6. Analyses of the olivines in the vugs of the Rose City meteorite, which show a slight increase in the Fe content of the silicate phase, suggest the meteoritic material submitted to the highest temperatures may undergo "relocation" of some of its constituent elements. Volatilization may encourage a small degree of oxidation of the iron to occur. Less strongly heated meteoritic material with more volatile elements (specifically carbon) may activate another process, namely the reduction of iron from the silicate phases.

Among the minor volatile elements there is a decrease in carbon and water from low to high petrologic types (Dodd, 1969). This is not at variance with impact-induced thermal metamorphism.

The volatile minor elements are depleted in ordinary chondrites with respect to carbonaceous chondrites, which represents, or is because of a different accretional history from the carbonaceous chondrites, i.e., the parent meteorite bodies of the ordinary chondrites accreted less minor volatiles than the carbonaceous chondrite parent body(s). Dodd (1969) points out that carbon, indium and the noble gases are depleted systematically from Type 3 to Type 6 in ordinary chondrites. These depletions could be the result of impact or shock metamorphism after accretion. The exception in minor volatiles are chlorine and mercury. These elements are more abundant in ordinary chondrites than would be expected from their estimated volatilities and neither shows a systematic depletion pattern within the ordinary chondrites. Chlorine

varies among the ordinary chondrites by roughly one order of magnitude, with no systematic difference in the chlorine contents of Type 5 and Type 6 chondrites (Dodd, 1969). However, chlorine resides in the thermally stable phase of apatite primarily. Therefore, except under severe conditions it would not be expected to be lost readily. Chlorine is present only in trace amounts in the calcium phosphate minerals in the Rose City meteorite (this study) although it is abundant in many ordinary chondrites (Dodd, 1969). Mason and Wiik (1966) found no chlorine in their analyses. Therefore, it is suggested that the unusual variation of chlorine within the ordinary chondrites is related to the intensity of shock-metamorphism each ordinary meteorite has undergone and the ability to melt or vaporize primarily the apatite. The Rose City meteorite is depleted in chlorine because the high temperatures from the shock metamorphism was sufficient to melt apatite and vaporize the chlorine. In an ejecta blanket of reasonable thickness the chlorine once mobilized would move from the highest temperature regions and be concentrated in lower temperature zones. This movement would occur along natural fissures and cracks leading to the surface of the ejecta blanket. Movement of chlorine within certain zones and areas (Figure 42) would explain the wide range in chlorine concentrations observed in the ordinary chondrites. It would be deposited, consequently, in the more porous, less consolidated material within the ejecta blankets.

It is proposed that the Rose City meteorite represents a sample that experienced the extreme pressures and temperatures of an impact event. If this impact occurred on the parent meteorite body, this sample would be part of the impact melt sheet, with non-melted clasts of the impacted

ACKNOWLEDGEMENTS

I wish to sincerely thank Dr. Elbert King, my thesis advisor for his patience, suggestions and guidance. Thanks are extended to Drs. Max F. Carman, John Butler, and W. W. Wentworth who served on my thesis committee and also offered many useful comments.

Appreciation is extended to the Geology and Geophysics Branch of the Johnson Space Center, NASA, for after hour use of equipment and facilities where the research for this thesis was accomplished. Thanks also are extended to Dr. Carleton Moore who generously loaned me the samples of the Rose City meteorite used in this study.

In addition I would like to express my sincere thanks to Drs. Don Bogard, D. S. McKay, U. S. Clanton and John Kerridge for their comments and discussions during the course of this work.

Appreciation is extended to Elinor Stockton who typed the preliminary and final drafts of this report.

REFERENCES

- Albee, A. C., Chodos, A. A. and Gancarz, A. J. (1972) Petrology of Apollo 15 sample 15486. In *The Apollo 15 Lunar Samples*, p. 20-25. The Lunar Science Institute, Houston.
- Alexeyeva, K. N. (1958) Physical properties of stony meteorites and their interpretation in the light of hypotheses regarding the origin of the meteorites. *Meteoritika*, Vol. 16, p. 67-77.
- Anders, E. and Mellick, P. J. (1969) Orbital clues to the nature of meteorite parent bodies. In *Meteorite Research*, Millman (Ed.), p. 559-572. Dordrecht: Reidel.
- Anders, E. (1964) Origin, age and composition of meteorites. *Space Sci. Rev.* Vol. 3, p. 583-714.
- Anderson, A. T., Braziunas, T. F., Jacoby, J. and Smith, J. V. (1972) Thermal and mechanical history of breccias 14306, 14063, 14270, and 14321. *Proc. Third Lunar Sci. Conf., Geochim. Cosmochim. Acta*, Suppl. 3, Vol. 1, p. 819-835.
- Begemann, F. and Wlotzka, F. (1969) Shock-induced thermal metamorphism and mechanical deformations in the Ramsdorf chondrite. *Geochim. Cosmochim. Acta*, Vol. 33, p. 1351-1370.
- Binns, R. A. (1967) Stony meteorites bearing maskelynite. *Nature*, Vol. 213, p. 1111-1112.
- Bowell, F. and Zellner, B. (1973) Polarization of asteroids and satellites. In *Planets, Stars, and Nebulae Studied with Photopolarimetry* (Ed. Gehrels). University of Arizona Press.
- Butkovich, T. R. (1968) Gas equation state of natural materials, in *Shock Metamorphism of Natural Materials*, Ed. by B.M. French and N.M. Short, p. 83-85.

- Carter, J. L. (1973) Morphology and chemistry of probable VLS (vapor-liquid-solid)-type of whisker structures and other features on the surface of breccia 15015,36. Proc. Fourth Lunar Sci. Conf., Geochim. Cosmochim. Acta, Suppl. 4, Vol. 1, p. 413-422, Pergamon.
- Carter, J. L. and MacGregor, I. D. (1970) Mineralogy, petrology, and surface features of some Apollo 11 samples. Proc. Apollo 11 Lunar Sci. Conf., Geochim. Cosmochim. Acta, Suppl. 1, Vol. 1, p. 247-265. Pergamon.
- Carter, J. L., Clanton, U. S., Fuhrman, R., Laughon, R. B., McKay, D. S. and UsseIman, T. M. (1975) Morphology and composition of chalcopyrite, chromite, Cu, Ni-Fe, pentlandite, and troilite in vugs of 76015 and 76215. Contribution No. 235, University of Texas at Dallas.
- Charles, R. W., Hewitt, D. A. and Wones, D. R. (1971) H₂O in lunar processes: The stability of hydrous phases in lunar samples 10058 and 12013. Proc. Second Lunar Sci. Conf., Geochim. Cosmochim. Acta, Suppl. 2, Vol. 1, p. 645-664. MIT Press.
- Christophe-Levy Michel (1971) On drusy chondrites. Meteoritics, Vol. 6, No. 4, p. 256.
- Clanton, U. S., McKay, D. S., Laughon, R. B. and Ladle, G. H. (1973) Iron crystals in lunar breccias. Proc. Fourth Lunar Sci. Conf., Geochim. Cosmochim. Acta, Suppl. 4, Vol. 1, p. 925-932. Pergamon.
- Dodd, R. T. (1975) H-group xenoliths in the St. Mesmin LL-group chondrite. Geochim. Cosmochim. Acta, in press.
- Dodd, R. T. and Van Schmus, W. R. (1971) Dark-zoned chondrules. Chem. Erde, Vol. 30, p. 59-69.

- Dodd, R. T. (1969) Metamorphism of ordinary chondrites. *Geochim. Cosmochim. Acta*, Vol. 33, p. 161-203.
- Duke, M. B. and Silver, L. T. (1967) Petrology of eucrites, howardites and mesosiderites. *Geochim. Cosmochim. Acta*, Vol. 31, p. 1637-1665.
- El Goresy, A. (1965) Baddeleyite and its significance in impact glasses. *Jour. Geophys. Res.*, 70, p. 3453-3456.
- Engelhardt, W. von (1963) Der Eukrit von stannern. *Contrib. Mineral. Petrol.*, Vol. 9, p. 65-94.
- Epstein, S. and Taylor, H. P. (1971) O^{18}/O^{16} , Si^{30}/Si^{28} , D/H and C^{13}/C^{12} ratios in lunar samples. In *Proc. Second Lunar Sci. Conf.*, *Geochim. Cosmochim. Acta*, Suppl. 2, p. 1421-1441. MIT Press.
- Evans, H. T., Jr. (1970) The crystallography of lunar troilite. *Proc. Apollo 11 Lunar Sci. Conf.*, *Geochim. Cosmochim. Acta*, Suppl. 1, Vol. 1, pp. 399-408. Pergamon.
- Fredriksson, K. (1963) Chondrules and the meteorite parent bodies. *Trans. N. Y. Acad. Sci. Series 11*, Vol. 25, p. 756-769.
- Fredriksson, K., DeCarli, P., Aaramae, A. (1963) Shock-induced veins in chondrites. *Space Res.*, Vol. 3, p. 974-983.
- Fredriksson, K. and Keil, K. (1963) The light-dark structure in the Pantar and Kapoeta stone meteorites. *Geochim. Cosmochim. Acta*, Vol. 27, p. 717-739.
- Fredriksson, K., Noonan, A. and Nelen, J. (1973) Meteoritic, lunar and Lunar impact chondrules. *The Moon*, vol. 7, p. 475-483.
- Gay, P., Bancroft, G. M. and Brown, M. G. (1970) Diffraction and Mossbauer studies of minerals from lunar soils and rocks. *Proc. Apollo 11 Lunar Sci. Conf.*, *Geochim. Cosmochim. Acta*, Suppl. 1, Vol. 1, p. 481-497. Pergamon.

- Gibbons, R. V., Hörz, F., Morris, R. V. and Thompson, T. D. (1975)
Petrographic and ferromagnetic resonance studies of experimentally
shocked regolith analogues. Proc. Sixth Lunar Sci. Conf., in press.
- Heymann, D. (1967) On the origin of hypersthene chondrites: ages and
shock effects of black chondrites. *Icarus*, Vol. 6, p. 189-221.
- Hintenberger, H., König, H., Schultz, L. and Wanke, H. (1965). *Z.
Naturforsch.* 20a, 983.
- Hörz, F. (1965) Untersuchungen an Riesgläsern. *Beiträge zur Mineral und
Petrologie*, Vol. 11, p. 621-661.
- Hovey, E. O. (1922) Aerolite from Rose City, Michigan. *Amer. Mus.
Novitates*, No. 53, 7p.
- James, O. (1972) Lunar anorthosite 15415: texture, mineralogy, and
metamorphic history, *Science*, Vol. 175, p. 432-434.
- Jedwab, J. (1971) Surface morphology of free-growing ilmenites and
chromites from vuggy rocks 10072,31 and 12036,2. Proc. Second
Lunar Sci. Conf., *Geochim. Cosmochim. Acta*, Suppl. 2, Vol. 1,
p. 923-935. MIT Press.
- Keil, K. and Fredriksson, K. (1964) The iron, magnesium, and calcium
distribution in coexisting olivines and rhombic pyroxenes of
chondrites. *J. Geophys. Res.*, Vol. 69, p. 3487-3515.
- King, E. A., Jr., Butler, J. C. and Carman, M. F. (1972) Chondrules in
Apollo 14 samples and size analyses of Apollo 14 and 15 fines.
Proc. Third Lunar Sci. Conf., *Geochim. Cosmochim. Acta*, Suppl. 3,
Vol. 1, p. 673-686.
- Kirsten, T., Krankowsky, D., and Zahringer, J. (1963) Edelgas- und Kalium
Bestimmungen an einer grösseren Zahl von Steinmeteoriten. *Geochim.
Cosmochim. Acta*, Vol. 27, p. 13.

- Kurat, G., Fredriksson, K. and Nelen, J. (1969) Der meteorit von Siena. *Geochim. Cosmochim. Acta*, Vol. 33, p. 765-773.
- Kurat, G., Keil, K., Prinz, M. (1974) Rock 14318: a polymict lunar breccia with chondritic texture. *Geochim. Cosmochim. Acta*, Vol. 38, p. 1133-1148.
- Kurat, G., Keil, K., Prinz, M. and Nehru, C. E. (1972) Chondrules of lunar origin. *Proc. Third Lunar Sci. Conf., Geochim. Cosmochim. Acta, Suppl. 3, Vol. 1*, p. 707-721.
- Mason, B. (1962) *Meteorites*. John Wiley and Sons, Inc., New York.
- Mason, B. (1963) The hypersthene achondrites. *Am. Mus. Novitates*, No. 2155, 13p.
- Mason, B. and Wiik, H. B. (1966) The composition of the Bath Frankfort, Kakangari, Rose City and Tadjera meteorites. *Amer. Mus. Novitates*, No. 2272, 23p.
- McKay, D. S., Clanton, U. S., Morrison, D. A. and Ladle, G. H. (1972) Vapor phase crystallization in Apollo 14 breccia. *Proc. Third Lunar Sci. Conf., Geochim. Cosmochim. Acta, Suppl. 3, Vol. 1*, p. 739-752. M.I.T. Press.
- McQueen, R. G., March, S. P., and Fritz, J. W. (1967) Hugoniot equation of state of twelve rocks, *J. Geophys. Res.*, Vol. 72, p. 4999-5036.
- Nelen, J., Noonan, A. and Fredriksson, K. (1972) Lunar glasses, breccias, and chondrules. *Proc. Third Lunar Sci. Conf., Geochim. Cosmochim. Acta, Suppl. 3, Vol. 1*, p. 723-737.

- Ramdohr, P. (1963) The opaque minerals in stony meteorites. *J. Geophys. Res.*, Vol. 68, No. 7, p. 2011-2036.
- Scott, R. (1966) Origin of chemical variations within ignimbrite cooling units. *Amer. J. Sci.*, Vol. 264, p. 273-288.
- Sheridan, M. F. (1970) Fumarolic mounds and ridges of the Bishop Tuff, California. *Bull. Geol. Soc. Amer.*, Vol. 81, p. 851-868.
- Simonds, C. (1975) Thermal regimes in impact melts and the petrology of the Apollo 17 Station 6 boulder. *Proc. Sixth Lunar Sci. Conf.* in press.
- Skinner, B. J. and Winchell, H. (1972) Vapor phase growth of feldspar crystals and fractionation of alkalis in feldspar crystals from 12038,22 (abstract). In *Lunar Science-III* (editor, C. Watkins), p. 710-711. Lunar Science Institute Contr. No. 88.
- Smith, R. L. (1960) Ash flows. *Bull. Geol. Soc. Amer.*, Vol. 71, p. 795-842.
- Sorby, H. C. (1877) On the structure and origin of meteorites. *Nature*, Vol. 15, p. 495-498.
- Stacey, F. D., Lovering, J. F. and Parry, G. G. (1961) Thermo-magnetic anisotropies of some chondritic meteorites. *J. Geophys. Res.*, Vol. 60, p. 1523-1534.
- Stöffler, D. (1972) Deformation and transformation of rock-forming minerals by natural and experimental shock processes. I. Behavior of minerals under shock compression. *Fortschr. Miner.* Vol. 49, p. 50-113.

- Stöffler, D. (1971) Progressive metamorphism and classification of shocked and brecciated crystalline rocks at impact craters. J. Geophys. Res., Vol. 76, No. 23, p. 5541-5551.
- Sunagawa, I. (1967) Surface microstructures of crystals grown from molten salts. J. Crystal Growth, Vol. 1, p. 102-109.
- Taylor, S. R. (1975) Lunar Science: A Post-Apollo View. Pergamon Press.
- Taylor, G. J., and Heymann, D. (1969) Shock, reheating, and the gas retention ages of chondrites. Earth Planet. Sci. Lett., Vol: 7, p. 151-161.
- Taylor, G. J. and Heymann, D. (1971) Postshock thermal histories of reheated chondrites. J. Geophys. Res., Vol. 76, No. 8, p. 1879-1893.
- Tschermak, G. (1883) The microscopic properties of meteorites, in Smithsonian Contrib. Astrophys., Vol. 4, No. 6, 1964.
- Urey, H. C. (1967) Parent bodies of the meteorites. Icarus, Vol. 7, p. 350-359.
- Urey, H. C. (1958) Comments on two papers by John F. Lovering concerning a typical meteorite parent body. Geochim. Cosmochim. Acta, Vol. 13, p. 335-338.
- Urey, H. C. and Craig, H. (1953) The composition of the stone meteorites and the origin of the meteorites. Geochim. Cosmochim. Acta, Vol. 4, p. 36-82.
- Van Schmus, W. R. (1967) Polymict structure of the Mesö-Madaras chondrite. Geochim. Cosmochim. Acta, Vol. 31, p. 2027-2042.
- Van Schmus, W. R. (1969) The mineralogy and petrology of chondritic meteorites. Earth-Sci. Rev., Vol. 5, p. 145-184.

- Van Schmus, W. R. and Wood, J. A. (1967) A chemical-petrologic classification for the chondritic meteorites. *Geochim. Cosmochim. Acta*, Vol. 31, p. 737-765.
- Wahl, W. (1952) The brecciated stony meteorites and meteorites containing foreign fragments. *Geochim. Cosmochim. Acta*, Vol. 2, p. 91-117.
- Walton, W. J. A., Jr. (1972) Phase equilibrium in the system $Mg_3(PO_4)_2$ - $Ca_3(PO_4)_2$ - Mg_2SiO_4 (Farringtonite-Whitlockite-Fosterite) at one atmosphere pressure. Unpubl. doctoral thesis, Ohio State University.
- Warner, J. L. (1972) Metamorphism of Apollo 14 breccias. *Proc. Third Lunar Sci. Conf.*, *Geochim. Cosmochim. Acta*, Suppl. 3, Vol. 1, p. 623-643. MIT Press.
- Warner, J. L., Simonds, C. H. and Phinney, W. C. (1973) Apollo 16 rocks: classification and petrogenetic model. *Proc. Fourth Lunar Sci. Conf.*, *Geochim. Cosmochim. Acta*, Suppl. 4, Vol. 1, p. 481-504.
- Warner, J. L., Simonds, C. H. and Phinney, W. C. (1974) Impact induced fractionation in the lunar highlands. *Proc. Fifth Lunar Sci. Conf.*, *Geochim. Cosmochim. Acta*, Suppl. 5, Vol. 1, p. 379-397. Pergamon.
- Wasson, J. T. (1974) *Meteorites*. Springer-Verlag, New York.
- Wilkening, L. L. and Clayton, R. N. (1974) Foreign inclusions in stony meteorites - II. Rare gases and oxygen isotopes in a carbonaceous chondritic xenolith in the Plainview gas-rich meteorite. *Geochim. Cosmochim. Acta*, Vol. 38, p. 937-945.
- Wlotzka, F. (1969) On the formation of chondrules and metal particles by "shock melting." In *Meteorite Research* (Millman, Ed.), p. 174-184. Dordrecht Reidel.
- Wood, J. A. (1968) *Meteorites and the Origin of Planets*. McGraw-Hill Book Company.

APPENDIX A

Definitions:

O1, Olivine

Px, Pyroxene

V, Vu, Vug occurrence

MAT, Matrix occurrence (as opposed to vug occurrence)

CHO, CHON, Chondrule

VEIN, Glassy shock-melted vein

MCR, Matrix crystals, preserved but recrystallized

RCM, Recrystallized matrix

MMC, Matrix mineral clast, unrecrystallized

COTECTIC, In cotectic association

ROSE CITY CLAST A, OLIVINE, PYROXENE

	OL3	OL4	OL5	PX6	OL6A	OL7	OLAMAT	OLA1VL
SI02	39.614	39.126	39.658	57.559	40.066	39.873	40.006	39.120
AL2O3	0.022	0.001	0.017	0.292	0.000	0.007	0.035	0.054
CR2O3	0.112	0.041	0.034	0.098	0.040	0.047	0.063	0.074
FFU	16.941	17.218	17.131	10.901	17.312	17.056	18.023	19.170
MGU	42.724	41.866	42.300	30.364	42.343	42.501	42.109	40.662
CAO	0.076	0.070	0.091	0.722	0.066	0.101	0.116	0.185
TOTAL	99.490	98.322	99.232	99.937	99.828	99.585	100.352	99.265
ITER	7	7	7	8	7	7	7	7

STRUCTURAL FORMULAE: 12 OXYGENS

SI	3.021	3.026	3.034	4.042	3.046	3.037	3.036	3.024
AL	0.002	0.000	0.002	0.024	0.000	0.001	0.003	0.005
CR	0.007	0.003	0.002	0.005	0.002	0.003	0.004	0.005
FE	1.081	1.113	1.096	0.640	1.101	1.087	1.144	1.239
MG	4.857	4.826	4.823	3.178	4.798	4.825	4.764	4.684
CA	0.006	0.006	0.007	0.054	0.005	0.008	0.009	0.015
TOTAL	8.974	8.973	8.964	7.944	8.953	8.961	8.960	8.972

	OLA2VU	OLA3VU	OLA4VU	OLA5VU	OLA6VU	OLA7VU	PXA	PXAVLG
SI02	40.118	39.173	39.085	39.387	39.247	40.246	57.823	58.116
AL2O3	0.096	0.059	0.000	0.129	0.041	0.000	0.101	0.200
CR2O3	0.068	0.050	0.057	0.056	0.062	0.048	0.103	0.110
FEU	19.485	18.583	19.023	18.835	19.380	18.982	10.827	10.577
MGU	39.014	40.793	40.629	40.878	40.264	40.423	30.668	30.505
CAU	0.132	0.130	0.115	0.116	0.117	0.127	0.884	0.774
TOTAL	98.914	98.789	98.909	99.402	99.110	99.826	100.406	100.282
ITER	7	7	7	7	7	7	8	8

STRUCTURAL FORMULAE: 12 OXYGENS

SI	3.104	3.033	3.029	3.032	3.039	3.080	4.042	4.058
AL	0.009	0.005	0.000	0.012	0.004	0.000	0.008	0.016
CR	0.004	0.005	0.003	0.003	0.004	0.003	0.006	0.006
FE	1.261	1.203	1.233	1.213	1.255	1.215	0.633	0.618
MG	4.500	4.708	4.694	4.691	4.647	4.611	3.196	3.175
CA	0.011	0.011	0.010	0.010	0.010	0.010	0.066	0.058
TOTAL	8.889	8.963	8.969	8.960	8.958	8.919	7.951	7.971

Clast A, continued

	DLB	PXVUGC	PXCHON	PXVEIN
SiO ₂	39.407	57.979	58.498	53.593
Al ₂ O ₃	0.000	0.189	0.257	2.076
Cr ₂ O ₃	0.044	0.124	0.125	0.283
FeO	17.546	10.922	10.432	12.386
MgO	42.567	30.975	29.930	27.712
CaO	0.076	0.829	0.752	2.062
	-----	-----	-----	-----
TOTAL	99.641	101.018	99.994	98.113
ITER	7	8	8	8

STRUCTURAL FORMULAE: 12 OXYGENS

SI	3.011	4.030	4.007	3.896
AL	0.000	0.015	0.021	0.178
CR	0.003	0.007	0.007	0.016
FE	1.121	0.635	0.610	0.753
MG	4.847	3.209	3.117	3.003
CA	0.006	0.062	0.056	0.161
TOTAL	8.988	7.959	7.899	8.027

HOSE CITY MATRIX, SI FE MG 6/21/75

	OLMCR4	OLV1	PX2	OLMCM2	OLV3	PXV5A	PXV5B	OLV7A
SIU2	38.982	38.548	51.270	39.237	39.631	50.957	49.860	38.395
AL2O3	0.000	0.000	0.206	0.000	0.059	4.800	1.117	0.000
CR2O3	0.005	0.089	0.127	0.065	0.036	0.074	0.447	0.075
FEU	16.069	17.370	11.222	16.458	16.173	9.922	9.266	17.120
MGO	43.430	42.754	29.059	42.445	42.640	25.640	24.725	42.167
CAU	0.073	0.100	0.106	0.123	0.029	0.082	4.386	0.095
TOTAL	99.360	98.916	91.991	98.327	98.569	91.481	89.801	97.853
ITEM	7	7	8	7	7	8	7	7

STRUCTURAL FORMULAE: 24 OXYGENS

SI	5.963	5.951	7.894	6.048	6.077	7.785	7.897	5.978
AL	0.000	0.000	0.037	0.000	0.011	0.864	0.209	0.000
CR	0.001	0.011	0.015	0.008	0.004	0.010	0.054	0.009
FE	2.158	2.240	1.445	2.121	2.074	1.268	1.227	2.229
MG	9.903	9.826	6.669	9.751	9.745	5.838	5.837	9.785
CA	0.012	0.017	0.018	0.020	0.005	0.013	0.704	0.016
TOTAL	18.036	18.044	16.079	17.948	17.916	15.778	15.970	18.018

	OLV7B	PXV7C	OLV7D	OLMCM7	OLMCM7	OLXLIN	OLCH02	OLCH03
SIU2	38.901	51.693	38.374	38.691	38.410	39.263	39.210	39.106
AL2O3	0.178	1.602	0.107	0.000	0.022	0.724	0.000	0.000
CR2O3	0.058	0.788	0.054	0.071	0.093	0.060	0.006	0.006
FEU	17.261	4.518	17.445	17.445	18.168	16.692	17.423	17.389
MGO	42.148	17.487	43.032	42.623	42.074	42.495	43.028	43.055
CAU	0.137	19.626	0.134	0.125	0.238	0.082	0.088	0.053
TOTAL	98.684	95.714	99.145	98.954	99.005	99.316	99.756	99.648
ITEM	7	7	7	7	7	7	7	7

STRUCTURAL FORMULAE: 24 OXYGENS

SI	6.001	7.851	5.908	5.963	5.942	5.992	5.985	5.976
AL	0.032	0.287	0.019	0.000	0.000	0.130	0.000	0.000
CR	0.007	0.095	0.007	0.000	0.011	0.007	0.001	0.006
FE	2.227	0.570	2.246	2.249	2.351	2.130	2.224	2.222
MG	9.090	3.959	9.876	9.792	9.702	9.666	9.790	9.808
CA	0.023	3.194	0.022	0.021	0.039	0.013	0.014	0.009
TOTAL	17.984	15.958	18.079	18.033	18.050	17.939	18.014	18.021

ROSE CITY MATRIX, SI FF MG 6/21/75

	OLMOC1	OLMOC3	OLMOC2	OLMOC4	OLMOC1	OLMOC2	OLMOC3
SI02	39.070	39.454	38.995	39.110	39.089	39.080	38.937
AL2O3	0.029	0.000	0.000	0.027	0.006	0.015	0.008
CR2O3	0.009	0.001	0.004	0.008	0.036	0.050	0.051
FE0	17.383	17.071	16.529	17.109	16.957	17.025	16.703
MGO	43.116	42.771	43.153	42.722	42.832	42.418	42.712
CAU	0.022	0.006	0.035	0.077	0.043	0.030	0.013
TOTAL	99.629	99.463	98.776	99.103	98.964	98.614	98.424
ITER	7	7	7	7	7	7	7

STRUCTURAL FORMULAE: 24 OXYGENS

SI	5.971	6.026	5.990	6.001	6.022	6.022	6.006
AL	0.005	0.000	0.000	0.005	0.001	0.003	0.001
CR	0.001	0.010	0.008	0.007	0.004	0.006	0.006
FE	2.222	2.181	2.123	2.196	2.178	2.194	2.155
MG	9.822	9.738	9.880	9.771	9.803	9.743	9.820
CA	0.004	0.014	0.006	0.013	0.007	0.005	0.002
TOTAL	18.025	17.969	18.006	17.993	17.995	17.973	17.950

	OLCH01	OLCH04	PXCH04	OLMOC8	OLMOC9
SI02	39.017	39.088	54.538	39.083	39.012
AL2O3	0.000	0.000	0.220	0.000	0.000
CR2O3	0.034	0.105	0.132	0.024	0.035
FE0	17.532	17.150	10.493	17.059	17.407
MGO	42.961	43.010	30.600	42.976	42.514
CAU	0.072	0.097	0.807	0.095	0.165
TOTAL	99.616	99.453	96.787	99.238	99.133
ITER	7	7	8	7	7

STRUCTURAL FORMULAE: 24 OXYGENS

SI	5.970	5.970	7.939	5.989	5.995
AL	0.000	0.000	0.038	0.000	0.000
CR	0.004	0.013	0.015	0.003	0.004
FE	2.243	2.194	1.277	2.186	2.237
MG	9.798	9.830	6.600	9.816	9.738
CA	0.012	0.016	0.126	0.016	0.027
TOTAL	18.028	18.013	16.035	18.010	18.002

METAL, SULFIDE GRAINS IN CLAST LITHOLOGY

	Fe	Ni	Fe	S	Ni
VUG	80.10	20.08	62.42	36.17	0.19
MATRIX	91.21	8.59	62.88	36.02	0.18
MATRIX	87.26	12.99	62.85	36.49	0.17
MATRIX	94.13	5.62	62.63	35.89	0.18
MATRIX	92.28	7.72	62.84	36.62	0.09
VUG	87.87	13.15	62.66	36.57	0.20
VUG	83.29	17.59	62.90	36.78	0.21
MATRIX	93.44	7.20	62.78	36.28	0.11

METAL, SULFIDE GRAINS IN MATRIX LITHOLOGY

	Fe	Ni	Fe	S	Ni
VUG	93.68	6.89	62.73	36.95	0.10
VUG	90.82	9.46	62.71	36.08	0.11
VUG	91.87	9.04	-	-	-
VUG	91.45	8.94	-	-	-
VUG	91.79	8.77	-	-	-
RCM	91.82	8.51	62.87	36.81	0.15
RCM	92.35	7.87	62.67	36.43	0.13
GLASSY	88.83	11.25	61.64	36.03	0.07
GLASSY	81.83	18.22	62.32	36.29	0.05
GLASSY	89.50	11.46	62.65	36.83	0.09
GLASSY	90.64	9.92	62.68	35.51	0.17
COTECTIC	91.49	8.79	63.13	37.07	0.18
COTECTIC	92.12	8.59	62.81	36.81	0.17